Atomistic modeling of thermodynamic properties, diffusion and ordering in Fe-Ni alloys

Yimi Wang

▶ **To cite this version:**

Yimi Wang. Atomistic modeling of thermodynamic properties, diffusion and ordering in Fe-Ni alloys. Material chemistry. Centrale Lille Institut, 2021. English. NNT : 2021CLIL0036 . tel-04027008

HAL Id: tel-04027008
https://theses.hal.science/tel-04027008

Submitted on 13 Mar 2023

HAL is a multi-disciplinary open access archive for the deposit and dissemination of scientific research documents, whether they are published or not. The documents may come from teaching and research institutions in France or abroad, or from public or private research centers.

L'archive ouverte pluridisciplinaire **HAL**, est destinée au dépôt et à la diffusion de documents scientifiques de niveau recherche, publiés ou non, émanant des établissements d'enseignement et de recherche français ou étrangers, des laboratoires publics ou privés.

CENTRALE LILLE

THESE

Présenté en vue d'obtenir le grade de

DOCTEUR

En

Science des matériaux

Par

WANG Yimi

DOCTORAT DELIVRE PAR CENTRALE LILLE

Modélisation atomique des propriétés thermodynamiques, de la diffusion et de la mise en ordre dans les alliages Fe-Ni

Soutenue le 01/12/2021 devant le jury d'examen :

Président	**Prof.**	**Michel Perez**	Université de Lyon, France
Rapporteur	**Prof.**	**Cristelle Pareige**	Université de Rouen, France
Rapporteur	**Dr.**	**Guy Tréglia**	CiNAM-CNRS, France
Membre	**Dr.**	**Anne Hemeryck**	LAAS-CNRS, France
Membre	**Dr.**	**Hickel Tilmann**	Max-Planck-Institut für Eisenforschung, Allemagne
Membre	**Dr.**	**Frédéric Soisson**	CEA-Saclay, France
Directeur de thèse	**Prof.**	**Charlotte Becquart**	Centrale Lille, France

Thèse préparée dans le Laboratoire SRMP
Ecole Doctorale SMRE 104

Introduction

Atomistic simulations of the kinetics of diffusive phase transformations (phase separation or ordering) in metallic alloys require interaction models that realistically describe the thermodynamic and diffusion properties of these materials. When diffusion occurs via vacancies - the most common case - this means accurately describing how the concentration and the jump frequencies of vacancies depend on the local atomic environment. In recent years, much progress has been made in this area, largely due to *ab initio* computational methods. However, to simulate kinetics of thermally activated processes, the models must also be sufficiently light. Pair interaction models on rigid lattices, used in atomistic kinetic Monte Carlo (AKMC) simulations, are in this respect a good compromise between realism and numerical cost, and have proven to be an efficient tool to simulate coherent phase transformation kinetics. Pairwise interactions can be fitted to *ab initio* calculations at 0 K of alloying properties (typically the enthalpies of formation of ordered or disordered structures) and / or of point defects (enthalpies of formation, migration barriers). It is, however, much more difficult to determine high temperature properties from first principle methods. Calculations of vibrational entropies are possible, but expensive, and are still mostly limited to pure metals or dilute alloys (in concentrated alloys, the number of atomic configurations to consider becomes a problem). In iron-based materials, magnetic effects are an additional difficulty for ab initio calculations: in paramagnetic materials, such as austenitic steels, magnetic disorder is added to chemical disorder. In spite of recent progress, mainly concerning pure metals (Körmann et al. 2008), it is difficult to predict the effect of a magnetic transition on, for instance, the stability of a phase, the enthalpy of formation or migration of a vacancy, a diffusion coefficient. Magnetic interaction models, based only on Density Functional Theory (DFT) calculations, have been proposed recently (for example at the SRMP, with the work of Chu-Chun Fu and coworkers (Schneider et al. 2020; Li and Fu 2020), or the Magnetic Cluster Expansion developed at Culham (Lavrentiev, Dudarev, and Nguyen-Manh 2009). However, these models are still too computationally costly to be used directly in AKMC simulations of precipitation or ordering kinetics, because one has to equilibrate the magnetic moments, in addition to the atomic configurations. Under these conditions, it is interesting and necessary to directly adjust the relevant parameters of the simulations on experimental data.

The idea is not new of course, but we propose here to apply it to Fe-Ni alloys with the face-centered cubic structure, in a more systematic way than in previous studies, in particular by establishing the link

between our model and the CALPHAD method (both with the formalism used in CALPHAD, and the data available for Fe-Ni alloys). Fe-Ni alloys are the base of many industrial alloys. At the SRMP, their modeling is an essential step before dealing with the Fe-Cr-Ni ternary alloys (the model system for austenitic steels) and the simulation of irradiation effects in these alloys. Fe-Ni alloys have interesting magnetic properties: the γ solid solutions, stable at high temperature, are paramagnetic, but Ni rich alloys become ferromagnetic at low temperatures. Because of their industrial importance, there are many experimental studies concerning both their thermodynamic and diffusion properties (the latter in particular have been studied more extensively than those of many other alloys). Nevertheless, as shown in Figure 1, some questions remain open: as always, the phase diagram is not well known at low temperatures, when the diffusion becomes too slow to bring the system to its equilibrium state. A FeNi-$L1_0$ phase has been observed in meteorites or under irradiation, and *ab initio* calculations suggest that it is stable at low temperatures, but its domain of existence is debated. They are few atomistic modeling of its diffusion properties and of the kinetics of ordering, and they often used empirical interatomic potentials whose predictive power is imperfect.

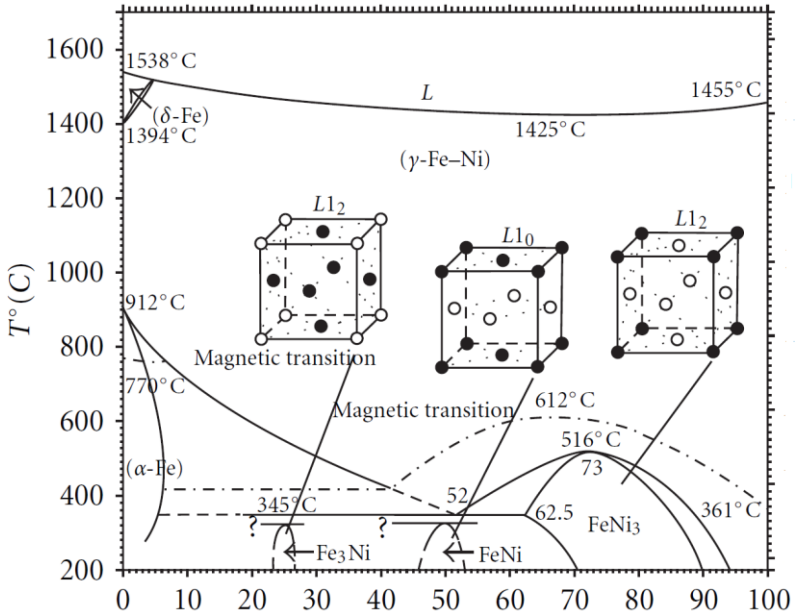

Figure 1. The phase diagram of the Fe-Ni system (Vernyhora, Tatarenko, and Bokoch 2012)

The manuscript is organized as follows: we model this system with a rigid lattice pair interaction model and AKMC simulations. The pair interactions depend on the local composition and temperature, which allows us to reproduce asymmetric mixing properties, and non-configurational entropic contributions (the entropy of configuration is treated by Monte Carlo simulation). The thermodynamic properties of Fe-Ni alloys are discussed in Chapter I. The interatomic pair interactions that control them are fitted to DFT calculations at T = 0 K of formation enthalpies in ordered and disordered structures,

performed by Kangming Li during his thesis (Li 2021). The high-temperature properties are fitted to a recent CALPHAD study (Cacciamani et al. 2010). This allows for an accurate description of the enthalpy and Gibbs free energy of the phases, in particular of their magnetic contribution - which are treated separately in this CALPHAD study. We build the Fe-Ni phase diagram, with Monte Carlo simulations performed in the semi-grand canonical ensemble. In particular, we study the effect of the magnetic contribution on the relative stability of the γ solid solution, the $L1_0$ phase and the $L1_2$ phase.

The diffusion properties are the subject of Chapter II. The pair interaction model is completed to include the diffusion of vacancies and the corresponding parameters are fitted to experimental measurements of tracer diffusion coefficients in dilute and concentrated solid solutions. AKMC simulations of diffusion phenomena require the knowledge of the equilibrium vacancy concentration, and how it depends on the temperature, the alloy composition and the state of order. We find that previously used techniques, developed for systems with an unmixing tendency, are inefficient in the case of Fe-Ni, an alloy with an ordering tendency. A new method is thus proposed, based on the Widom insertion technique. We then use AKMC simulations to evaluate the interdiffusion coefficients in disordered solid solutions, and to test the Darken equation which relates the tracer coefficients, the interdiffusion coefficients, and the thermodynamic factor. Finally, we study the diffusion in the ordered $FeNi_3$-$L1_2$ phase, for which no experimental data are available.

In the last chapter, we model the ordering kinetics in the $FeNi_3$ alloy, with the same interaction model and AKMC simulations. We compare our results with three experimental studies that provide measurements of the time evolution of the long-range order parameter and of the size of the ordered domains in alloys of the same composition. We conclude by considering possible improvements to our model, and possible applications to other systems.

List of acronyms

1nn: first nearest neighbors

AFM: Anti-Ferro Magnetic

AKMC: Atomic Kinetic Monte Carlo

DD: Differential Dilatometry

DFT: Density Functional Theory

fcc: face-centered cubic

FM: ferromagnetic

GGA: Generalized Gradient Approximation

k-PIM: kinetic Pair Interaction Model

LDA: Local Density Approximation

MC: Monte Carlo

MD: Molecular Dynamics

NM: Non Magnetic

PAW: projector augmented wave

PAS: positron annihilation spectroscopy

PBE: Perdew-Burke-Ernzerhof

PIM: Pair Interaction Model

PM: paramagnetic

SIA: Self-Interstitial Atoms

SP: Saddle Point

SQS: Special Quasi-random Structures

TEM: Transmission Electron Microscopy

TIP: Thermodynamics of Irreversible Phenomena

VASP: Vienna Ab initio Simulation Package

List of symbols

a_0: lattice parameter

C: concentration of an element in a material

$c_{A\alpha}$: concentration of atoms A on the α site

$c_{V\alpha}$: concentration of vacancies on the α siteC_V^{eq}: equilibrium concentration of mono-vacancies

C_V^{MC}: vacancy concentration in the Monte Carlo simulations

C_I^{eq}: equilibrium concentration of interstitials

D: self-diffusion coefficient

D_0: pre-factor of diffusion coefficient

D_2: diffusion coefficient of solute in dilute solution

D_A^{Intr}, D_B^{Intr}: intrinsic diffusion coefficient of component A and B

D_{AB}^{A*}: tracer diffusion coefficient of atom A in alloy A-B

D_A^{A*}: self-diffusion coefficient of A

D_A^{B*}: impurity diffusion coefficient of dilute B in element A

$\widetilde{D}$: inter-diffusion coefficient

e_i: atom energy of atom i

$e_{A\alpha}$: energy of atom A on the α sublattice

f, f_2: correlation factor of self-diffusion and interdiffusion coefficients

g_i: Gibbs free energy of atom i

g_{Ai}^{SP}: interactions between the atom A on the saddle point position and atoms on its neighboring sites (i)

$g_{Vj}^{(n)}$: interactions between the vacancy V and atoms j on the lattice (nth nearest neighbor)

$g_{Ak}^{(n)}$: interactions between the atom A and other atoms k on lattice (nth nearest neighbor)

$G_V^{mig}, H_V^{mig}, S_V^{mig}$: Gibbs free energy, enthalpy and entropy of vacancy migration

$G_V^{for}, H_V^{for}, S_V^{for}$: Gibbs free energy, enthalpy and entropy of vacancy formation

$G_{V_{Fe}}^{for}, G_{V_{Ni}}^{for}$: Gibbs free energy of vacancy formation in ordered phases: a vacancy replace an atom Fe or Ni on its sub lattice

G_{S-V}^{bin}: Gibbs free binding energy between a solute and a vacancy ($G_{S-V}^{bin} > 0$ for attractive interactions)

G_{V_i}: Gibbs free energy of the system with a vacancy on site i

G_0: Gibbs free energy of the system without vacancy

$G^{\gamma}, G_{ref}^{\gamma}, G_{ex}^{\gamma}, G_{mag}^{\gamma}, G_{id}^{\gamma}$: the total Gibbs free energy of a system and its different contribution part (reference part, excess part, magnetic part and ideal part)

$H_0^{mig}, H_1^{mig}, H_2^{mig}, H_3^{mig}, H_4^{mig}$: migration barriers corresponding respectively to the frequencies $\omega, \omega_1, \omega_2, \omega_3, \omega_4$ of the five-frequency model.

$\boldsymbol{J}$: flux of a species

k_B: Boltzmann constant

$\boldsymbol{L}, L_{ij}$: the matrix of transport coefficients and its coefficients

M: magnetic moment

Q: activation energy of diffusion

t_{MC}: calculated time in Monet Carlo simulations

t_{real}: physical time of the real system

$T_{Curie}^{Fe}, T_{Curie}^{Ni}$: Curie temperature of Fe and Ni

$T_C^{L1_2}$: critical temperature of the ordered phase $FeNi_3$-$L1_2$

x_A, x_B: mole fraction of element A and B

$\boldsymbol{X_J}$: driving force of the flux $\boldsymbol{J}$

β_{FeV}, β_{NiV}: ratio between the second and first nearest neighbors of vacancy and Fe/Ni atoms

λ: wave length

η: long-range order parameter

σ_1, σ_2: short range order parameter measured by the first and second nearest neighbors

μ_i: chemical potential of element i

ϑ_0: attempt frequency

$\omega, \omega_1, \omega_2, \omega_3, \omega_4$: frequencies in the five-frequency model

υ_n: ordering parameters of the Fe-Ni system, with $n = 1, 2$

γ_i: coefficient of thermodynamic activity of species i

Φ: thermodynamic factor

Chapter I Thermodynamic properties in fcc Fe-Ni alloys

This first chapter presents the thermodynamic part of our pair interaction model (PIM), which will be extended in the following chapters to deal with the formation and migration and vacancies, and diffusion and ordering phenomena. This is a reproduction of an article published in Physical Review Materials: *Combining DFT and CALPHAD for the development of on-lattice interaction models: The case of Fe-Ni system*, Yimi Wang, Kangming Li, Frédéric Soisson, and Charlotte S. Becquart, Phys. Rev. Materials 4, 113801 (2020)

Combining DFT and CALPHAD for the development of on-lattice interaction models: the case of Fe-Ni system

Yimi Wang,* Kangming Li,† and Frédéric Soisson‡

Université Paris-Saclay, CEA, Service de Recherches de Métallurgie Physique, 91191, Gif-sur-Yvette, France

Charlotte S. Becquart§

Univ. Lille, CNRS, INRAE, Centrale Lille, UMR 8207, UMET, Unité Matériaux et Transformations, F 59000, Lille, France

Abstract

We present a model of pair interactions on rigid lattice to study the thermodynamic properties of iron-nickel alloys. The pair interactions are fitted at 0 K on ab initio calculations of formation enthalpies of ordered and disordered (special quasi-random) structures. They are also systematically fitted on the Gibbs free energy of the γ Fe-Ni solid solution as described in a CALPHAD (CALculation of PHAse Diagrams) study by Cacciamani et al. This allows the effects of finite temperature, especially those of magnetic transitions, to be accurately described. We show that the ab initio and CALPHAD data for the γ solid solution and for the $FeNi_3$-$L1_2$ ordered phase can be well reproduced, in a large domain of composition and temperature, using first and second neighbor pair interactions which depend on temperature and local alloy composition. The procedure makes it possible to distinguish and separately compare magnetic, chemical and configuration enthalpies and entropies. We discuss the remaining differences between the pair interaction model and CALPHAD, which are mainly due to the treatment of the short-range order and configurational entropy of the solid solution. The FCC phase diagram of the Fe-Ni system is determined by Monte Carlo simulations in the semi-grand canonical ensemble and is compared with experimental studies and other models. We especially discuss the stability of the FeNi-$L1_0$ phase at low temperature.

I. INTRODUCTION

Atomistic Monte Carlo simulations of phase transformation kinetics in metallic alloys (precipitation, ordering, etc. [1–13]) require interaction models that allow a precise description of the thermodynamic and kinetic properties of the materials, while remaining simple enough to model systems of a few million atoms over long periods of time (their evolution being controlled by thermally activated diffusion mechanisms). Models using effective interactions on rigid lattices – although limited to coherent problems – are among the most widely used and have become more reliable since they are systematically fitted to ab initio calculations of materials properties at 0 K (such as the formation energies of ordered phases or special quasi-random structures, point defect formation and migration energies, etc.) [5, 7, 13].

* yimi.wang@cea.fr

† kangming.li@cea.fr

‡ frederic.soisson@cea.fr

§ charlotte.becquart@univ-lille.fr

Evaluating non-zero temperature effects from ab initio methods is more difficult: calculations of vibration entropy, for example, are in principle possible but are computationally expensive and are usually limited to simple systems (e.g. pure metals, perfectly ordered phases, or dilute alloys). Modeling the effect of magnetic transitions and magnetic disorder – especially important in iron based alloys – is also very challenging. Alternatively, the temperature dependence of pair interactions can be adjusted on experimental data, for example on phase diagrams, but these adjustments are often made on a case-by-case basis. We propose here a new approach to systematically fit a pair interaction model both on ab initio calculations at 0 K and, for high temperatures, on a CALPHAD-type model. CALPHAD models provide an accurate description of the Gibbs free energies of the different phases of an alloy, based on empirical thermodynamic models fitted (mainly) on large numbers of experimental measurements. They also provide a specific description of some important contributions (e.g. magnetic contributions in iron-based alloys). The objective of this paper is to show how to establish a term-to-term correspondence between the empirical models used in CALPHAD and the effective interactions of a lattice model; to show the improvements that this brings to the description of a particular alloy; but also to discuss the limits of such a correspondence.

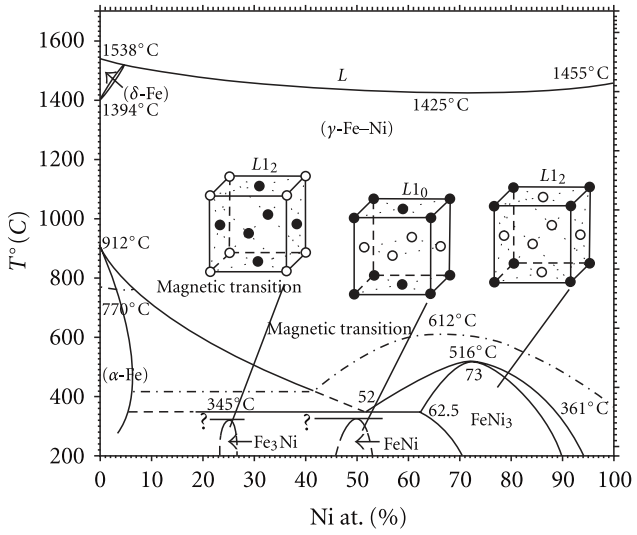

FIG. 1. The phase diagram of the Fe-Ni system (from [14] and [15])

We apply this approach to Fe-Ni alloys with a face-centered cubic structure (FCC). Recent ab initio [16, 17] and CALPHAD [18, 19] studies are available for this system. The thermodynamic properties of Fe-Ni alloys have been much studied, because of their industrial

interest and because they still raise unresolved questions. The phase diagram of the Fe-Ni system (Fig. 1) is well known at temperatures above 400°C [20]: the FCC solid solution γ is stable over the whole composition range and over a wide temperature range. The body centered cubic (BCC) solid solution α is stable below 912°C, and only with nickel contents below approximately 10%. A two-phase domain $\alpha - \gamma$ is observed in iron-rich alloys, and an ordered $FeNi_3$ phase (with the $L1_2$ structure) is formed below 516°C.

At lower temperatures, the phase diagram is – as usual – more difficult to establish, because of slow diffusion processes. However, irradiation experiments [21–23], observations of meteorites [15, 24], and ab initio studies [16, 17] suggest that other ordered FCC phases may be stable or metastable (notably the FeNi phase of $L1_0$ structure and the Fe_3Ni phase of $L1_2$ structure). Many CALPHAD studies have sought to complement the Fe-Ni phase diagram by extrapolating at low temperatures the empirical thermodynamic models fitted to experiments at high temperatures. This is especially difficult in the case of Fe-Ni, and as a result, the proposed phase diagrams show significant differences [15, 18, 20, 25]. A particular difficulty of this system is that the experimental data are obtained essentially in paramagnetic phases, whereas the ordered phases are ferromagnetic. Magnetic contributions are indeed taken into account in CALPHAD approaches, but again by empirical models using experimental data and still under discussion [25].

Atomistic models combining the information from experiments and first principle methods may provide additional insight on these issues. A few rigid lattice interaction models, fitted to ab initio calculations, have been developed for Fe-Ni alloys: Mohri et al. [26] proposed a cluster expansion to study the stability of the ordered compound FeNi-$L1_0$ in the framework of a CVM approximation: they found an ordering temperature of 483 K (taking into account the vibration entropy, which lowers it by about 40 K). But they did not study the $FeNi_3$ phase, nor the effect of the ferro-to-paramagnetic transition. Effective interactions models including an explicit description of the magnetic moments have been proposed for Fe-Ni alloys, using Ising [27–30] or Heisenberg [30, 31] models for the magnetic interactions and parameters fitted to the experimental transition temperatures. Similar magnetic models have been also used in phase-field simulations of ordering and precipitation of the $FeNi_3$ phase [32]. More recently Lavrentiev, Wrobel et al. [33, 34] developed a Magnetic Cluster Expansion (MCE), based on a Heisenberg-Landau Hamiltonian, fitted to ab initio calculations. Its properties have been studied by Monte Carlo methods, but the combined equilibration of

the chemical and magnetic configurations is very costly in computational time, and the complete phase diagram of the MCE model of Fe-Ni remains to be established.

In the present paper, we propose a pair interaction model (PIM) based on a rigid lattice approximation, aiming at modelling the Fe-Ni system. The model does not describe explicitly the magnetic moments, nor the lattice relaxations, which makes it faster to process in Monte Carlo simulations. It only involves pair interactions between atoms that depends both on the local composition and temperature. Finite temperature effects of magnetic transitions or of lattice vibrations (harmonic and non-harmonic), on the energetic proprieties are taken into account through these dependencies.

The outline of this article is as follows: section II is devoted to the thermodynamic models of FCC phases in the Fe-Ni system. We briefly recall the Gibbs free energy models used in the CALPHAD approaches, focusing on the recent study of Cacciamani et al. [18] (II A); then the available ab initio results on the properties of Fe-Ni alloys (in particular those of K. Li and C.-C. Fu [17]) (II B). We then show how to reproduce these results with the PIM in section (II C). In section III, we use Monte Carlo simulations in the semi-canonical grand ensemble, to measure the Gibbs free energies of the FCC alloys, and to build the FCC phase diagram.

II. THERMODYNAMIC MODELS

Our PIM is built using both a CALPHAD study and ab initio calculations. We therefore recall the main information provided by these two approaches before to explain how it can be reproduced with effective interactions on a rigid lattice.

A. CALPHAD Models

Several CALPHAD-type studies have been proposed for the Fe-Ni system: the most recent are those of Cacciamani et al. [18] and Ohnuma et al. [19] (for older ones, see the reviews in refs. [15, 20]). Within the CALPHAD framework, a Gibbs free energy model can be defined for each of the phases to be considered (e.g. in the Fe-Ni system, the α and γ solid solutions and the different ordered phases). This gives great flexibility to fit the parameters to the experimental data. We will fit our PIM parameters to the study by Cacciamani

et al. [18] (which will be hereafter simply referred to as the "CALPHAD model" or even as "CALPHAD"), but the following presentation and procedure could easily be adapted to other CALPHAD studies.

1. The γ solid solution

The Gibbs free energy per atom of the solid solution γ (FCC) $Fe_{1-x}Ni_x$ is:

$$G^\gamma = G^\gamma_{ref} + G^\gamma_{ex} + G^\gamma_{mag} + G^\gamma_{id} \tag{1}$$

This is the total Gibbs free energy, including the entropy of configuration. (Note that in CALPHAD one rather uses molar energies, in J.mol^{-1}. We convert them in energies per atom, in eV).

G^γ_{ref} is the non-magnetic contribution of pure metals:

$$G^\gamma_{ref} = (1-x)G^\gamma_{Fe} - xG^\gamma_{Ni} \tag{2}$$

where G^γ_{Fe} and G^γ_{Ni} are the Gibbs free energy of pure Fe and pure Ni.

G^γ_{ex} is the excess Gibbs free energy, written as a sum of Redlich-Kister polynomials:

$$G^\gamma_{ex} = x(1-x)\sum_i L^\gamma_i(T)(1-2x)^i \tag{3}$$

(from $i = 0$ to 2 in [18])

G^γ_{mag} is the magnetic contribution:

$$G^\gamma_{mag} = -k_B T f(\tau)\ln(\beta(x)+1) \tag{4}$$

$\tau = T/T_c(x)$, where $T_c(x)$ is the Curie temperature, $\beta(x)$ the average magnetic moment of the γ solid solution and $f(\tau)$ is a polynomial function of the reduced temperature. $T_c(x)$ and $\beta(x)$ are also given by Redlich-Kister polynomials of the composition x, fitted to experimental measurements. Different expressions and values have been proposed [25], those used by Cacciamani et al. are given in [18].

G^γ_{id} corresponds to an ideal entropy of configuration:

$$G^\gamma_{id} = -TS^\gamma_{id} = k_B T\left[x\ln x + (1-x)\ln(1-x)\right] \tag{5}$$

i.e. to the configuration entropy of a perfectly disordered solid solution with no short-range order. Note that the excess term (eq. 3) may include a non-ideal configurational part, but it is not identified as such.

Finally, the Gibbs free energy of mixing is:

$$G^{\gamma}_{mix} = G^{\gamma} - (1-x)G'^{\gamma}_{Fe} - xG'^{\gamma}_{Ni} \tag{6}$$

where $G'^{\gamma}_{Fe} = G^{\gamma}_{Fe} + G^{\gamma}_{mag}(x=0)$ and $G'^{\gamma}_{Ni} = G^{\gamma}_{Ni} + G^{\gamma}_{mag}(x=1)$ are the total Gibbs free energies of the pure metals, including the magnetic part.

2. Ordered Phases

In the study by Cacciamani et al. [18], the ordered phases $FeNi_3$ ($L1_2$), Fe_3Ni ($L1_2$) and FeNi ($L1_0$) are modeled within the framework of the Compound energy formalism (CEF) with 4 sublattices. An additional term is added to the Gibbs free energy of the γ phase, which depends on the distribution of species on the different sublattices and on interaction energies (limited to the first nearest neighbors) fitted to ab initio calculations of the formation enthalpy of the perfectly ordered phase.

In the present work, we will use more detailed ab initio studies, involving both ordered and disordered configurations and summarized in the following section.

B. Ab initio calculations

1. Density functional theory method

In this work, the 0 K formation enthalpies of Fe-Ni ordered and disodered phases are fitted to those computed in the *ab initio* study of Ref. [17]. The essential computational points are presented in the following.

The *ab initio* calculations were performed using density functional theory (DFT) with the projector augmented wave method [35, 36] as implemented in the VASP (Vienna Ab-initio Simulation Package) [37–39]. The generalized gradient approximation for the exchange-correlation functional in the Perdew-Burke-Ernzerhof parametrization [40] was employed. All the calculations are spin-polarized. $3d$ and $4s$ electrons were considered as valence electrons. The plane-wave basis cutoff was set to 400 eV. The Methfessel-Paxton broadening

scheme with a smearing width of 0.1 eV was used [41]. The k-point grids were generated according to the cell size to achieve a k-sampling equivalent to a cubic unit cell with a $16 \times 16 \times 16$ shifted grid following the Monkhorst-Pack scheme [42]. The zero-point energies, which can be significant for light elements, have been calculated in the ordered phases. Their contribution to the mixing enthalpies is very small (typically 0.001 to 0.003 eV) and has been neglected in the following. FCC solid solutions were represented by Special Quasirandom Structures (SQS) [43] minimizing Warren-Cowley short-range order parameters [44, 45], with 128-atom and 108-atom supercells for anti-ferromagnetic-double-layer and ferromagnetic phases, respectively.

2. Ordered Phases

TABLE I. Formation enthalpies of FCC ordered phases in Fe-Ni (DFT calculations from [17]).

Ordered phase	H_{for} (eV/atom)
Fe_7Ni-cI32	0.039273
Fe_3Ni-$L1_2$	-0.01636
Fe_3Ni-Z1	-0.04414
Fe_2Ni-$C11_f$	-0.06991
FeNi-$L1_1$	-0.04040
FeNi-$L1_0$	-0.10797
Fe_2Ni-$C11_f$	-0.08064
$FeNi_2$-$L1_2$	-0.10879
$FeNi_7$-cI32	-0.04541

The formation enthalpies of nine ordered structures on the FCC lattice, calculated by Kangming et al. [17] using the DFT method presented in the previous section, are given in Table I and Fig. 2. The ordered structures are ferromagnetic, except for Fe_7Ni-cI32 which is ferrimagnetic. The formation enthalpies are defined with the anti-ferromagnetic FCC iron and the ferromagnetic FCC nickel as reference states. The trends are the same as in a previous study by Mishin et al. [16]: only the FeNi-$L1_0$ and $FeNi_3$-$L1_2$ phases are located on the convex hull (Fig. 2) and must therefore be stable at low temperature on the FCC

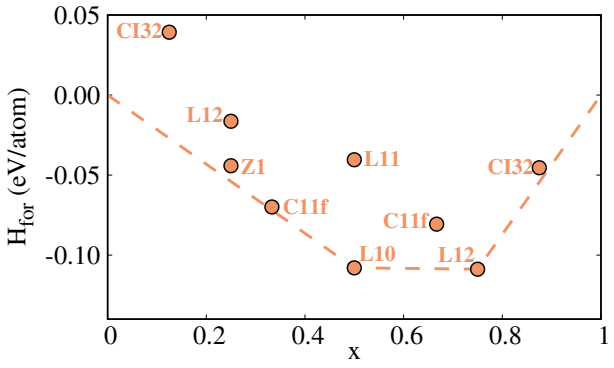

FIG. 2. Formations enthalpies of ordered FCC structures at 0 K (DFT calculations from [17]).

lattice. However the $FeNi_7$-cI32 and Fe_2Ni-$C11_f$ phases are close to the stability limit.

3. Special Quasi-Random Structures

The formation enthalpies H_{for} of special quasi-random structures (SQS) of different compositions have also been calculated in the same study with different magnetic states. These structures are representative of random solid solutions. They were generated by standard methods, with a minimization of Warren-Cowley short-range order parameters. They are described in Ref. [17], with a detailed analysis of their volume and magnetic moments. We just recall here the energetic results used for the PIM parametrization.

The most stable SQS are found to be double-layered anti-ferromagnetic for $x < 0.184$ and ferromagnetic for $x > 0.184$ (red circles in Fig. 3). One observes an asymmetrical evolution of H_{for} with the composition, as already predicted in the study by Cacciamani et al., with mainly negative values (i.e. a tendency to order) and a minimum in the vicinity of the composition of the $FeNi_3$ phase. However, the SQS values are significantly larger than the CALPHAD ones (Fig. 3), and are even slightly positive for $x < 0.20$ (as already obtained by Sansa et al. [46], using a tight-binding approach).

C. Pair interaction model

We propose to reproduce the properties of Fe-Ni alloys with a model of concentration- and temperature-dependent pair interactions on a perfect FCC lattice. This pair interaction model (PIM) is based on a similar one developed for Monte Carlo simulations of BCC Fe-Cr

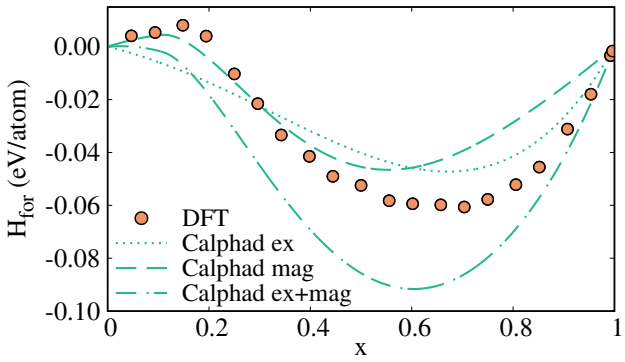

FIG. 3. Formations enthalpies at 0 K of quasi-random FCC structures (DFT calculations [17]) and FCC solid solutions (CALPHAD [18], with separate magnetic and excess contributions).

alloys [9, 47], which had however not been fitted systematically on a CALPHAD model, and did not explicitly distinguish a magnetic contribution.

The essential assumption of the PIM is that the Gibbs free energy (per atom) of a given configuration, i.e. a given distribution of n_{Fe} Fe atoms and n_{Ni} Ni atoms ($N = n_{Fe} + n_{Ni}$) on the FCC lattice, can be written as a sum of interactions $g_{ij}^{(n)}(x,T)$ between pairs of i and j atoms on n^{th} neighboring sites:

$$G_{conf} = \frac{1}{N} \sum_{ij} g_{ij}^{(n)}(x,T) \tag{7}$$

The pair interactions depend on the temperature, T, and the Ni concentration, x (we will omit these dependencies in the following, to simplify the notations). The dependence on concentration is required to reproduce an asymmetric evolution of formation enthalpies, as observed in Fig. 2 and Fig. 3. The dependence on temperature describes the entropic contributions (electronic, vibrational and magnetic) other than the configuration entropy, so the $g_{ij}^{(n)}$ are indeed "pair Gibbs free energies" and can be written as: $g_{ij}^{(n)} = h_{ij}^{(n)} - Ts_{ij}^{(n)}$ [48].

To facilitate the comparison with CALPHAD models, each interaction $g_{ij}^{(n)}$ is written as a sum of a non-magnetic (nm) and a magnetic term (mag). G_{conf} is therefore the sum of:

$$G_{conf}^{nm} = \frac{1}{N} \sum_{ij} g_{ij}^{nm(n)} \tag{8}$$

which accounts for the chemical and vibrational contributions, and of:

$$G_{conf}^{mag} = \frac{1}{N} \sum_{ij} g_{ij}^{mag(n)} \tag{9}$$

The total Gibbs free energy of the alloy is:

$$G = G_{conf} - TS_{conf} \tag{10}$$

where S_{conf} is the entropy of configuration, which will be evaluated from Monte Carlo simulations.

The Gibbs free energy of mixing G_{mix} is:

$$G_{mix} = G - (1-x)G'_{Fe} - xG'_{Ni} \tag{11}$$

G'_{Fe} is the Gibbs free energy of pure iron, on the same FCC lattice:

$$G'_{Fe} = G^{nm}_{Fe} + G^{mag}_{Fe} \tag{12}$$

$$= \sum_n \frac{z_n}{2}(g^{nm(n)}_{FeFe} + g^{mag(n)}_{FeFe}) \tag{13}$$

$$= \sum_n \frac{z_n}{2} g^{(n)}_{FeFe} \tag{14}$$

where z_n is the coordination number for the nearest neighbors n. The same expressions apply to pure nickel.

1. High temperatures: fitting of the pair interactions to CALPHAD

In the PIM, the Gibbs free energy of mixing of a perfectly disordered solid solution is:

$$G_{mix}(x,T) = x(1-x)\sum_n z_n v_n(x,T) - TS_{id} \tag{15}$$

where the ordering parameters v_n are defined as:

$$v_n(x,T) = g^{(n)}_{FeNi} - \frac{1}{2}\left(g^{(n)}_{FeFe} + g^{(n)}_{NiNi}\right) \tag{16}$$

To reproduce the properties of the CALPHAD model, we identify the non-magnetic part of the ordering parameters (in eq. 15) to the excess Gibbs free energy of CALPHAD (eq. 3):

$$\sum_n v^{nm}_n(x,T) = \frac{G^{\gamma}_{ex}}{x(1-x)} \tag{17}$$

and their magnetic part to the magnetic Gibbs free energy of CALPHAD (eq. 4):

$$\sum_n v^{mag}_n(x,T) = \frac{G^{\gamma}_{mag}}{x(1-x)} \tag{18}$$

The fitting of the PIM parameters on CALPHAD can be summarized to the equations 16-18. It is worth to notice that it is based on an approximation: eq. 15 is exact only for a disordered solid solution, i.e. at sufficiently high temperatures. In the real solid solution, a short-range order may exist, and the configuration entropy does not reduced to an ideal term.

2. Low temperatures: fitting of the pair interactions to ab initio calculations

To reproduce the properties of a solid solution at 0 K, the same method can be used by fitting $v_n(x,T)$ on the formation enthalpies of SQS calculated by DFT. The magnetic part remains fitted to the magnetic model of CALPHAD (eq. 18) and the non-magnetic part is fitted so that the sum of the magnetic and non-magnetic contributions of the PIM reproduces the DFT formation enthalpies. A good agreement is obtained with a Redlich-Kister polynomial of order 5 (instead of 2 for G^{γ}_{ex} in ref. [18]), as shown in Fig. 4 (with respectively the magnetic part, the non-magnetic part and the total mixing enthalpies of the PIM). The fitting coefficients L_j^{DFT} of the polynomial are given in Table II, corresponding to the orange curve in Fig. 4. As mentioned above, this gives mixing enthalpies above those predicted by CALPHAD at 0 K.

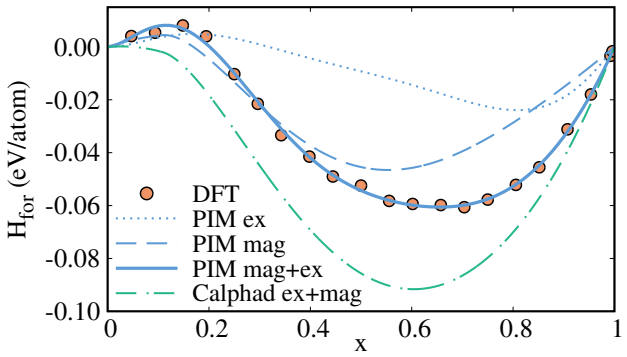

FIG. 4. Formations enthalpies of quasi-random FCC Structures at 0 K: ab initio calculations (DFT) and pair interaction model (PIM, with the excess and magnetic contributions). The formations enthalpy of the γ solid solution of CALPHAD is also shown for comparison.

This fit of pair interactions (using eq. 15) to the CALPHAD model or to the formation enthalpies of SQS, only involves the sum of v_n and can be done with any range n of interac-

TABLE II. The coefficients L_j^{DFT} of the Redlich-Kister polynomial for the excess enthalpy of mixing of the γ solid solution of the PIM (in eV).

L_0^{DFT}	L_1^{DFT}	L_2^{DFT}	L_3^{DFT}	L_4^{DFT}	L_5^{DFT}
-0.03696	0.09631	-0.04722	0.21141	-0.04752	-0.18389

tions. However, it is well known that in FCC ordered structures, the phase diagram and in particular the order-disorder temperatures, depend strongly on the ratio $= v_2/v_1$ [49]. The fit is also independent of the choice of the composition x (local or global) in eq. 18 and 17. Therefore, it does not provide a very accurate description of the interatomic interactions in Fe-Ni alloys.

To get a better description of the thermodynamic properties, the range of interactions and the ratio between the interactions at different distances is fitted to the DFT calculations of the formation enthalpies of the ordered phases (Table I).

With only first nearest neighbors (nn) interactions (Fig. 5(a)), the PIM model underestimates the formation enthalpies of the ordered phases, especially those of the FeNi-$L1_0$ and $FeNi_3$-$L1_2$ phases.

A better result (Fig. 5(b)) is obtained with first and second nn pair interactions, taking a constant ratio $\alpha = v_2/v_1 = -0.7$ (the agreement is very sensitive to the value of α, except in the range $\alpha \in [-0.6, -0.7]$). The formation enthalpies obtained with first and second nn interactions are close to those of the DFT calculations, in particular for the two stable phases FeNi-$L1_0$ and $FeNi_3$-$L1_2$ (Fig. 5). The least well reproduced is that of the iron-rich cI32 phase, which is unstable.

Note that in this fitting procedure, the local composition around a Fe-Ni pair has been defined as the average Ni atomic fraction around the first and second nearest neighbors of the pair, excluding the two atoms which compose it. An atom neighboring the two atoms of the pair is counted twice (so that with 12 first and 6 nearest neighbors, a pair is surrounded by 0 to 34 Ni atoms). Using this definition, the formation enthalpies of the different ordered phases are the functions of v_2 and v_1 given in Table III, together with the values of the local composition x_1 and x_2 around the first and second nn Fe-Ni pairs. Other definitions of the local composition are possible and we have tested some of them (taking into account the two atoms of the pairs, or counting each surrounding Ni atom only once). The definition

chosen here gives a slightly better fit, although the differences are small.

We did not obtain significantly better results by introducing third and fourth nn interactions. In the following we will therefore restrict to the PIM with first and second nn interactions and $\alpha = -0.7$, corresponding to the results shown in Fig. 4 and 5(b).

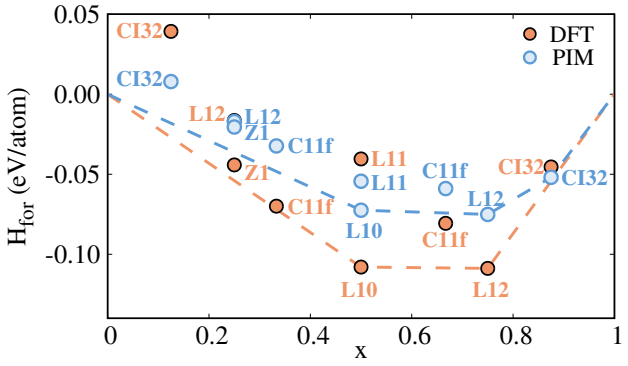

(a)

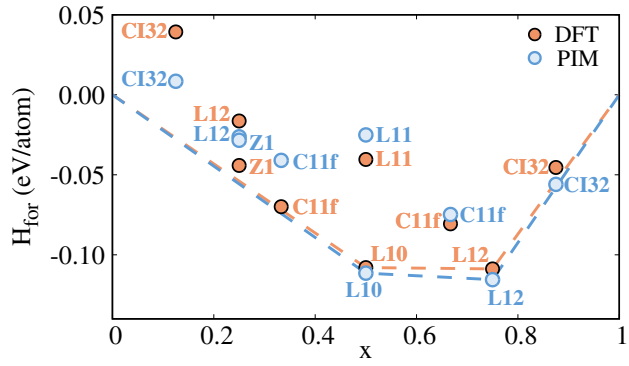

(b)

FIG. 5. Formations enthalpies of FCC ordered phases at 0 K: ab initio calculations (DFT, full circles) and pair interaction model (PIM, open circles) with (a) only first nn interactions, (b) first and second nn interactions, $\alpha = v_2/v_1 = -0.7$

3. Transition between parameters at high and low temperatures

The final PIM will therefore use first and second neighbor pair interactions with a constant $\alpha = v_2/v_1 = -0.7$ ratio:

- At 0 K the variations of v_2 and v_1 with the composition are fitted to the formation enthalpies of SQS and ordered structures calculated by Li and Fu [17] using DFT methods,

TABLE III. Formation enthalpies of FCC ordered phases in a pair interaction model with first and secong nearest neighbor interactions.

Ordered phases	x_1	x_2	H_{for}^{PIM}
Fe_7Ni-cI32	$\frac{1}{34}$	$\frac{5}{34}$	$\frac{3}{2}v_1 + \frac{3}{4}v_2$
Fe_3Ni-$L1_2$	$\frac{9}{34}$	0	$3v_1$
Fe_3Ni-Z1	$\frac{11}{34}$	$\frac{9}{34}$	$2v_1 + \frac{1}{2}v_2$
Fe_2Ni-$C11_f$	$\frac{6}{17}$	$\frac{6}{17}$	$\frac{8}{3}v_1 + \frac{2}{3}v_2$
$FeNi$-$L1_1$	$\frac{1}{2}$	$\frac{1}{2}$	$3v_1 + 3v_2$
$FeNi$-$L1_0$	$\frac{1}{2}$	0	$4v_1$
$FeNi_2$-$C11_f$	$\frac{11}{17}$	$\frac{11}{17}$	$\frac{8}{3}v_1 + \frac{2}{3}v_2$
$FeNi_3$-$L1_2$	$\frac{25}{34}$	1	$3v_1$
$FeNi_7$-cI32	$\frac{33}{34}$	$\frac{29}{34}$	$\frac{3}{2}v_1 + \frac{3}{4}v_2$

as summarized in fig. 5 and 4;

- At high temperatures the variations of v_2 and v_1 with the composition are fitted to the Gibbs free energies of the γ solid solution, from the CALPHAD study of Cacciamani et al. [18];

These two sets of parameters differ only in the non-magnetic part of parameters v_2 and v_1, which is described by Redlich-Kister polynomials having different order and coefficients (respectively L_i^{DFT} and $L_i^{CALPHAD}$). The final parameters are obtained by using coefficients $L_i^{PIM}(T)$ which evolves gradually from one to the other according to:

$$\begin{aligned} L_j^{PIM}(T) = & \exp\left(-\frac{T}{T_j}\right) L_j^{DFT} \\ & + \left[1 - \exp\left(-\frac{T}{T_j}\right)\right] L_j^{CALPHAD}(T) \end{aligned} \tag{19}$$

with $T_j = 400$ K for $j = 0, 1, 2$ and $T_j = 80$ K for $j = 3, 4, 5$. The example of coefficient L_2^{PIM} is given in fig. 6. The temperatures T_j have been chosen so as to give the Gibbs free energy of CALPHAD for $T > 1000$ K, at temperatures where it is derived from numerous and reliable experimental data. The influence of these transition temperatures on the phase diagram will be discussed later.

Let us note finally that the Gibbs free energy of mixing of the solid solution, the formation enthalpies of of SQS or ordered structures and the FCC phase diagram, depend only on the

parameters v_n. We have chosen to take $g^{(n)}_{FeFe}$ and $g^{(n)}_{NiNi}$ interactions independent of the concentration, but dependent on the temperature and adjusted to the free enthalpies of the pure metals (eq. 12). Only the $g^{(n)}_{FeNi}$ interactions are dependent on local concentration. This choice does not affect the results of the present study, but it allows a better description of the properties of point and diffusion defects [9], which we will address in future work. It also makes the Monte Carlo simulations slightly less time consuming.

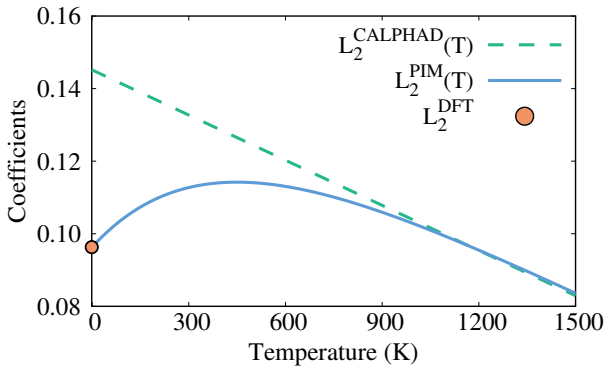

FIG. 6. The evolution of the coefficient $L_2^{PIM}(T)$ with the temperature.

III. MONTE CARLO SIMULATIONS

We will now use Monte Carlo simulations to measure the Gibbs free energies of the PIM (including the configuration entropy) at different compositions and temperatures and build the FCC phase diagram.

A. Semi-grand canonical isotherms

The equilibrium properties of the PIM are determined by Monte Carlo simulations carried out in the semi-grand canonical ensemble. In general, we use a system of $N = 4 \times 16^3$ atoms, with periodic boundary conditions. Exchanges are tried between a randomly chosen atom of the system and an atom taken in a reservoir, with a given difference of chemical potential $\Delta\mu = \mu_{Ni} - \mu_{Fe}$. By changing $\Delta\mu$, one modifies the equilibrium concentration (Fig. 8 and 9). A total of 500 increments for a interval of 1 eV in $\Delta\mu$ are used to go from pure iron to pure nickel, and then 500 increments to go the other way. For each value of $\Delta\mu$, 5×10^6 attempts of atomic exchange (or Monte Carlo steps, MCS) are performed

before measuring the equilibrium composition and order parameters. For building the phase diagram of Fig. 16, a larger system of $N = 4 \times 24^3$ atoms and much smaller increments of $\Delta\mu$ are used, in order to get a better precision (up to 100 increments for a interval of 0.04 in $\Delta\mu$).

To identify the different ordered phases, the FCC lattice is divided into 4 simple cubic sublattices, shifted by a distance $a/2$ in the x, y, z directions [50]. We measure the Ni concentration on each sublattice, and the long range order parameter defined as:

$$\eta = \frac{1}{4} \sum_{i=1}^{4} \left| \frac{x_i}{x} - 1 \right| \tag{20}$$

where x_i is the Ni concentration on the sublattice i. With this definition, $\eta = 1$ in the perfect FeNi-$L1_0$ structure and $\eta = 0.5$ in the perfect $FeNi_3$-$L1_2$ structure.

The short range order is characterized by the Warren-Cowley parameters for the first and second nearest neighbors:

$$\sigma_i = 1 - \frac{f_{Ni}^{(i)}}{x} \tag{21}$$

where $f_{Ni}^{(i)}$ is the average fraction of Ni atoms among the i^{th} nn of the Fe atoms. For a perfect $L1_2$ ordered phase, $\sigma_1 = -0.33$ and $\sigma_2 = +1$.

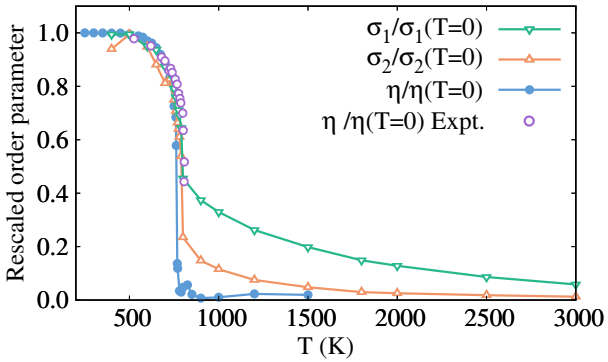

FIG. 7. Evolution the long-range parameter η and of the short-range order parameters σ_1 and σ_2 in $FeNi_3$ as a function of T (Monte Carlo simulations and experiments by Kozlov et al. [51]).

The evolution of the long-range η (eq. 20), and of the short range order parameters σ_1 and σ_2 (eq. 21), in an alloy of composition $FeNi_3$ as a function of the temperature, is shown in Fig. 7. The $L1_2$ ordered phase is found to be stable up to 765 K (instead of 790 K for CALPHAD [18]). The evolution of η is in good agreement with the experiments of Kozlov et al. [51] (which gives a slightly higher ordering temperature: 807 K). The discontinuity at

the order/disorder temperature indicates a first-order transition. A significant short range order remains well above the disordering temperature, especially between the first nearest neighbors.

Two examples of isotherms $x = f(\Delta\mu)$, at $T = 1000$ K and $T = 600$ K are shown in Fig. 8 and 9. At 1000 K, $x(\Delta\mu)$ evolves continuously, with $\eta \simeq 0$: the disordered solid solution is stable in the whole composition range. At 600 K, $\eta \simeq 0.76$ to 0.53 between $\Delta\mu = -0.188$ and -0.068 eV, which corresponds to an over stoichiometric $L1_0$ phase; and $\eta \simeq 0.49$ between $\Delta\mu = -0.05$ and $+0.3$ eV, which corresponds to an almost stoichiometric $L1_2$ phase. Discontinuities and hysteresis on the $x(\Delta\mu)$ curve indicate first order transitions and the limits of two-phase domains.

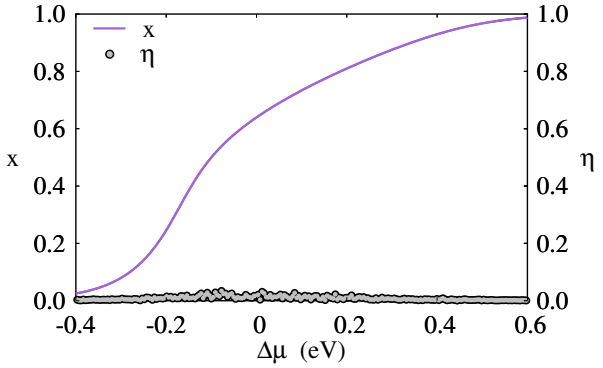

FIG. 8. Monte Carlo simulations: evolution of the Ni concentration x and long-range order parameter η of the PIM for Fe-Ni alloys at 1000 K, as a function of the difference in chemical potentials $\Delta\mu = \mu_{Ni} - \mu_{Fe}$.

B. Gibbs free energy of mixing

Using the definition of chemical potentials: $\mu_i = (\partial G/\partial n_i)_{T,P,n_j}$ and integrating the $\Delta\mu(x)$ curve, we obtain the Gibbs free energy of mixing G_{mix}. The results obtained at different temperatures can be directly compared with the G_{mix} of the CALPHAD study [18]. In each case, one can also compare separately, the enthalpy H_{mix} and entropy S_{mix} of mixing, as well as the magnetic, excess and configuration contributions.

Fig. 10 for example, gives the Gibbs free energy of mixing of the Fe-Ni solid solution at $T = 1500$ K. The PIM is in very good agreement with the CALPHAD study. At this high temperature (well above T_c), the magnetic contribution is negligible. However it is

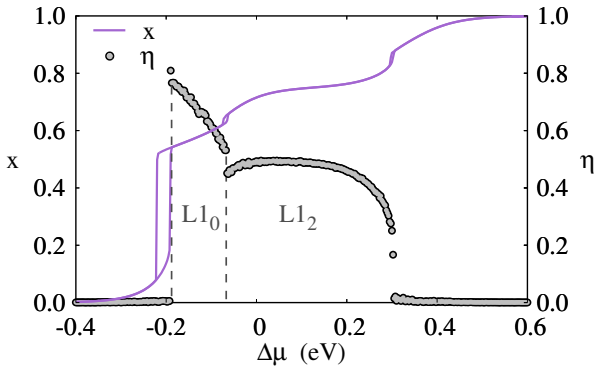

FIG. 9. Monte Carlo simulations: evolution of the Ni concentration x and long-range order parameter η of the PIM for Fe-Ni alloys at 600 K, as a function of the difference in chemical potentials $\Delta\mu = \mu_{Ni} - \mu_{Fe}$.

worth to notice that the excess contribution is slightly lower in the PIM, with a minimum of -0.038 eV at $x = 0.69$ instead of -0.033 eV in CALPHAD. The difference is due to the fact that in the PIM, some short range order remains in the γ solid solution, even at this high temperature (Fig. 7).

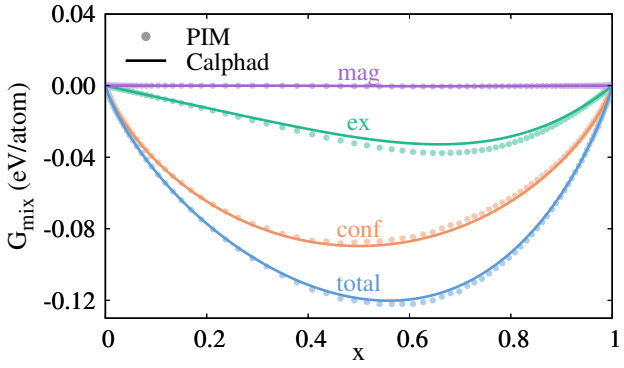

FIG. 10. Gibbs free energy of mixing of the Fe-Ni solid solutions at 1500 K: PIM (dotted lines) vs CALPHAD (full lines), with the separate magnetic, excess and configurational entropic contributions.

The effect is clearer if one separates the enthalpic and entropic contributions of $G_{mix} = H_{mix} - TS_{mix}$. The enthalpy of mixing (Fig. 11) is dominated by the excess term. Due to the remaining short range order ($\sigma_1 = -0.066$ and $\sigma_2 = 0.048$), the PIM gives a minimum of $H_{mix} = -0.054$ eV at $x = 0.67$ instead of -0.047 eV in CALPHAD. This discrepancy on H_{mix} only disappear at very high temperature. At 3000 K (i.e. above the liquidus),

the maximum difference between the PIM and CALPHAD is still $\Delta H_{mix} = 0.0022$ eV (for $\sigma_1 = 0.06$ and $\sigma_2 = 0.013$). It becomes negligible only above 5000 K.

The entropy of mixing of the the PIM (Fig. 12) is dominated by the entropy of configuration, which is very close to the ideal S_{id} of CALPHAD. In the PIM as in CALPHAD, the excess and magnetic contributions to the entropy of mixing are less important, and negative (except below $x \simeq 0.1$). At $x = 0.67$, the discrepancy due to the short range order is only $S_{conf} - S_{id} = 0.15 \times 10^{-5}$ eV/(atom·K), which corresponds to a difference of $T(S_{conf} - S_{id}) = -0.00225$ eV/atom. The difference on S_{mix} partly compensate the one on H_{mix}, which explain the good agreement on G_{mix} between the PIM and CALPHAD, even below 1500 K, when the short range order increases. The G_{mix} of the PIM and CALPHAD are therefore in very good agreement in the whole range of composition and temperature where the γ solid solution is stable (Fig. 13).

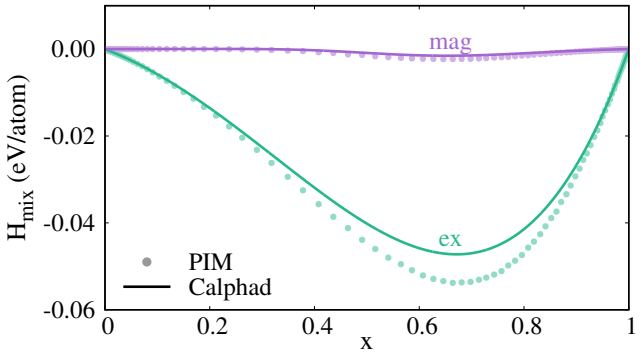

FIG. 11. Enthaply of mixing of the Fe-Ni solid solutions at 1500 K: PIM (dotted lines) vs CALPHAD (full lines), with separate magnetic and excess contributions.

The difference between the Gibbs free energy of mixing of the PIM and CALPHAD [Fig. 14(a)] slightly increases at lower temperatures, when the ordered phase $L1_2$ stabilizes, i.e. when the long-range order parameter η is close to 0.5, between $x \simeq 0.6$ and $x \simeq 0.82$ [Fig. 14(b)]. This is not surprising since the PIM parameters at low temperatures are not fitted on CALPHAD, but on DFT calculations which give a different energetic landscape, especially for the disordered phase (section II C). In spite of this difference, the $G_{mix}(x)$ curve of the PIM is still in good agreement with CALPHAD at $T = 700$ K.

At 650 K, the agreement between the Gibbs free energy of mixing of the PIM and CALPHAD is still quite good for the compositions where the γ solid solution and the $L1_2$ phase

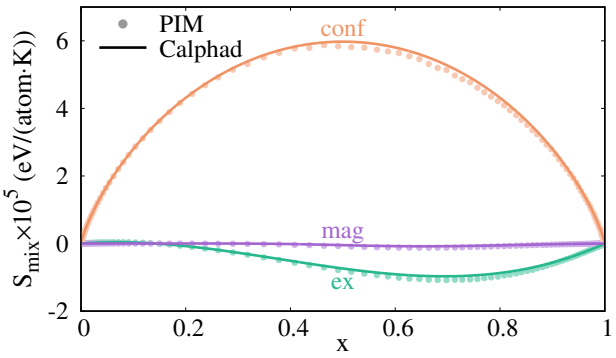

FIG. 12. Entropy of mixing of the Fe-Ni solid solutions at 1500 K: PIM (dotted lines) vs CALPHAD (full lines), with separate magnetic, excess and configurational contributions.

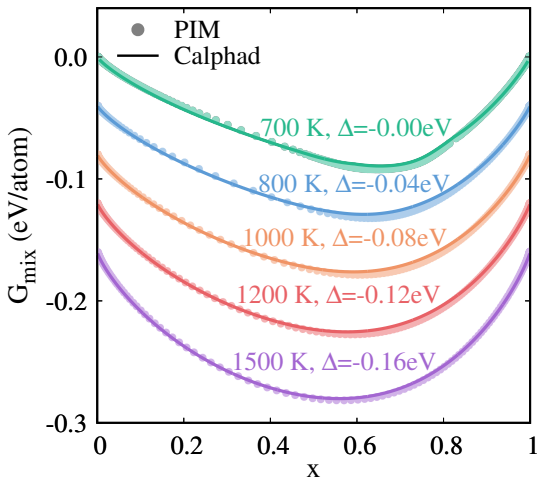

FIG. 13. Gibbs free energy of mixing of the Fe-Ni solid solution of the PIM and CALPHAD [18], at different temperatures. For the sake of clarity, each curve is shifted downwards by a constant Δ given on the figure.

are stable [Fig. 15(a)]. However the evolution of the long-range parameter η as a function of the nickel concentration x now displays two bumps [Fig. 15(b)]. The second one (between $x \simeq 0.63$ and $x \simeq 0.85$) still corresponds to the $L1_2$ phase. The phase is almost perfectly ordered for the stoichiometric composition $FeNi_3$ ($\eta \simeq 0.5$ for $x = 0.75$)). However, the PIM predicts that the FeNi-$L1_0$ phase is stable between $x \simeq 0.52$ and 0.63, while it only appears at lower temperature (below 316 K) according to the CALPHAD model [18]. Note that it is not perfectly ordered ($\eta \simeq 0.6$ instead of 1 for the perfect order), because it is slightly

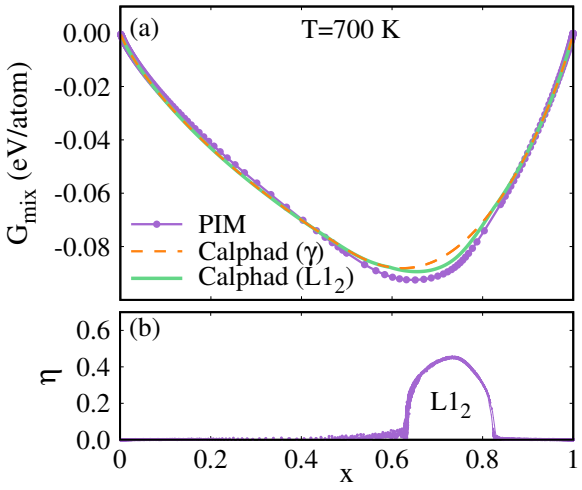

FIG. 14. (a) Gibbs free energy of mixing of Calphad and the PIM and (b) long range order parameter of the PIM, for Fe-Ni alloys at 700 K.

non-stoichiometric ($x > 0.5$) and because 650 K is close to its order disorder-temperature (680 K).

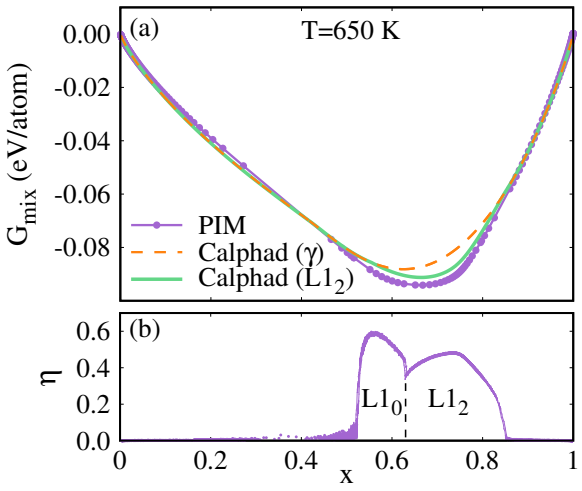

FIG. 15. (a) Gibbs free energy of mixing of Calphad and the PIM and (b) long range order parameter of the PIM, for Fe-Ni alloys at 650 K.

C. FCC phase diagram

The FCC phase diagram of the Fe-Ni system predicted by the PIM is shown in Fig. 16 and compared with experimental data [52–55]. It can be also compared to the FCC diagram

of Cacciamani et al. (Fig. 8 in [18]).

The ordering temperatures of the $FeNi_3$-$L1_2$ phase are slightly different: the PIM gives 765 K, a little lower than 790 K for the CALPHAD study of Cacciamani et al. [18] (which is adjusted to the experimental value). As in CALPHAD, the limits of the two-phase domain $FeNi_3$+γ for $x > 0.75$, are slightly shifted towards lower values ($\Delta x \simeq -0.04$ at 571 K) by comparison with the experiments by Heumann et al. [53]. And as in CALPHAD, the width of the two-phase domain γ+$FeNi_3$ at $x < 0.75$ is smaller than the one of the two-phase domain at $x > 0.75$ (earlier CALPHAD studies predicted a larger two-phase field, as in Fig. 1). Here it should be noted that, except in the vicinity of the ordering temperature at $x = 0.75$, the experimental data for these two-phase fields are going back to 1963 [53] and are only available for one temperature.

The discrepancy is more important for the FeNi-$L1_0$ phase: the PIM predicts an ordering temperature of 680 K instead of 316 K for CALPHAD. The CVM study of Mohri et al. [26] predicts an intermediate ordering temperature (483 K). A direct estimation by DFT calculations (taking into account the vibrational entropy, but not the configurational entropy of the FeNi-$L1_0$ phase) gives 640 K. There is no precise experimental measurement available for the evolution of the degree of order as a function of the temperature (as for the $FeNi_3$ phase, in Fig. 7), but the experimental observations under electron irradiation by Reuter et al. [23] suggest an ordering temperature of approx. 593 K.

As in CALPHAD, the FCC phase diagram of the PIM also displays a two-phase field with an equilibrium between a ferromagnetic (γ_f) and a paramagnetic (γ_p) solid solution, at $x = 0.4$ and below $T = 660$ K. This phase separation has been first predicted by Chuang et al. [56], but it has not been confirmed experimentally. The PIM is able to reproduce this two-phase field because it includes the magnetic contribution of the CALPHAD model. It is however more limited in temperatures than in ref. [18], because of the higher stability of the FeNi-$L1_0$ phase in the PIM, which limits its extension below 680 K.

The phase diagram of the PIM without the magnetic contribution is shown in Fig. 17. As in the study by Cacciamani et al., the non-magnetic phase diagram reduces the critical temperature of $L1_2$ by approx. 118 K and shows no $\gamma_f - \gamma_p$ two-phase field.

Finally, let us recall that the parameters of the PIM and the results of section III have been obtained with parameters fitted to DFT calculations at 0 K, the CALPHAD data of ref. [18] at high temperatures, and a transition between the high and low temperature regimes

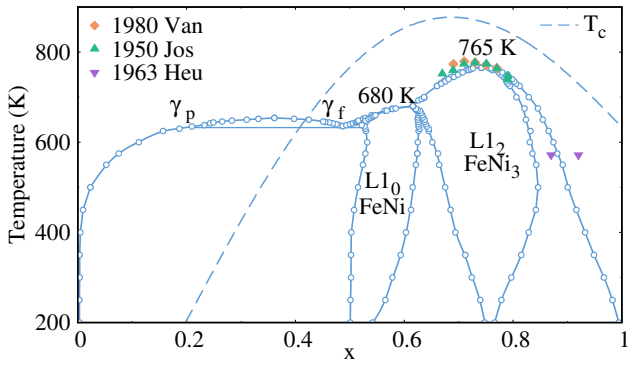

(a)

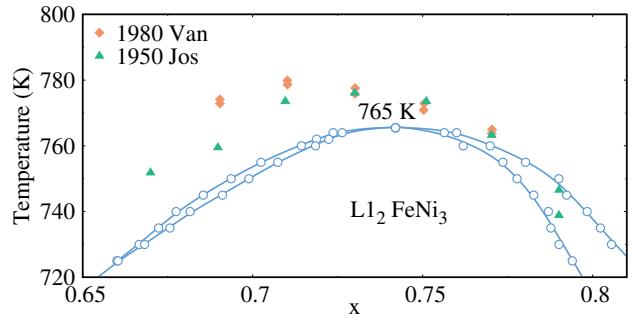

(b)

FIG. 16. (a) The Fe-Ni FCC phase diagram: comparison between the PIM and experiments (1950 Jos = [52], 1963 Heu = [53], 1980 Van = [54, 55]., (b) zoom in the region of the $L1_2$ ordering temperature.

controlled by the exponential interpolation of Eq. 17. With the chosen T_j temperatures, the Redlich-Kister coefficients of the PIM are almost identical to those of CALPHAD above approximately 1000 K. To assess the effect of this choice on the phase diagram, we have performed some simulations with a different set of paramaters: $T_j = 50$ K for $j = 0, 1, 2$ and $T_j = 10$ K for $j = 3, 4, 5$ (using the same notation as in II C 3). With these parameters, the Redlich-Kister coefficients of the PIM becomes almost identical to those of CALPHAD at a lower temperature (approx. 315 K). The resulting phase diagram is shown in Fig. 18. It is not very different from the previous one (Fig. 16(a)), except from a moderate increase of the ordering temperatures of the $L1_0$ and $L1_2$ phases. The reason is that with the new parameters, the ordering tendency is a little more pronounced below 1000 K (Fig. 4). As a consequence, the $\gamma_p - \gamma_f$ two-phase domain almost completely disappears.

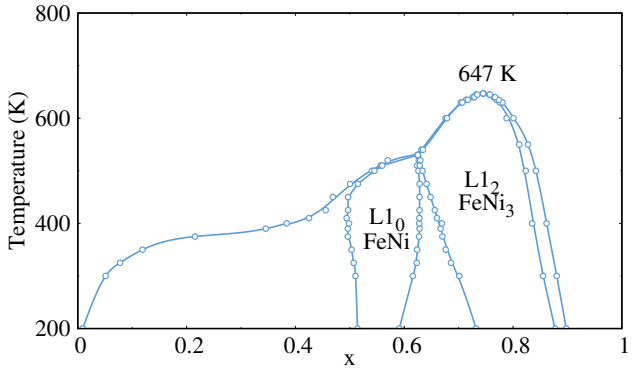

FIG. 17. The Fe-Ni FCC phase diagram of the PIM without magnetic contribution

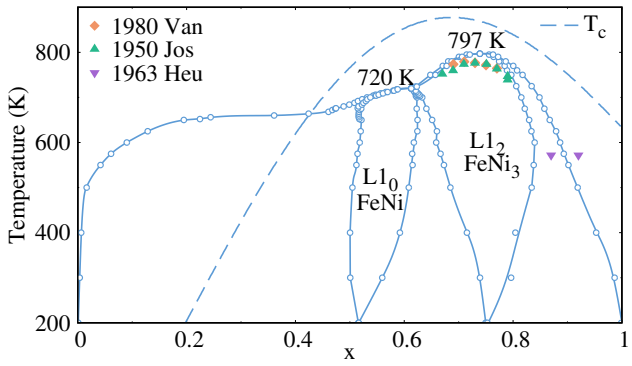

FIG. 18. The Fe-Ni FCC phase diagram of the PIM using a different transition between high and low temperature parameters.

IV. DISCUSSIONS AND CONCLUSIONS

We have presented in this study a method for developing a pair interaction model for Fe-Ni alloys, fitted at 0 K on the enthalpies of formation of ordered and disordered structures (computed by first-principle methods) and at high temperatures on the Gibbs free energy of the γ solid solution (as given by a CALPHAD study and its underlying experimental data).

Thanks to the temperature and concentration dependence of the pair interactions, the PIM is able to reproduce precisely these two types of energetic properties, and to distinguish between excess, magnetic and configurational entropic contributions. The identification between CALPHAD and the PIM is not perfect, because the configurational entropy and short-range order in the solid solution is described more approximately in CALPHAD methods than in the Monte Carlo simulations used to determine the equilibrium properties

of the PIM. The CALPHAD method is more flexible than an atomistic model: the properties of each phase can be adjusted very precisely and independently on the experiments. The PIM imposes some constraints but, combined with Monte Carlo simulations, it ensures a consistent description of the short- and long-range order and of the entropy of configuration.

Despite these differences, the Gibbs free enthalpies of mixing of the γ solid solution, as given by CALPHAD, are very well reproduced by the PIM, throughout the composition and temperature range of stability of the phase. The Gibbs free enthalpy of the $FeNi_3$-$L1_2$ phase is also well reproduce, although the parameters of the PIM and CALPHAD for that phase are not fitted on the same DFT calculations. At high temperatures, the FCC phase diagram involves only these two phases, and both methods give similar results (especially for the order-disorder transition in the vicinity of $FeNi_3$, and for the $\gamma_p - \gamma_f$ phase separation).

On the other hand, both models predict that the FeNi-$L1_0$ phase is stable at low temperature, but with different ordering temperatures. Taking the electron irradiation experiments [23] as a reference, it seems that CALPHAD underestimates the ordering temperature, while the PIM overestimates it. It should be noted here that alloys under irradiation may be not fully at equilibrium, so that no real experimental thermodynamic data are available for this phase; and that both the CALPHAD model and the PIM are only fitted to DFT calculations of enthalpies of formation at 0 K. The PIM and CALPHAD should therefore be both improved to properly describe this phase. One possibility is to use DFT methods to compute finite temperature contributions. These methods are computationally expansive, but can separate each energetic contribution and provide results at intermediate temperature (say, between 0 and 400°C), where experimental results are rarer and perhaps less accurate. An example is given in the study of K. Li and C.-C. Fu [17], which shows that the vibrational entropy decreases the ordering temperatures of the $L1_0$ and $L1_2$ phases by respectively 280 and 200 K.

In spite of this limitation, the PIM model gives a satisfactory description of the γ solid solution and of the $L1_2$ phase. Of course, such a model is necessarily dependent on the CALPHAD data it uses. For the magnetic contribution for example, we rely on the recent study by Cacciamani et al., which is itself based on a large experimental database (with measurements of specific heats, Curie temperatures, magnetic moments, etc. of γ solid solutions with various compositions, described in ref. [18, 57]). For the same reason, our model takes into account, but cannot distinguish between energetic contributions that are

not identified separately in CALPHAD (for example, harmonic and non-harmonic vibrational contributions – which are both gathered in the excess Gibbs free energy, together with the non-ideal part of the configurational entropy). However it could easily be updated to take into account future improvement on that points. It could also be easily extended to Fe-Ni-Cr ternary alloys or to other binary or ternary systems. Finally the PIM is simple enough to be used as a basis for Atomistic Kinetic Monte Carlo methods to simulate the kinetics of homogeneous ordering or of heterogeneous precipitation of the $L1_2$ phase; or to model the interdiffusion properties in the γ solid solution at high temperature. It is indeed not more numerically expensive than the PIM for BCC Fe-Cr alloys described in Ref. [47], which has been used for the simulations of precipitation kinetics [8, 9] or irradiation effects [11, 12]. As in these studies, the modeling of kinetics will require the extension of the PIM to describe the formation and migration properties of point defects.

ACKNOWLEDGMENTS

We thank our colleagues Chu-Chun Fu and Maylise Nastar for many fruitful discussions. The research leading to these results has been carried out in the frame of EERA Joint Program for Nuclear Materials and is partly funded by the European Commission HORIZON 2020 Framework Programme under grant agreement No. 755269. Yimi Wang and Kangming Li are supported by the CEA NUMERICS program, which has received funding from the European Union's Horizon 2020 research and innovation program under the Marie Sklodowska-Curie grant agreement No. 800945.

[1] C. Pareige, F. Soisson, G. Martin, and D. Blavette, Ordering and phase separation in Ni–Cr–Al: Monte carlo simulations vs three-dimensional atom probe, Acta Materialia **47**, 1889 (1999).

[2] E. Clouet, M. Nastar, and C. Sigli, Nucleation of Al_3Zr and Al_3Sc in aluminum alloys: From kinetic monte carlo simulations to classical theory, Phys. Rev. B **69**, 064109 (2004).

[3] E. Vincent, C. Becquart, and C. Domain, Solute interaction with point defects in α-Fe during thermal ageing: A combined ab initio and atomic kinetic Monte Carlo approach, Journal of Nuclear Materials **351**, 88 (2006), proceedings of the Symposium on Microstructural Processes in Irradiated Materials.

[4] M. Y. Lavrentiev, R. Drautz, D. Nguyen-Manh, T. P. C. Klaver, and S. L. Dudarev, Monte Carlo study of thermodynamic properties and clustering in the bcc Fe-Cr system, Phys. Rev. B **75**, 014208 (2007).

[5] F. Soisson and C.-C. Fu, Cu-precipitation kinetics in α-Fe from atomistic simulations: Vacancy-trapping effects and Cu-cluster mobility, Phys. Rev. B **76**, 214102 (2007).

[6] C. S. Becquart and C. Domain, Introducing chemistry in atomistic kinetic Monte Carlo simulations of fe alloys under irradiation, Physica Status Solidi (b) **247**, 9 (2010).

[7] R. Ngayam-Happy, C. Becquart, C. Domain, and L. Malerba, Formation and evolution of MnNi clusters in neutron irradiated dilute fe alloys modelled by a first principle-based AKMC method, Journal of Nuclear Materials **426**, 198 (2012).

[8] E. Martínez, O. Senninger, C.-C. Fu, and F. Soisson, Decomposition kinetics of Fe-Cr solid solutions during thermal aging, Phys. Rev. B **86**, 224109 (2012).

[9] O. Senninger, E. Martínez, F. Soisson, M. Nastar, and Y. Bréchet, Atomistic simulations of the decomposition kinetics in Fe–Cr alloys: Influence of magnetism, Acta Materialia **73**, 97 (2014).

[10] C. Liebscher, V. Radmilović, U. Dahmen, N. Vo, D. Dunand, M. Asta, and G. Ghosh, A hierarchical microstructure due to chemical ordering in the bcc lattice: Early stages of formation in a ferritic Fe–Al–Cr–Ni–Ti alloy, Acta Materialia **92**, 220 (2015).

[11] O. Senninger, F. Soisson, E. Martinez, M. Nastar, C.-C. Fu, and Y. Brechet, Modeling radiation induced segregation in iron-chromium alloys, Acta Materialia **103**, 1 (2016).

[12] F. Soisson, E. Meslin, and O. Tissot, Atomistic modeling of precipitation in fe-cr alloys under charged particles and neutron irradiations: Effects of ballistic mixing and sink densities, Journal of Nuclear Materials **508**, 583 (2018).

[13] C. S. Becquart and F. Soisson, Monte carlo simulations of precipitation under irradiation, in *Handbook of Mechanics of Materials*, edited by S. Schmauder, C.-S. Chen, K. K. Chawla, N. Chawla, W. Chen, and Y. Kagawa (Springer Singapore, Singapore, 2019) pp. 703–731.

[14] I. V. Vernyhora, V. A. Tatarenko, and S. M. Bokoch, Thermodynamics of f.c.c. Ni-Fe Alloys in a Static Applied Magnetic Field, ISRN Thermodynamics **2012**, 1 (2012).

[15] C. Yang, D. Williams, and J. I. Goldstein, A revision of the Fe-Ni phase diagram at low temperatures (< 400°c), Journal of Phase Equilibria **17**, 522 (1996).

[16] Y. Mishin, M. Mehl, and D. Papaconstantopoulos, Phase stability in the Fe–Ni system: In-

vestigation by first-principles calculations and atomistic simulations, Acta Materialia **53**, 4029 (2005).

[17] K. Li and C.-C. Fu, Ground-state properties and lattice-vibration effects of disordered Fe-Ni systems for phase stability predictions, Phys. Rev. Materials **4**, 023606 (2020).

[18] G. Cacciamani, A. Dinsdale, M. Palumbo, and A. Pasturel, The Fe–Ni system: Thermodynamic modelling assisted by atomistic calculations, Intermetallics **18**, 1148 (2010).

[19] I. Ohnuma, S. Shimenouchi, T. Omori, K. Ishida, and R. Kainuma, Experimental determination and thermodynamic evaluation of low-temperature phase equilibria in the Fe–Ni binary system, Calphad **67**, 101677 (2019).

[20] L. J. Swartzendruber, V. P. Itkin, and C. B. Alcock, The Fe-Ni (iron-nickel) system, Journal of Phase Equilibria **12**, 288 (1991).

[21] J. Paulevé, D. Dautreppe, J. Laugier, and L. Néel, Une nouvelle transition ordre-désordre dans Fe-Ni (50-50), J. Phys. Radium **23**, 841 (1962).

[22] A. Chamberod, J. Laugier, and J. Penisson, Electron irradiation effects on iron-nickel invar alloys, Journal of Magnetism and Magnetic Materials **10**, 139 (1979).

[23] K. Reuter, D. B. Williams, and J. Goldstein, Ordering in the Fe-Ni system under electron irradiation, Metallurgical Transactions A **20**, 711 (1989).

[24] K. Reuter, D. B. Williams, and J. Goldstein, Determination of the Fe- Ni phase diagram below 400°C, Metallurgical Transactions A **20**, 719 (1989).

[25] W. Xiong, H. Zhang, L. Vitos, and M. Selleby, Magnetic phase diagram of the Fe–Ni system, Acta Materialia **59**, 521 (2011).

[26] T. Mohri, Y. Chen, and Y. Jufuku, First-principles calculation of $L1_0$-disorder phase equilibria for Fe–Ni system, Calphad **33**, 244 (2009).

[27] P. J. Lawrence and P. L. Rossiter, Chemical and magnetic interactions in FCC Fe-Ni alloys using the cluster variation method, Journal of Physics F: Metal Physics **16**, 543 (1986).

[28] M. B. Taylor, B. L. Gyorffy, and C. J. Walden, Magnetic and compositional order in nickel-rich Ni_cFe_{1-c} alloys, Journal of Physics: Condensed Matter **3**, 1575 (1991).

[29] M.-Z. Dang and D. G. Rancourt, Simultaneous magnetic and chemical order-disorder phenomena in Fe_3Ni, FeNi, and $FeNi_3$, Phys. Rev. B **53**, 2291 (1996).

[30] I. Vernyhora, D. Ledue, R. Patte, and H. Zapolsky, Monte carlo investigation of the correlation between magnetic and chemical ordering in nife alloys, Journal of Magnetism and Magnetic

Materials **322**, 2465 (2010).

[31] M. Taylor and B. Gyorffy, Monte carlo simulations of an fcc Ni_cFe_{1-c} alloy with vector magnetic freedom, Journal of Magnetism and Magnetic Materials **104-107**, 877 (1992), proceedings of the International Conference on Magnetism, Part II.

[32] I. Vernyhora, H. Zapolsky, R. Patte, and D. Ledue, Atomic density function modeling of microstructure evolution in $Ni_{3-x}Fe_x$ alloys, Journal of Magnetism and Magnetic Materials **351**, 52 (2014).

[33] M. Y. Lavrentiev, J. S. Wróbel, D. Nguyen-Manh, and S. L. Dudarev, Magnetic and thermodynamic properties of face-centered cubic fe–ni alloys, Phys. Chem. Chem. Phys. **16**, 16049 (2014).

[34] J. S. Wróbel, D. Nguyen-Manh, M. Y. Lavrentiev, M. Muzyk, and S. L. Dudarev, Phase stability of ternary fcc and bcc Fe-Cr-Ni alloys, Phys. Rev. B **91**, 024108 (2015).

[35] P. E. Blöchl, Projector augmented-wave method, Phys. Rev. B **50**, 17953 (1994).

[36] G. Kresse and D. Joubert, From ultrasoft pseudopotentials to the projector augmented-wave method, Phys. Rev. B **59**, 1758 (1999).

[37] G. Kresse and J. Hafner, Ab initio molecular dynamics for liquid metals, Phys. Rev. B **47**, 558 (1993).

[38] G. Kresse and J. Furthmüller, Efficiency of ab-initio total energy calculations for metals and semiconductors using a plane-wave basis set, Comput. Mater. Sci. **6**, 15 (1996).

[39] G. Kresse and J. Furthmüller, Efficient iterative schemes for ab initio total-energy calculations using a plane-wave basis set, Phys. Rev. B **54**, 11169 (1996).

[40] J. P. Perdew, K. Burke, and M. Ernzerhof, Generalized Gradient Approximation Made Simple, Phys. Rev. Lett. **77**, 3865 (1996).

[41] M. Methfessel and A. T. Paxton, High-precision sampling for Brillouin-zone integration in metals, Phys. Rev. B **40**, 3616 (1989).

[42] H. J. Monkhorst and J. D. Pack, Special points for Brillouin-zone integrations, Phys. Rev. B **13**, 5188 (1976).

[43] A. Zunger, S.-H. Wei, L. G. Ferreira, and J. E. Bernard, Special quasirandom structures, Phys. Rev. Lett. **65**, 353 (1990).

[44] J. M. Cowley, An approximate theory of order in alloys, Phys. Rev. **77**, 669 (1950).

[45] E. Martinez, C. C. Fu, M. Levesque, M. Nastar, and F. Soisson, Simulations of Decomposition

Kinetics of Fe-Cr Solid Solutions during Thermal Aging, Solid State Phenom. **172-174**, 1016 (2011).

[46] M. Sansa, A. Dhouib, F. Ribeiro, B. Legrand, G. Tréglia, and C. Goyhenex, Tight-binding modelling of ferromagnetic metals and alloys, Modelling and Simulation in Materials Science and Engineering **25**, 084004 (2017).

[47] M. Levesque, E. Martínez, C.-C. Fu, M. Nastar, and F. Soisson, Simple concentration-dependent pair interaction model for large-scale simulations of fe-cr alloys, Phys. Rev. B **84**, 184205 (2011).

[48] M. Hillert, in *Phase Equilibria, Phase Diagrams and Phase Transformations: Their Thermodynamic Basis* (Cambridge University Press, 2007) Chap. 22, 2nd ed.

[49] U. Gahn, Ordering in face-centered cubic binary crystals confined to nearest-neighbour interactions—monte carlo calculations, Journal of Physics and Chemistry of Solids **47**, 1153 (1986).

[50] G. Inden, Atomic ordering, in *Phase Transformations in Materials*, edited by G. Kostorz (VCH, 2001) Chap. 8, p. 519.

[51] E. V. Kozlov, A. S. Tailashev, and D. M. Shtern, Order-discharge transition in ni_3fe alloy, Soviet Physics Journal **20**, 583–588 (1977).

[52] E. Josso, Equilibrium Diagram for the Order to Disorder Transformation of Iron-Nickels near Ni_3Fe, C. R. Acad. Sci. **230**, 1467 (1950).

[53] T. Heumann and G. Karsten, Karbonylverfahren und aufdampfverfahren zur bestimmung von phasengleichgewichten im temperaturbereich geringer beweglichkeit am beispiel der eisen-nickel-legierungen, Archiv für das Eisenhüttenwesen **34**, 781 (1963).

[54] Van Deen, J. K. and Van Der Woude, F., Phase diagram of the order-disorder transition in ni3fe, J. Phys. Colloques **41**, C1 (1980).

[55] J. V. deen] and F. V. D. Woude], Phase diagram of the order-disorder transition in ni3fe, Acta Metallurgica **29**, 1255 (1981).

[56] Y. G. Chuang, Y. A. Chang, R. Schmid, and J. C. Lin, Magnetic contributions to the thermodynamic functions of alloys and the phase equilibria of Fe-Ni system below 1200 K, Metallurgical Transactions A **17**, 1361 (1986).

[57] G. Cacciamani, J. De Keyzer, R. Ferro, U. Klotz, J. Lacaze, and P. Wollants, Critical evaluation of the fe–ni, fe–ti and fe–ni–ti alloy systems, Intermetallics **14**, 1312 (2006), eUROMAT 2005

'European Congress on Advanced Materials and Processes'.

Chapter II Diffusion properties in fcc Fe-Ni alloys

II.1 Introduction

There are many experimental studies on diffusion in the Fe-Ni alloys, which have been reviewed by Jönsson in 1994 for fcc alloys (Jönsson 1994) and in 1995 for bcc alloys (Jönsson 1995). Most of them deal with alloys at relatively high temperatures, in paramagnetic (PM) Fe-Ni solid solutions. They include data on self-diffusion coefficients, impurity diffusion coefficients, and tracer and interdiffusion coefficients in the whole concentration range from Fe to Ni. All these results will be reviewed in II.2.2. On the other hand, there are almost no experimental data at low temperatures, in ferromagnetic (FM) solid solutions and in ordered structures. As a result, diffusion coefficients at low temperatures are usually obtained by extrapolations from high temperatures, using Arrhenius expressions.

Available modelling studies will be presented in II.2.3. Recent analytical approaches, combining diffusion models and first principle calculations, are very promising (see e.g. Schuler, Messina, and Nastar 2020; Messina et al. 2014; Ding et al. 2012; Mantina et al. 2008). However, in concentrated metallic alloys, it is still very difficult to build analytical models that accurately predict the point defect concentrations and the correlation factors. It is also difficult to estimate finite temperature effects by *ab initio* methods. Therefore, most recent studies still deal with dilute alloys and low temperatures regimes (e.g. in bcc Fe based alloys, with ferromagnetic states). Assumptions must be made – based e.g. on Ruch's diffusion model (Ruch et al. 1976) – to model the effect of the FM/PM transition (such as in the study Ding et al. 2012, on solute diffusion in α-Fe). From that point of view, fcc Fe-Ni alloys are especially challenging, since they combine chemical and magnetic disorder. As a consequence, only the Fe and Ni diffusion coefficients in pure Ni have been estimated from first principles (Tucker et al. 2010; Toijer et al. 2021).

In the present study, we have chosen an alternative approach, presented in II.3, combining an effective interaction model and atomistic kinetic Monte Carlo (AKMC) simulations. A similar method has been used in previous studies of bcc Fe-Cr alloys (Martínez et al. 2012; Senninger et al. 2014). In this approach, the magnetic moments are not explicitly considered. More complex magnetic interaction models – taking into explicit account the magnetic moments and with parameters fitted to DFT calculations – have been developed very recently at the SRMP by Fu et al. (Schneider et al. 2020; Tran, Fu, and Schneider 2020; Li and Fu 2020). They have been used to model the effects of magnetism on

the diffusion coefficients of bcc Fe-alloys (Schneider et al. 2020) or the thermodynamic and point defect properties of fcc Fe-Ni alloys (Li and Fu 2020; Li, Fu, and Schneider 2021). However, dealing with spins makes them too time consuming to model interdiffusion in concentrated alloys, or the kinetics of phase transformations. As in Chapter I, we will therefore use a simpler approach, which only considers the effects of magnetism (but also of the vibration entropy) on the energetic properties of Fe-Ni alloys, through the composition and temperature dependence of effective pair interactions. When possible however, we will use the information provided by the *ab initio* calculations and the magnetic interaction model developed by Kangming Li for Fe-Ni alloys, for example the work just published by Li (Li, Fu, and Schneider 2021).

To do that, it is necessary to extend the thermodynamic PIM of Chapter I into a kinetic pair interaction model (hereafter referred to as k-PIM). The k-PIM describes the vacancy migration barriers and jump frequencies in fcc Fe-Ni alloys, and the way they depend on the local atomic environments. Self-diffusion and impurity diffusion can then be directly investigated using Le Claire diffusion model (Le Claire 1978) (section II.3.2). However, for the study of diffusion in concentrated alloys, one must also know the evolution of the vacancy concentration with the alloy composition and temperature, including possible short- and long-range ordering effects. No general analytical model exists to estimate this concentration. Previous AKMC methods used for alloys with phase separation tendencies, such as Fe-Cu or Fe-Cr (Soisson and Fu 2007; Nastar and Soisson 2012) do not work well for the ordering case. We therefore propose a new method based on the Widom integration technique (II.3.4). Using this method, the tracer diffusion and interdiffusion coefficients in concentrated Fe-Ni alloys are estimated and compared to experimental data (II.3.5.1). The Darken equation, which relates tracer and interdiffusion coefficients, is tested (II.3.5.2). Last, the effect of the $L1_2$ order-disorder transition on the tracer diffusion coefficients in $FeNi_3$ alloys, which has not yet measured experimentally, is predicted (II.3.5.3).

II.2 Diffusion in Fe-Ni alloys: a bibliography

II.2.1 Diffusion properties in alloys: general results

Diffusion is the transport of matter from one point to another by motion of atoms or molecules. A phenomenological description of the diffusion at the macroscopic scale within a continuous medium is obtained by Fick's equations. The first law of Fick connects the flux of a species to its concentration gradient by:

$$\boldsymbol{J} = -D\boldsymbol{\nabla}C \tag{II-1}$$

where $\boldsymbol{J}$ is the species flux, D is the diffusion coefficient and $C(x, y, z, t)$ is the concentration of the species at position (x, y, z) and at the time t. The equation predicts that the diffusion of a species and its concentration gradient are in opposite directions, revealing that substances have often the tendency to diffuse spontaneously from places of high concentration to where the concentration is lower. As for Fick's second law, it relates the variation of the species concentration over time with the concentration itself by:

$$\frac{\partial C}{\partial t} = \boldsymbol{\nabla} \cdot (D \boldsymbol{\nabla} C) \tag{II-2}$$

If the diffusion coefficient is independent of the concentration, the equation above simplifies to:

$$\frac{\partial C}{\partial t} = D \Delta \mathrm{C} \tag{II-3}$$

where Δ denotes the Laplace operator. By solving the diffusion equation, one gets the variation of the concentrations over time and space. Thus the evolution of the concentration profile will depend on the diffusion coefficient, D.

From an atomistic point of view, one can relate the macroscopic diffusion coefficient D to the jump frequencies ω of the diffusing species, using random walk theories. Einstein's relation states that the diffusion coefficient is related to its mean-square displacement $\langle R^2 \rangle$ during the time t (Mehrer 2007):

$$D = \frac{\langle R^2 \rangle}{6t} \tag{II-4}$$

In the case of a completely random walk, $\langle R^2 \rangle = nd^2$, where n is the number of jumps and d the jump distance. In a fcc lattice, $n = 12\omega t$ and $d = a_0/\sqrt{2}$, and one simply gets: $D = a_0^2 \omega$. However, in real situations, the jump probabilities often depend on the direction of previous jumps. As a result, successive atom jumps are correlated. Therefore, correlation effects must be taken into account, which is one of the main difficulties of diffusion models.

Diffusion occurs through different mechanisms, which vary according to the type of point defects being involved. In Fe-Ni alloys, it is widely accepted that diffusion occurs through the vacancy mechanism. Furthermore, different diffusion coefficients correspond to different situations and will be considered in this study. From the simplest to most complicated, they are respectively the self-diffusion coefficients, the impurity diffusion coefficients, the intrinsic diffusion coefficients. We assign D as the general diffusion coefficient, $D_A^{B^*}$ as the diffusion coefficient of tracer B in matrix A, $D_{AB}^{B^*}$ the tracer diffusion in the alloy A-B and $\widetilde{D}$ the interdiffusion coefficient for a binary system. We will discuss whether these different diffusion coefficients can be analytically calculated by different models.

In general, the temperature dependence of diffusion coefficients is found to be ruled by the Arrhenius formula:

$$D = D_0 \exp\left(-\frac{Q}{k_B T}\right) \tag{II-5}$$

where D_0 denotes the pre-exponential factor and Q is the activation energy of diffusion. These two quantities are assumed to be constant, at least within some temperature range.

II.2.1.2 Self-diffusion

Beginning with the simplest situation of pure A, the self-diffusion coefficient is related to the Gibbs free energy of the formation (G_V^{for}) and migration (G_V^{mig}) of the vacancies as:

$$D_A^{A^*} = f a_0^2 \vartheta^0 \exp\left(-\frac{G_V^{for} + G_V^{mig}}{k_B T}\right) \tag{II-6}$$

where a_0 is the lattice parameter, f is the correlation factor, and ϑ^0 is the attempt frequency.

This equation can be also written as:

$$D_A^{A^*} = f a_0^2 C_V^{eq} \omega \tag{II-7}$$

where $C_V^{eq} = \exp\left(-G_V^{for}/k_B T\right)$ is the equilibrium vacancy concentration and $\omega = \vartheta^0 \exp\left(-G_V^{mig}/k_B T\right)$ is the jump frequency of the vacancy.

Here a correlation factor f is considered. It decreases the diffusion coefficient with respect to its theoretical value in the case of a purely random walk. To better understand its origin, consider the simple case of a vacancy jumps in a fcc lattice. After the exchange of the vacancy with one of its nearest neighboring atom, the vacancy is in a position which permits a reverse jump. The probability of jumping backwards is 1/12. If it occurs, two consecutive jumps are cancelled. Therefore the correlation factor can be estimated to $f \approx 1 - 2/12 = 0.833$. Cancellations may occur after several jumps (the probability decreases rapidly), so the exact value for the self-diffusion in the fcc structure is $f = 0.7815$ (Mehrer 2007).

Since the Gibbs free energy can be separated into two parts, the enthalpy and the entropy, according to $G = H - TS$, equation (II-6) can be set as the same form as equation (II-5), with:

$$D_0 = f a_0^2 \vartheta^0 \exp\left(\frac{S_V^{for} + S_V^{mig}}{k_B}\right) \text{ and } Q = H_V^{for} + H_V^{mig} \tag{II-8}$$

II.2.1.3 Diffusion in dilute alloys

Another situation of interest is the diffusion of a solute B in a dilute solvent A. According to Le Claire, one solution is considered to be dilute when (a) all solute atoms are present as isolated atoms or as small grouping of atoms (pairs, triplets etc.), and (b) each isolated atom or group of atoms can diffuse independently (Le Claire 1978). For expressing such diffusion coefficients, there are two other factors to be introduced: the binding energy between solute-vacancy G_{B-V}^{bin} (in the following we will use the convention $G_{B-V}^{bin} > 0$ for an attraction between a solute B and a vacancy V) and the migration barrier for the solute-vacancy exchange $G_{2,V}^{mig}$. Considering the diffusion of a tracer B* into a pure metal A, we have:

$$D_A^{B^*} = f_2 a_0^2 \vartheta_2^0 \exp\left(-\frac{G_V^{for} - G_{S-V}^{bin}}{k_B T}\right) \exp\left(-\frac{G_{2,V}^{mig}}{k_B T}\right) \quad \text{(II-9)}$$

where f_2 is the correlation factor, which is usually calculated via the five-frequency model by Le Claire (Le Claire 1978), a_0 is the lattice constant of the solvent and ϑ_2^0 is the attempt frequency of the solute in the solvent. The index 2 denotes the diffusion of the solute in a dilute solution. The model is valid when the interactions are limited to the first nearest interactions. In fcc alloys, five jump frequencies are then to be considered (Figure II.1):

ω_2: solute-vacancy exchange rate

ω_1: rotation rate of the solute-vacancy pair

ω_3: dissociation rate of the solute-vacancy pair

ω_4: association rate of the solute-vacancy pair

ω: vacancy-atom exchange rate in the solvent

They are related to their corresponding migration barrier G_i^{mig} by:

$$\omega_i = \vartheta_i^0 \exp\left(-\frac{G_i^{mig}}{k_B T}\right) = \vartheta_i^0 \exp\left(\frac{S_i^{mig}}{k_B}\right) \exp\left(-\frac{H_i^{mig}}{k_B T}\right) \quad \text{(II-10)}$$

with ϑ_i^0 the attempt frequency. The impurity diffusion coefficient can be calculated as a function of these five frequencies:

$$D_A^{B^*} = f_2 a_0^2 \omega_2 \exp\left(-\frac{G_V^{for}}{k_B T}\right) \frac{\omega_4}{\omega_3} \quad \text{(II-11)}$$

An exact expression for f_2 was derived by Manning:

$$f_2 = \frac{\omega_1 + 7F_3\omega_1/2}{\omega_2 + \omega_1 + 7F_3\omega_1/2} \quad \text{(II-12)}$$

with F_3 a function of the ratio $\alpha = \omega_4/\omega$ (Manning and Bruner 1968).

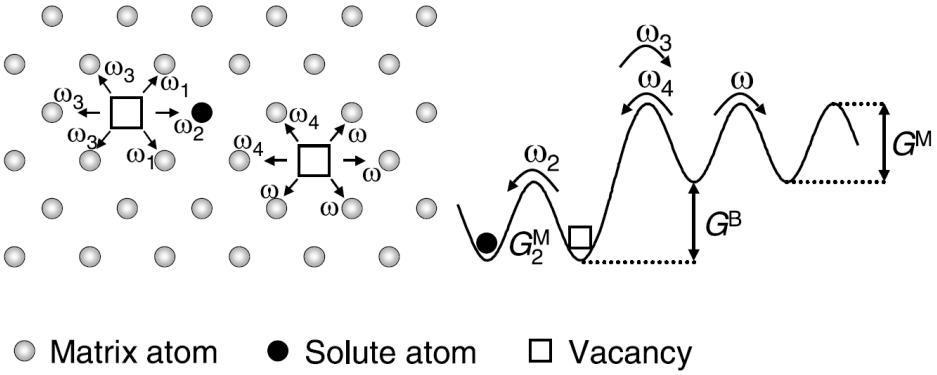

Figure II.1. Left: Five-frequency model for the diffusion of impurities in dilute fcc alloys. Right: Energy landscape for vacancy jumps in the neighborhood of a solute atom (Mehrer 2007)

The association and dissociation rates are related to the binding Gibbs free energy (G_{S-V}^{bin}) of the vacancy and the solute:

$$\frac{\omega_4}{\omega_3} = \exp\left(\frac{G_{B-V}^{bin}}{k_B T}\right) \tag{II-13}$$

Therefore $\omega_4/\omega_3 > 1$ corresponds to $G_{S-V}^{bin} > 0$ i.e. to attractive interactions between the solute and the vacancy. On the other hand, if vacancy-solute exchanges occur much faster than vacancy-solvent exchanges, i.e. for $\omega_2 \gg \omega_1, \omega_3, \ldots$, then we have $f_2 \ll 1$. The movement of the solute atom is then highly correlated.

For more concentrated, but still dilute alloys (with B atomic fraction limited to a few percent), other analytical models exit. The tracer diffusion coefficients A and B can be expressed as:

$$D_{AB}^{A^*}(x_B) = D_A^{A^*}[1 + b_1 x_B + \cdots] \tag{II-14}$$

and:

$$D_{AB}^{B^*}(x_B) = D_B^{B^*}[1 + B_1 x_B + \cdots] \tag{II-15}$$

where the coefficients b_1 and B_1 are respectively the factors revealing the change in the jump rates of those atoms A and B influenced by the solute (Mehrer 2007).

The factor b_1 is sometimes called the linear enhancement factor of solvent diffusion and has attracted particular interest. Taking into account its relation of jump rates in the neighborhood of the solute, the following expression of b_1 has been proposed by Howard and Manning (Howard and Manning 1967):

$$b_1 = -18 + \frac{\omega_4}{\omega}\left[4\frac{\chi_1}{f}\frac{\omega_1}{\omega_3} + 14\frac{\chi_2}{f}\right] \quad \text{(II-16)}$$

where f is the self-diffusion correlation factor, all the jump frequencies ω are those defined in the five-frequency model (Figure II.1), and the quantities χ_1 and χ_2 are the partial correlation factors given in the article of Howard and Manning (Howard and Manning 1967).

Let us point out that these results are valid within the framework of the five-frequency model, i.e. in fcc alloys with solute-vacancy interactions limited to the first-nearest neighbors. If vacancy-atom interactions between further sites are considered, more complicated models are proposed to calculate the correlation factor. For example, Manning calculated the correlation factor of impurity diffusion taking into account the association or the dissociation of the vacancy jump towards its second-nearest neighbor (Manning 1964). Very recently, the KineClue code has been developed by Schuler *et al*. (Schuler, Messina, and Nastar 2020) to account for long-range interactions and for the cases of concentrated alloys.

In general, even in more complicated multiple frequency models, the correlation factor can be still written as the form of (Allnatt and Lidiard 1993):

$$f_2 = \frac{H}{2\omega_s + H} \quad \text{(II-17)}$$

where ω_s is the jump frequency of the solute and the quantity H is independent of the solute jump frequency.

II.2.1.4 Diffusion in concentrated alloys

The interdiffusion of A and B atoms in a binary alloy is characterized by the interdiffusion coefficient, $\widetilde{D}$. The interdiffusion coefficient is concentration-dependent and can be expressed in Fick's second law. In one dimension, in the *x*-direction:

$$\frac{\partial C}{\partial t} = \frac{\partial}{\partial x}\left[\widetilde{D}(C)\frac{\partial C}{\partial x}\right] \quad \text{(II-18)}$$

where C is the concentration of component B.

The interdiffusion coefficient can be measured experimentally by the Boltzmann-Matano method. The principle is the following: a binary diffusion couple consisting of two semi-infinite bars is joined at time $t = 0$, with different concentrations at the two sides of the interface. During a diffusion annealing over a time t, a concentration profile $C(x)$ develops. The interdiffusion coefficient $\widetilde{D}$ for each composition C can be directly calculated from one profile $C(x)$ (Matano 1933).

The interdiffusion involves the diffusion of both atom A and atom B. In general they have different intrinsic diffusion coefficients, which are denoted as D_A^{Intr} and D_B^{Intr} respectively. These diffusion coefficients can be related to the concentration gradient by the Fick's law:

$$J_A = -D_A^{Intr}\frac{\partial C_A}{\partial x}, \qquad J_B = -D_B^{Intr}\frac{\partial C_B}{\partial x} \tag{II-19}$$

The intrinsic and interdiffusion coefficients are defined in different reference frames. The intrinsic diffusion coefficients are defined for a flux in the reference of the local crystalline lattice, while the interdiffusion coefficients are defined in the reference of the laboratory.

Diffusion models in concentrated alloys are more rigorously developed within the framework of the thermodynamics of irreversible phenomena (TIP), using Onsager transport equations:

$$\boldsymbol{J} = \sum_{j=1}^{n} L_{ij}\boldsymbol{X_J} \tag{II-20}$$

with $\boldsymbol{J}$ the flux, $\boldsymbol{L}$ the matrix of transport coefficients L_{ij} and $\boldsymbol{X_J}$ the driving forces causing to the flux $\boldsymbol{J}$. For investigating the diffusion phenomenon, they deal with the real driving forces: the gradient of chemical potentials, namely $\boldsymbol{X_J} = -\nabla\mu_i$. If we consider the diffusion in a binary A-B system by vacancy diffusion, we have:

$$\begin{aligned} J_A &= L_{AA}X_A + L_{AB}X_B + L_{AV}X_V \\ J_B &= L_{AB}X_A + L_{BB}X_B + L_{BV}X_V \\ J_V &= L_{AV}X_A + L_{BV}X_B + L_{VV}X_V \end{aligned} \tag{II-21}$$

(here we have used the symmetry of the matrix $\boldsymbol{L}$, using, what is known as Onsager reciprocity theorem). If we assume that the vacancies are always maintained at their equilibrium concentration, namely $X_V = 0$, the flux becomes $J_A = L_{AA}X_A + L_{AB}X_B$ and $J_B = L_{AB}X_A + L_{BB}X_B$. For a real solid solution, the chemical potential can be written as:

$$\mu_i = \mu_i^0 + k_B T ln(x_i\gamma_i) \tag{II-22}$$

where x_i is the atomistic fraction of the element i and γ_i the activity coefficient. Thus we have:

$$\begin{aligned} J_A &= -\left(\frac{L_{AA}}{x_A} - \frac{L_{AB}}{x_B}\right)k_B T\left(1 + \frac{\partial \ln\gamma_A}{\partial \ln x_A}\right)\frac{dx_A}{dx} \\ J_B &= -\left(\frac{L_{BB}}{x_B} - \frac{L_{AB}}{x_A}\right)k_B T\left(1 + \frac{\partial \ln\gamma_B}{\partial \ln x_B}\right)\frac{dx_B}{dx} \end{aligned} \tag{II-23}$$

The Gibbs-Duhem relation imposes: $1+\frac{\partial \ln \gamma_A}{\partial \ln x_A}=1+\frac{\partial \ln \gamma_B}{\partial \ln x_B}$. This quantity is referred to as the thermodynamic factor Φ. We can notice that equation (II-23) has the form of Fick's law, with:

$$D_A^{Intr}=-\frac{L_{AA}}{x_A}\left(1-\frac{L_{AB}x_A}{L_{AA}x_B}\right)k_BT\Phi$$
$$D_B^{Intr}=-\frac{L_{BB}}{x_B}\left(1-\frac{L_{AB}x_B}{L_{BB}x_A}\right)k_BT\Phi \quad \text{(II-24)}$$

where D_A^{Intr} and D_B^{Intr} are the intrinsic diffusion coefficients of A and B, respectively.

In general, the interdiffusion coefficient $\widetilde{D}$ can be related to the intrinsic diffusion coefficients by:

$$\widetilde{D}=\left(x_AD_B^{Intr}+x_BD_A^{Intr}\right) \quad \text{(II-25)}$$

If the off-diagonal terms of the matrix $\boldsymbol{L}$ are negligible, by relating the intrinsic and tracer diffusion coefficients of a component by the thermodynamic factor, $\widetilde{D}$ can be expressed as:

$$\widetilde{D}=\left(x_AD_{AB}^{B^*}+x_BD_{AB}^{A^*}\right)\Phi \quad \text{(II-26)}$$

where $D_{AB}^{B^*}$ and $D_{AB}^{A^*}$ are the tracer diffusion coefficients of B and A in the alloy respectively. Equation (II-26) is called the Darken equation. We see that the interdiffusion coefficient will tend towards the self-diffusion coefficient $D_A^{A^*}$ if x tends towards 0, and the impurity diffusion coefficient $D_A^{B^*}$ if x tends towards 1.

The Darken equation is obtained under the assumption that the concentration of vacancies is in thermal equilibrium during the interdiffusion process. But vacancy sources and sinks exist so that a vacancy flux is created to maintain a local equilibrium. A correction term must be added against this so-called vacancy-wind effect. Manning and Brunner proposed to correct this effect by adding a factor S and then we have the Darken-Manning equation as (Manning and Bruner 1968):

$$\widetilde{D}=\left(x_AD_{AB}^{B^*}+x_BD_{AB}^{A^*}\right)\Phi S=\widetilde{D}S \quad \text{(II-27)}$$

with $S=\frac{C_AD_{AB}^{B^*}r_B+C_BD_{AB}^{A^*}r_A}{C_AD_{AB}^{B^*}+C_BD_{AB}^{A^*}}$, where r_A and r_B are vacancy-wind factors (Manning and Bruner 1968). Another important approximation used to get the Darken equation is that the non-diagonal terms L_{ij} of the Onsager matrix are negligible.

In concentrated alloys, if the Darken equation is not verified, then by supposing that the vacancy concentration is at equilibrium, these non-diagonal terms L_{ij} of the Onsager matrix can be measured.

II.2.2 Diffusion properties in FeNi alloys: experimental results

There are several experimental measurements of self-diffusion and impurity diffusion coefficients in pure Fe and Ni. Different methods have been also used to get some information on the formation and migration properties of point defects. They include the classical Differential Dilatometry (DD), rapid quenching, Positron Annihilation Spectroscopy (PAS) and electric resistivity measurements. We will first present those experimental results for self-diffusion in fcc Ni and fcc Fe systems respectively.

II.2.2.1 Self-diffusion in fcc Fe and fcc Ni

- *Pure Ni*

Pure fcc nickel undergoes a transition from a ferromagnetic to a paramagnetic state above the Curie temperature $T_{Curie}^{Ni} = 633$ K (Dinsdale 1991). Several measurements of $D_{Ni}^{Ni^*}$ have been carried out, only in paramagnetic Ni. They are summarized in Table II.1 and Figure II.2. One observes an almost perfect Arrhenius behavior over about 10 orders of magnitudes. Slightly different values of D_0 and Q have been proposed to fit the results with the Arrhenius law (Table II.1). In his review, Ehrhart proposes $D_{Ni}^{Ni^*} = 0.92 \times 10^{-4}\exp(-2.88/k_BT)$ (Ehrhart 1991). Our k-PIM correspond to $D_{Ni}^{Ni^*} = 0.696 \times 10^{-4}\exp(-2.83/k_BT)$ m^2s^{-1} (see section II.3.3.4). Both give practically the same values of $D_{Ni}^{Ni^*}$. The k-PIM estimation is shown in advance, for comparison, in Figure II.2.

Table II.1. Experimentally measured self-diffusion coefficients in fcc Ni

$D_0(10^{-4}m^2s^{-1})$	Q(eV)	T range (K)	Method	Reference
1.77	2.955	1253 K-1673 K	radioisotope ^{63}Ni with electron analysis	(Bakker 1968)
1.33	2.91	879 K-1193 K	Ion-beam sputtering as micro-sectioning	(Maier et al. 1976)
1.9	2.95	1315 K-1677 K	lathe sectioning technique	(Monma 1964)
1.9	2.90	773 K-923 K	radioactive counting of the surface	(Wazzan 1965)
0.4	2.77	1373 K-1448 K	lathe sectioning technique	(Reynolds, Averbach, and Cohen 1957)
3.44	3.0	1258 K-1578 K	radioisotope ^{59}Fe and ^{63}Ni with electron analysis	(Million et al. 1981)

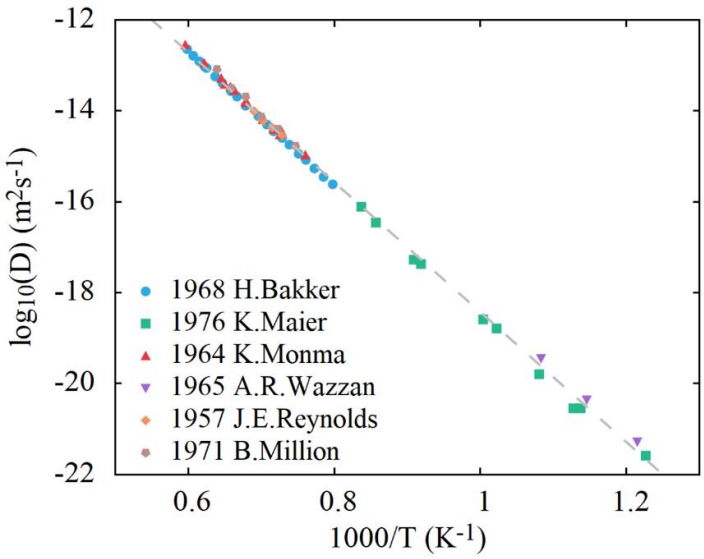

Figure II.2. Self-diffusion coefficient in fcc Ni: experiments are represented by points and the dashed line gives the values of our k-PIM : $0.696 \times 10^{-4} exp(-2.83/k_B T)\ m^2 s^{-1}$ *(see section II.3.3.4)*

The vacancy formation enthalpy $H_{Ni,V}^{for}$ (Table II.2) and migration enthalpy $H_{Ni,V}^{mig}$ (Table II.3) have been measured independently and reviewed by Ehrhart who recommends the values $H_{Ni,V}^{for} = 1.79 \pm 0.05$ eV and $H_{Ni,V}^{mig} = 1.04 \pm 0.04$ eV (Ehrhart 1991). The formation enthalpies were mostly obtained by positron annihilation spectroscopy and the migration enthalpies by electrical resistivity recovery after irradiation, quenching or cold work. These two values give $Q = H_{Ni,V}^{for} + H_{Ni,V}^{mig} = 2.83$ eV, in good agreement with the measurements of diffusion coefficients (Table II.1), which confirms that diffusion in Ni operates by a mono-vacancy mechanism.

It is interesting to note that diffusion coefficients and the formation enthalpy have been measured in paramagnetic Ni, but that the migration enthalpy have been measured by resistivity recovery in ferromagnetic Ni (the peak of the corresponding stage III is located at $T \sim 400$ K). The fact that the relation $Q = H_{Ni,V}^{for} + H_{Ni,V}^{mig}$ is fulfilled therefore suggests that in pure Ni, the magnetic transition has little influence on the vacancy migration enthalpy.

Table II.2. Experimental measurements of the vacancy formation enthalpy in fcc Ni (Ehrhart 1991)

$H_{Ni,V}^{for}$ (eV)	Method	Reference*
1.60	Quenching	69M2
1.45-1.73	PAS	77C1
1.65-1.74	PAS	77N1
1.6-1.8	PAS	77D1
1.58-1.63	Quenching	76W
1.55	PAS	79M1
1.76	PAS	79M2
1.54	PAS	80L1
1.8	PAS	81S3
1.79$\pm$0.05	Recommended value	Ehrhart

*the full references can be found in (Ehrhart 1991)

Table II.3. Experimental measurements of the vacancy migration enthalpy in fcc Ni (Ehrhart 1991)

$H_{Ni,V}^{mig}$ (eV)	Method	Reference*
1.05	Irradiation, cold work	59 S1
1.03	Irradiation	65 M
1.1$\pm$0.01	Cold work	66 M
1.3-1.9	Quenching	78 W 3
1.2	TEM	78 k1
1.1	Irradiation	78 A
1.04	irradiation	81 K 2
1.04$\pm$0.04	Recommended value	Ehrhart

* the full references can be found in (Ehrhart 1991)

- *Pure Fe*

Pure iron has two different crystal structures: bcc (α-Fe below 1183 K and δ-Fe above 1653 K) and fcc (γ-Fe). γ-Fe is stable between 1183 K and 1653 K and is always paramagnetic. Several experimental measurements of the self-diffusion coefficients are available for fcc Fe. A summary of the results is shown in Table II.4 and Figure II.3. An Arrhenius behavior is observed, over 3-4 orders of magnitude, much less than in pure Ni, due to the limited range of temperature for γ-Fe. The estimations of D_0 and Q (Table II.4) are therefore less precise. Our k-PIM gives $0.549 \times 10^{-4}\exp(-2.94/k_BT)$ $\mathrm{m^2 s^{-1}}$ (see section II.3.3.4).

Table II.4. Experimentally measured self-diffusion coefficients in fcc Fe

$D_0(10^{-5}m^2s^{-1})$	Q(eV)	T range (K)	Method	Reference
1.8	2.797	973 K-1711 K	Fe electroplated absorption	(Buffington, Hirano, and Cohen 1961)
4.9	2.943	1443 K-1634 K	tracer-sectioning technique	(Heumann and Imm 1968)
0.2	2.78	1429 K-1622 K	tracer-sectioning technique	(Graham and Tomlin 1963)
5.8	3.2	1243 K-1630 K	radioisotope ^{59}Fe with electron analysis	(Birchenall and Mehl 1950)
0.41	2.91	1373 K-1523 K	tracer-sectioning technique	(Fillion and Calais 1977)
7.21	2.89	1258 K-1578 K	radioisotope ^{59}Fe and ^{63}Ni with electron analysis	(Million et al. 1981)

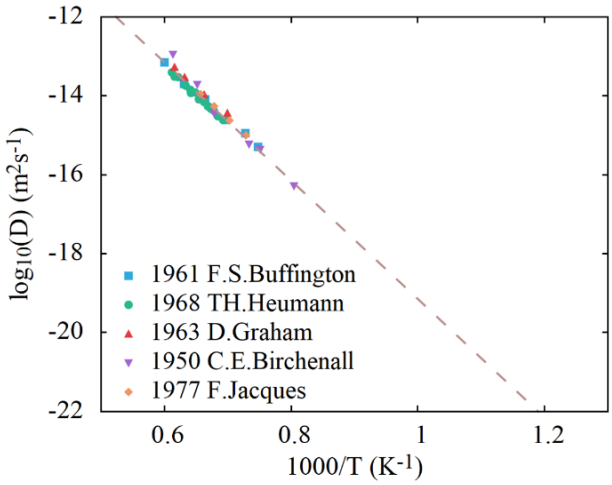

Figure II.3. Self-diffusion coefficient in fcc Fe: experiments are represented by points and the dashed line gives the values of the k-PIM : $0.594 \times 10^{-4} exp(-2.94/k_B T)\ m^2 s^{-1}$ *(see section II.3.3.4)*

For the properties of the vacancies, there are less experimental data than for the pure fcc Ni system. There are a few measurements of the vacancy formation enthalpies by PAS (Table II.5), but to our knowledge, no independent measurements of the vacancy migration enthalpy. Heumann and Imm deduced a value of $H_{Fe,V}^{mig} = 1.54$ eV from $H_{Fe,V}^{mig} = Q - H_{Fe,V}^{for}$ (Heumann and Imm 1968).

Table II.5. Experimental vacancy formation and migration enthalpy of fcc Fe

Method	$H_{Fe,V}^{for}$ (eV)	$H_{Fe,V}^{mig}$ (eV)	Condition	Reference
positron annihilation	1.7 ± 0.2		293 K-1593K	(Kim and Buyers 1978)
Positron annihilation	1.4 ± 0.15	1.54 ± 0.15 *	1183 K-1663 K	(Matter, Winter, and Triftshäuser 1979)

* deduced from the experimental activation energy Q (Heumann and Imm 1968)

II.2.2.2 Impurity diffusion in fcc Fe and fcc Ni

The experimental measurements for the impurity diffusion coefficients of Ni in fcc Fe, D_{Fe}^{Ni*} and of Fe in fcc Ni, D_{Ni}^{Fe*} have been reviewed by Jönsson (Jönsson 1994) and are shown in Figure II.4 and Figure II.5 respectively.

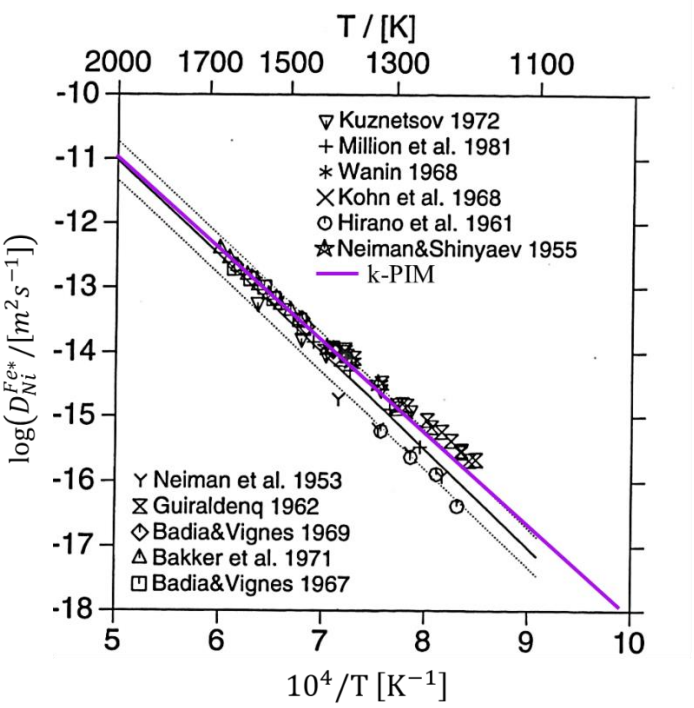

Figure II.4. Impurity diffusion coefficients of Fe in fcc Ni, the black line corresponds to the assessment of Jönsson (Jönsson 1994), the purple line gives the value of our k-PIM: $1.44 \times 10^{-4} exp(-2.84/k_B T)\ m^2 s^{-1}$ *(see section II.3.3.5) and the points are different experimental studies*

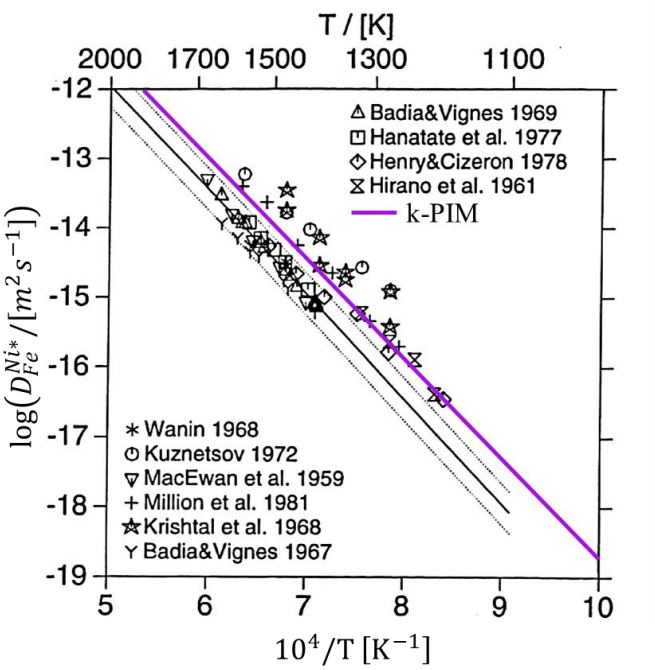

Figure II.5. Impurity diffusion coefficients of Ni in fcc Fe, the black line corresponds to the assessment of Jönsson (Jönsson 1994), the purple line gives the value of our k-PIM: $0.53 \times 10^{-4} exp(-2.88/k_B T)\ m^2 s^{-1}$ *(see section II.3.3.5) and the points are different experimental studies*

From Figure II.4 and Figure II.5 we see that the dispersion of impurity diffusion coefficients is larger than that of self-diffusion coefficients. The impurity diffusion coefficients of Ni in Fe (D_{Fe}^{Ni*}) are more scattered than that of Fe in Ni (D_{Ni}^{Fe*}). Jönsson suggests to exclude the extreme values and to keep only those between the dotted lines of Figure II.4 and Figure II.5. It is important to note that the values of Million *et al.* for D_{Fe}^{Ni*} are larger than the average ones (by approximately a factor 3, see Figure II.5): these values are part of a systematic study on diffusion in Fe-Ni solid solutions (Million et al. 1981) which will be discussed in detail later.

In Figure II.6, we compare the impurity and self-diffusion coefficients in Fe and in Ni. In pure iron, the solute and the solvent diffuse approximately at the same rate ($D_{Fe}^{Ni*} \sim D_{Fe}^{Fe*}$), but it is difficult to conclude due to the dispersion of the data. In pure nickel: according to most studies, $D_{Ni}^{Fe*} > D_{Ni}^{Ni*}$, the solute diffuses slightly faster than the solvent, at least at $T > 1200$ K. There are no data for D_{Ni}^{Fe*} at lower temperatures.

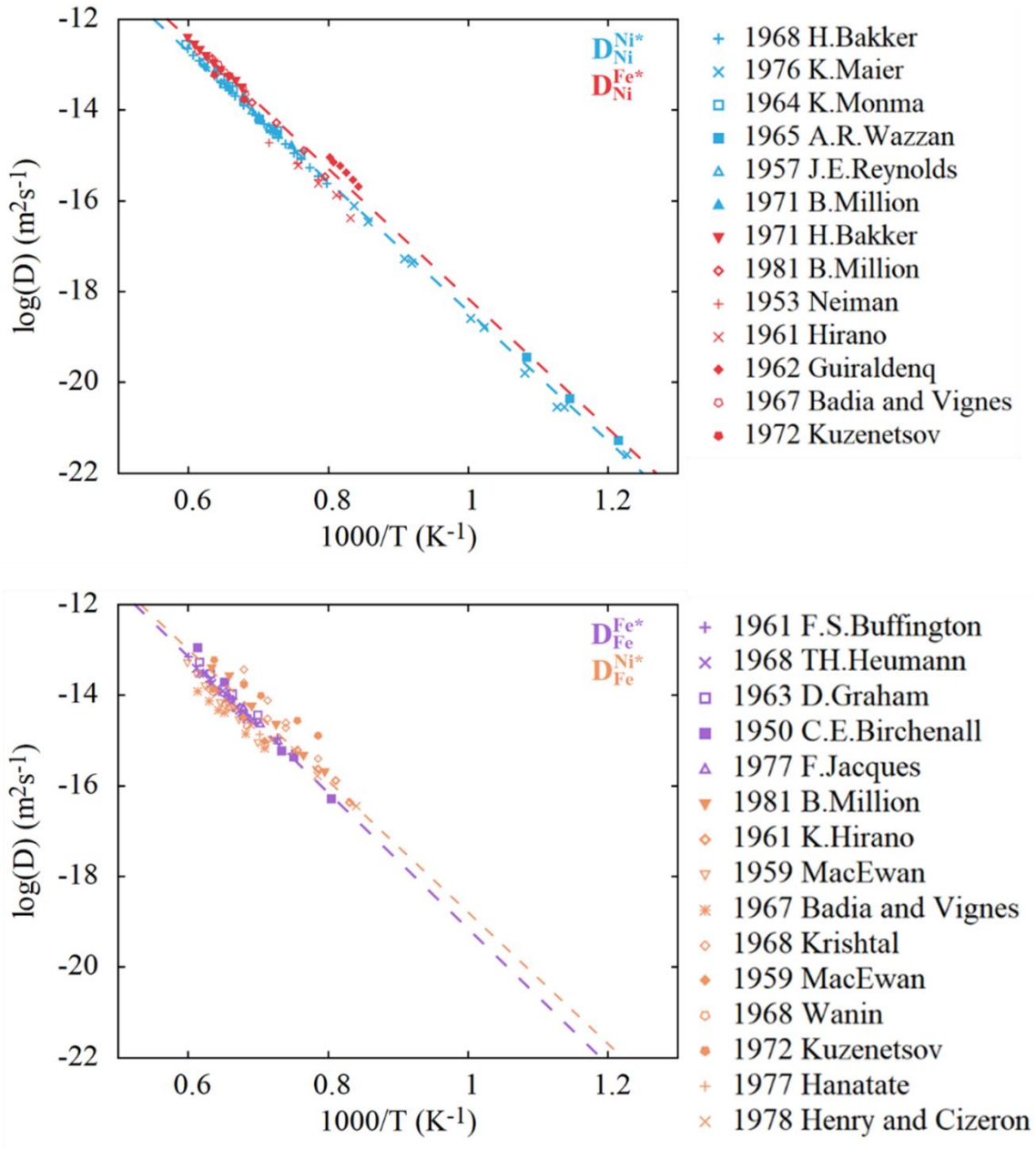

Figure II.6. Self-diffusion and impurity diffusion coefficients in fcc Ni (top) and Fe (bottom): experiments are represented by points and the dashed lines correspond to the k-PIM.

II.2.2.3 Diffusion in concentrated Fe-Ni alloys

- *Tracer diffusion coefficients*

Million *et al*. have measured the Fe and Ni tracer diffusion coefficients in Fe-Ni solid solutions, D_{FeNi}^{Fe*} and D_{FeNi}^{Ni*}, in the whole range of compositions and at different temperatures (Million et al. 1981). Their results are shown in Figure II.7 and compared with previous studies (Okada 1966; MacEwan, MacEwan, and Yaffe 1959; Hancock and Leak 1967; Zemskii, L'vov, and Makashova 1976; De Reca and Pampillo 1967). The "Million mean values" are the average values in pure Fe and Ni, calculated

with other data obtained by Million *et al.* in previous studies (Růžičková and Million 1981; Million and Kučera 1971).

The experimental data are very scattered, except those of Million which show a linear variation of the tracer diffusion coefficients of Fe and Ni as a function of concentration. The difference between pure Fe and pure Ni is limited: D_{FeNi}^{Fe*} and D_{FeNi}^{Ni*} increase by a factor of 3~5 between $x_{Ni} = 0$ and $x_{Ni} = 1$.

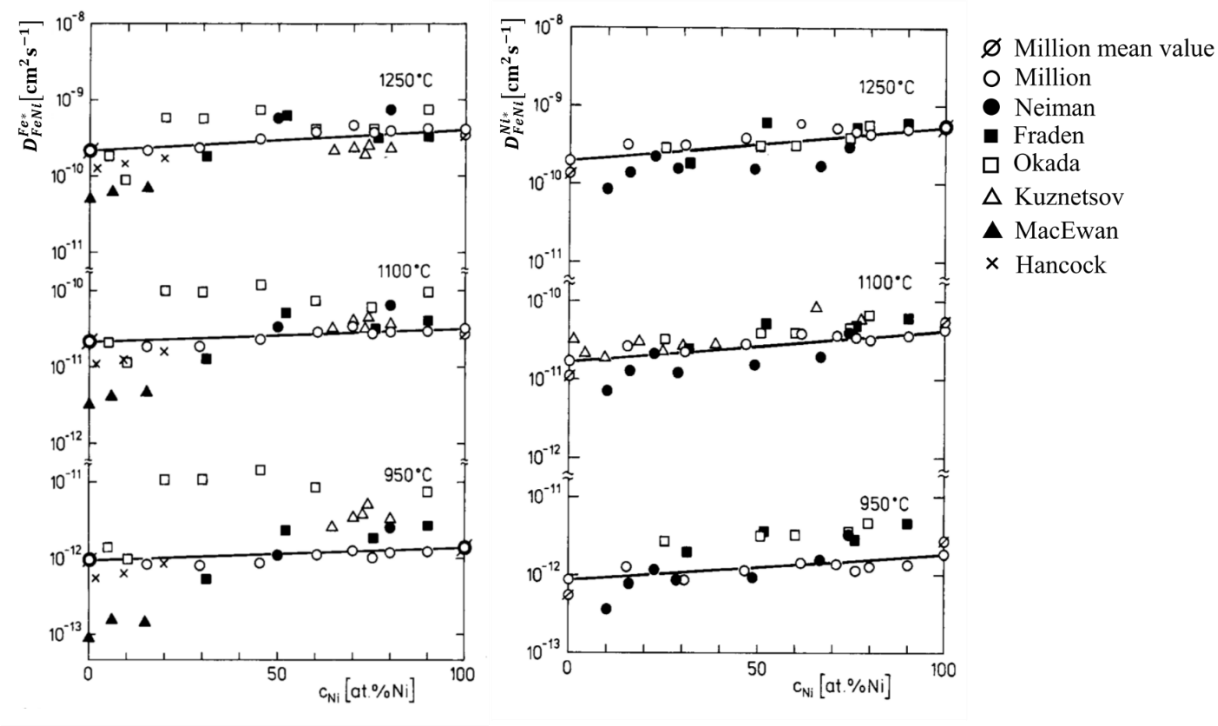

Figure II.7. Concentration dependence of the tracer diffusion coefficients in Fe-Ni solid solutions (Million et al. 1981): left: Fe tracer ; right: Ni tracer.

Jönsson has collected the tracer diffusion coefficients of Fe and Ni in alloys from the different experimental studies and proposed an interpolation function for their concentration and temperature dependence (Jönsson 1994). The result is shown in Figure II.8.

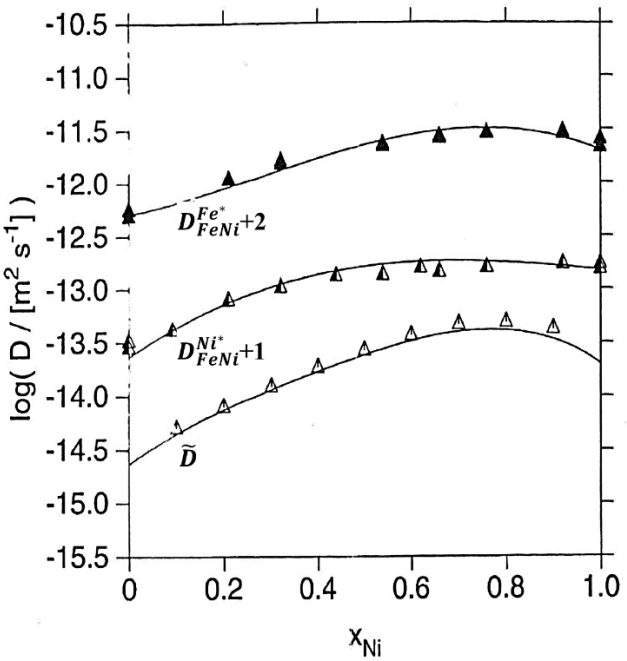

Figure II.8. Comparison of the tracer diffusion coefficients $D^{Fe^*}_{FeNi}$, $D^{Ni^*}_{FeNi}$ and the interdiffusion coefficients $\widetilde{D}$ at 1200 °C (Jönsson 1994)

There are some minor differences between these data. Compared to the linear dependence of the tracer diffusion coefficients with the Ni concentration, observed by Million et al. (Figure II.7), Jönsson's interpolation presents a significant curvature (Figure II.8), because it includes the more scattered data of other authors, and because it is fitted on accepted values in pure metals. On Figure II.7, the limit of at $x_{Ni} = 0$ and $x_{Ni} = 1$, correspond to the self and impurity diffusion coefficients of Million *et al.* and are compared to those of other authors (Figure II.9). Their values of $D^{Ni^*}_{Fe}$ are slightly larger than most of the other ones (as already seen in Figure II.5), and a similar difference is observed for their values of the self-diffusion coefficients in iron, $D^{Fe^*}_{Fe}$. Their values of $D^{Ni^*}_{Ni}$ and $D^{Fe^*}_{Ni}$ are close to those of other studies. To summarize, the values of Million *et al*. are less scattered than other ones, but they seem to overestimate the diffusion coefficients in pure Fe. These differences remain within a factor 2 or 3, which corresponds to the standard uncertainty for diffusion experiments.

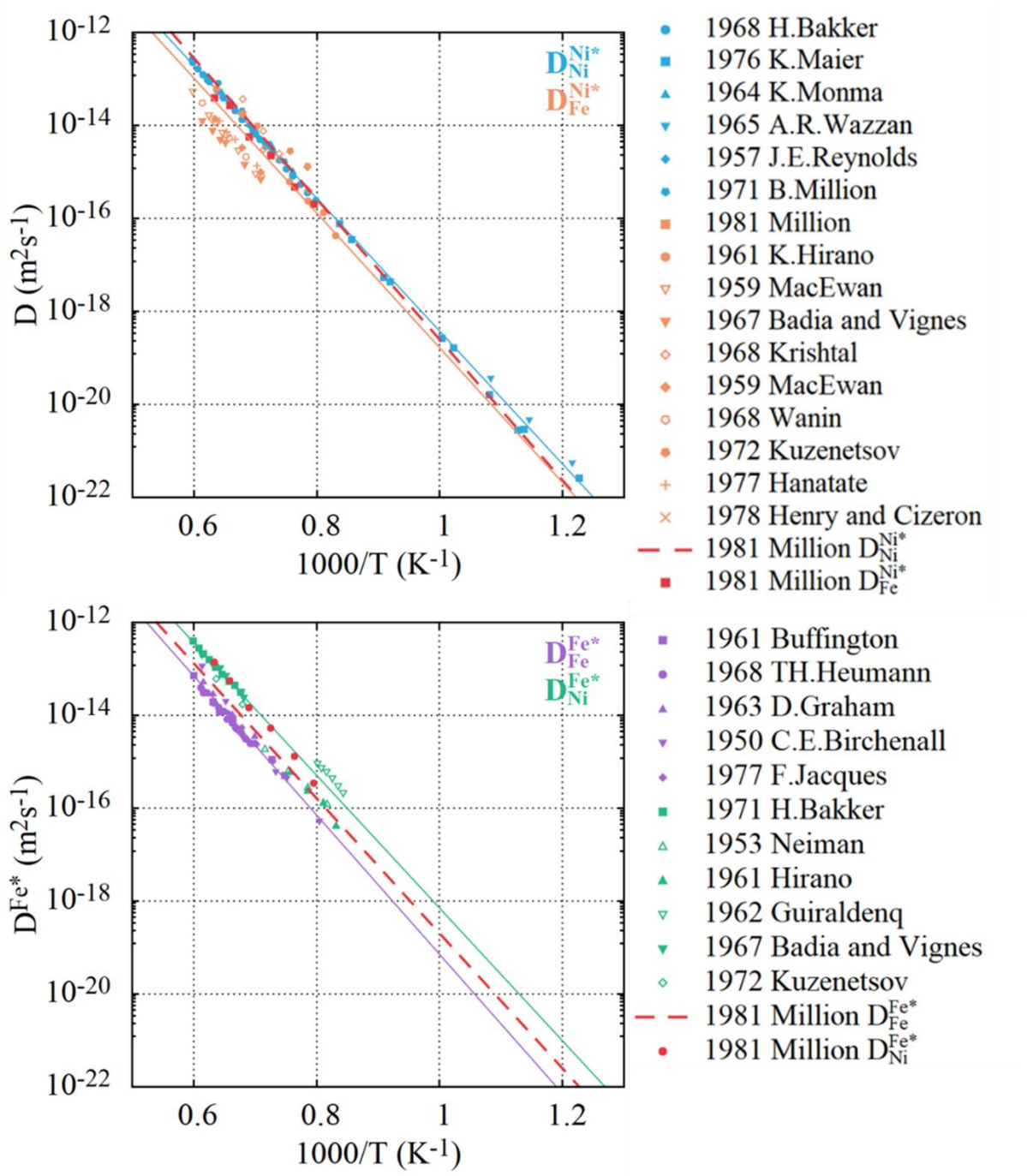

Figure II.9. Comparison of self and impurity diffusion coefficients of Million et al and other experimental studies (solid lines are the values of k-PIM). Top : Ni, bottom : Fe.

- *Interdiffusion coefficients*

Interdiffusion in Fe-Ni alloys has been measured in several studies (Million et al. 1981; Liu and Barmak 2015; Ganesan, Seetharaman, and Raghunathan 1984). Ganesan *et al*. found that between 1173 K and 1373 K, $\widetilde{D}$ in Fe-Ni alloys increases with the iron concentration up to 30 wt% Fe, and thereafter decreases (Ganesan, Seetharaman, and Raghunathan 1984), which is in agreement with the results of Million *et al.* (Million et al. 1981). Later, Jönsson did a review work for the diffusion in Fe-Ni alloys. In his review, Jönsson (Jönsson 1994) proposed a fitting function for the interdiffusion coefficients

dependence on temperature and concentration of based on different experiments, as shown in Figure II.10.

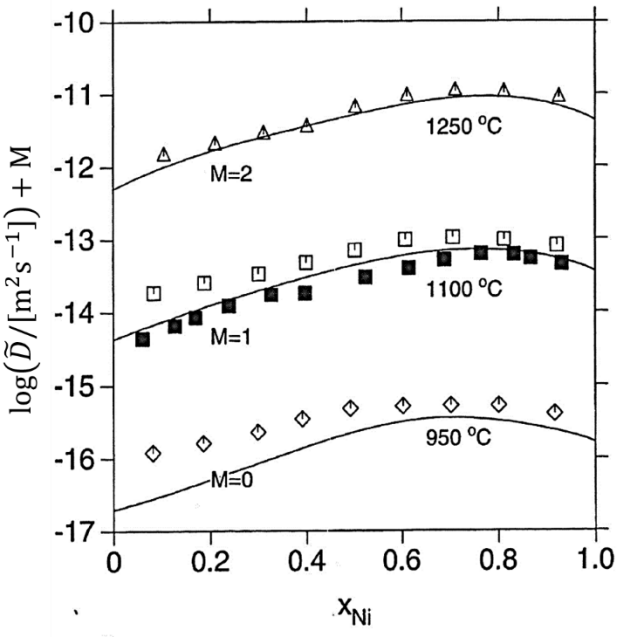

Figure II.10. Interdiffusion coefficient $\widetilde{D}$ of Jönsson (Jönsson 1994): different experiments collected are represented by points and the lines are the fitting functions of Jönsson.

- *Test of the Darken equation*

Million *et al*. tested the Darken equation (II-26) by comparing their measurements of tracer and interdiffusion coefficients at different compositions. According to the Darken equation, in FeNi solid solutions, $\widetilde{D} = \left(x_{Fe}D_{FeNi}^{Ni*} + x_{Ni}D_{FeNi}^{Fe^*}\right)\Phi$, with Φ the thermodynamic factor. The "calculated values" (□ in Figure II.11) are obtained with this equation, their experimental values of $D_{FeNi}^{Fe^*}$ and D_{FeNi}^{Ni*} (the same as in Figure II.7) and an estimation of the thermodynamic factor (see Figure 4 in Million et al. 1981). Compared to experimental values of $\widetilde{D}$ (○ in Figure II.11), the calculated values are in general higher. According to the author however, this discrepancy could be explained by the effects of grain boundaries and lattice defects on the diffusion processes, which are difficult to avoid in experiments, rather than to the assumptions underlying the Darken equation.

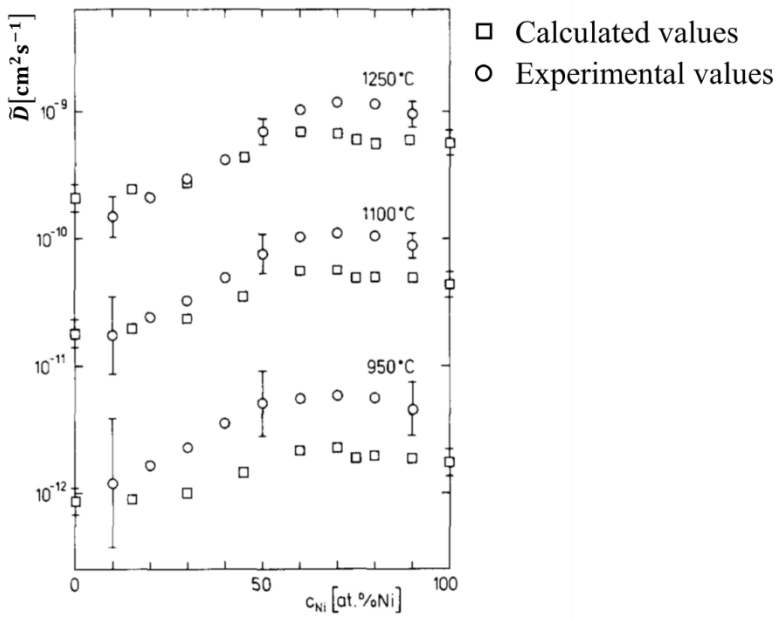

Figure II.11: Concentration dependence of the interdiffusion coefficients in Fe-Ni solid solutions at different temperatures. ○: experimental values; □: values calculated from self-diffusion and the Darken equation (Million et al. 1981)

- *Point defects properties*

Besides measurements of diffusion coefficients, there are few experimental data on the properties of vacancies in binary Fe-Ni alloys. Chambron and Caplain did some experiments after quenching from temperature between 600 °C and 700 °C in a Fe-Ni system containing 70% of Ni (Chambron and Caplain 1974). Both vacancy formation and migration enthalpies were measured by analysis of induced magnetic anisotropy. The values obtained are: $H_V^{for} = 1.57 \pm 0.03$ eV and $H_V^{mig} = 1.10 \pm 0.02$ eV. The activation enthalpy was measured independently as well. With a value of $Q = 2.72 \pm 0.02$ eV, the authors concluded that the relation $Q = H_V^{for} + H_V^{mig}$ is verified within the allowable range of experimental error. With the same method of vacancy quenching, Caplain and Chambron investigated the vacancy formation enthalpy in the FeNi system in a composition range of $x_{Ni} = 0.5$ to $x_{Ni} = 0.94$ (Caplain and Chambron 1977). They found that the vacancy formation enthalpy does not depend on the composition and obtained a value of $H_V^{for} = 1.80 \pm 0.03$ eV. No difference for the vacancy formation enthalpy was observed between paramagnetic and ferromagnetic states.

II.2.2.4 Possible effects of chemical and magnetism ordering on the diffusion coefficients

All the experiments mentioned above (except when pointed out directly) were done at high temperatures, in paramagnetic solid solutions. To our knowledge, there are no experimental data for the diffusion in ordered phases and in ferromagnetic fcc FeNi alloys. However, it is well known that for some metals and alloys, the effect of magnetic and chemical ordering on diffusion cannot be neglected.

Such effect would affect the kinetics of ordering, e.g. in $FeNi_3$ alloys, where diffusion occurs in a ferromagnetic $L1_2$ ordered structure.

Let us take the case of self-diffusion in bcc Fe to explain the effects that could be expected (Figure II.12). Bcc α-Fe is paramagnetic above and ferromagnetic below the Curie temperature, $T_c = 1043$ K. The self-diffusion coefficient is a continuous function around T=1043 K. However, there is a significant curvature just below the Curie temperature. Extrapolating the Arrhenius behavior of the paramagnetic phase at low temperature (indicated by the red dashed line on Figure II.12) would lead to a significant overestimation of the diffusion coefficient (by e.g. two orders of magnitude at 800 K). The simplest model which describes this is a modified Arrhenius equation proposed by Ruch *et al.*:

$$D^* = D^0_{para} \exp\left[-\frac{\Delta H_{para}(1+\alpha M^2)}{k_B T}\right] \tag{II-28}$$

where ΔH_{para} and D^0_{para} are the activation enthalpy and the exponential factor for the paramagnetic state, M is the ferromagnetic order parameter and α is a fitting coefficient (Ruch et al. 1976).

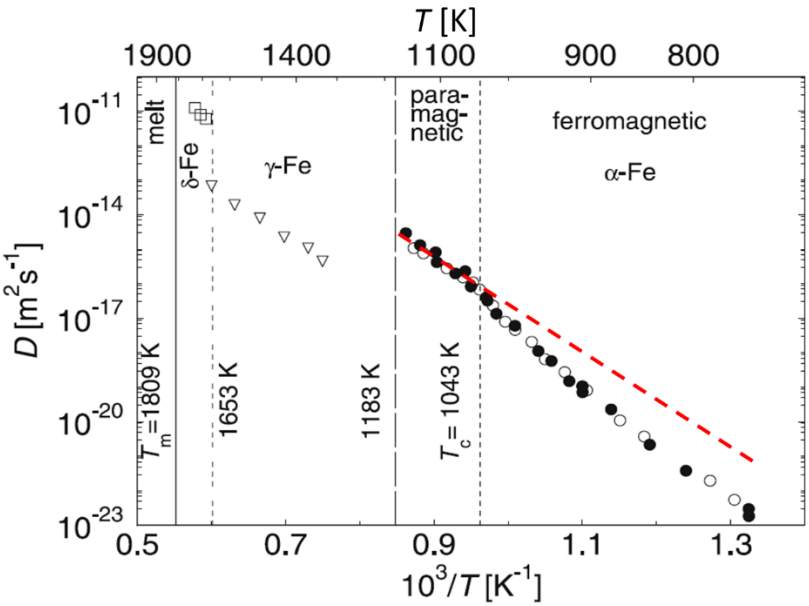

Figure II.12. Experimental self-diffusion coefficients in α-, γ- and δ-Fe (Mehrer 2007). The dashed line shows the extrapolation of the diffusion coefficient in paramagnetic iron (Iijima, Kimura, and Hirano 1988) at low temperatures.

A similar effect is often observed in chemical order-disorder transitions, e.g. in the Cu-Zn system, which undergoes an A2/B2 transition below 468°C (Figure II.13). In that case, the deviation of the diffusion coefficient from the Arrhenius behavior can also be described by (Girifalco 1964):

$$D^* = D^0_{dis} \exp\left[-\frac{\Delta H_{dis}(1+\alpha S^2)}{k_B T}\right] \tag{II-29}$$

where ΔH_{dis} and D^0_{dis} are the activation enthalpy and the exponential factor for the disordered phases and *S* is the long range order parameter.

In the following, we will try to determine if similar effects occur in Fe-Ni alloys.

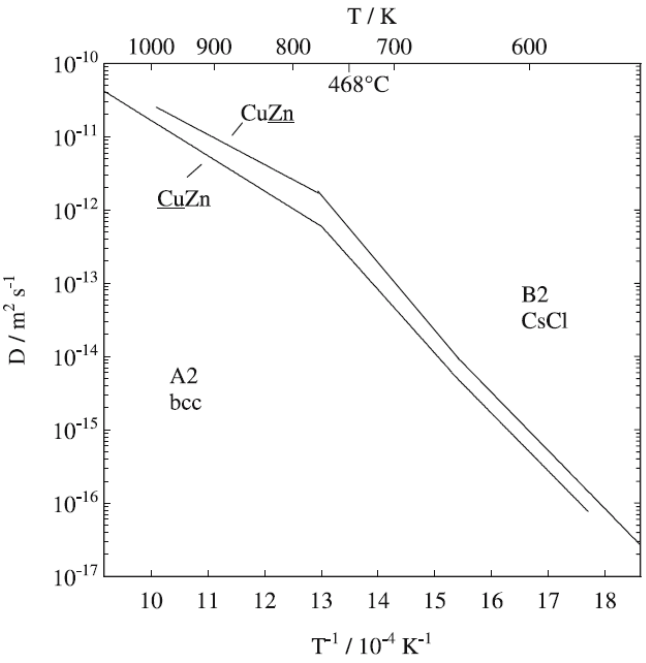

Figure II.13. Tracer diffusion coefficients of ^{65}Cu and ^{65}Zn in CuZn (Mehrer 2007)

II.2.3 Point defect and diffusion properties in FeNi alloys: theoretical results

In addition to the experimental results, *ab initio* calculations have recently provided some insight on point defects properties and diffusion in pure fcc iron and nickel, or dilute alloys. In concentrated alloys, only a few calculations or simulations, based on empirical potentials, are available. These methods have the advantage over experiments that they may deal with systems out of the experimental conditions, for example at very low temperatures, where the Fe-Ni alloys are ferromagnetic and sometimes ordered. On the other hand, the calculation from first principles of diffusion coefficients at high temperature, in ferromagnetic materials, is very challenging, because it has to deal with magnetic disorder. Nevertheless, DFT calculations can provide some information on the effect of the magnetic configuration on vacancy properties. In fcc Ni, there are DFT calculations in the non-magnetic (NM) and ferromagnetic (FM) states. In fcc Fe, there are DFT calculations in the NM but no calculation in the FM state as many FM states are unstable mechanically: other magnetic anti-ferromagnetic structures have been considered.

II.2.3.2 Self-diffusion in fcc Fe and fcc Ni

From section II.2, equation (II-6) and (II-8), self-diffusion coefficients in pure metals depends on the Gibbs formation and migration energies of vacancies, respectively G_V^{for} and G_V^{mig}. The activation energy can be written as $Q = H_V^{for} + H_V^{mig}$ and the pre-exponential factor as $D_0 = a^2 \upsilon_0 f \exp\left[\left(S_V^{for} + S_V^{mig}\right)/k_B\right]$.

- *Pure Nickel*

DFT calculations have been carried out to determine the self-diffusion coefficient as well as the vacancy formation and migration enthalpies in pure fcc Ni. Calculations for both non-magnetic and ferromagnetic state exist. The results and the calculation conditions are summarized in Table II.6 and Table II.7. We also give the results obtained with an EAM potential by Ortega, which include an estimation of the migration entropy that we will use later.

Table II.6. Vacancy formation/migration enthalpy/entropy in fcc Ni

$H_{Ni,V}^{for}$(eV)	$H_{Ni,V}^{mig}$(eV)	$S_{Ni,V}^{for}(k_B)$	$S_{Ni,V}^{mig}(k_B)$	Method	Reference
1.63-1.73	1.01-1.15			Ab-initio LDA NM	(Hargather et al. 2014)[1]
1.70-1.87	1.14-1.15			Ab-initio LDA FM	(Hargather et al. 2014)[1]
1.65	1.09	1.82		Ab-initio GGA FM	(Tucker et al. 2010)[2]
1.4	1.05	1.83		Ab-initio GGA FM	(Toijer et al. 2021)[3]
1.56	0.97		1.58	Classical MD	(Garcia Ortega, Ramos de Debiaggi, and Monti 2002)[4]

1: Ecut=350 eV; supercell=2×2×2=32 atoms; k-point=9^3; convergence condition: 0.01 eV.
2: Ecut=270 eV; supercell=3×3×3=108 atoms; k-point=3^3; convergence condition: 35 meV.
3: Ecut=350 eV; supercell=4×4×4=256 atoms; k-point=3^3; convergence condition: 20 meV/Å in force convergence
4: EAM potential by Voter and Chen (Voter and Chen 1986).

Table II.7. Activation energy and pre-exponential factor for the self-diffusion in fcc Ni

D_0 $(m^2 s^{-1})$	Q (eV)	Method	Reference
$1.99 \times 10^{-5} - 2.14 \times 10^{-4}$	2.85-3.03	Ab-initio LDA NM	(Hargather et al. 2014)[1]
$2.32 \times 10^{-6} - 4.34 \times 10^{-5}$	2.64-2.88	Ab-initio LDA FM	(Hargather et al. 2014)[1]
	2.74	Ab-initio GGA FM	(Tucker et al. 2010) [2]
7.3×10^{-6}	2.44	Ab-initio GGA FM	(Toijer et al. 2021)[3]
1.35×10^{-5} (CO)	2.53	MD	(Garcia Ortega, Ramos de Debiaggi, and Monti 2002)[4]
0.30×10^{-5} (IO)	2.53	MD	(Garcia Ortega, Ramos de Debiaggi, and Monti 2002)[4]

1: Ecut=350 eV; supercell=2×2×2, 32 atoms; k-point=9^3; convergence condition: 0.01 eV.
2: Ecut=270 eV; supercell=3×3×3, 108 atoms; k-point=3^3; convergence condition: 35 meV.
3: Ecut=350 eV; supercell=4×4×4, 256 atoms; k-point=3^3; convergence condition: 20 meV/Å in force convergence
4: EAM potential by Voter and Chen (Voter and Chen 1986), calculation approximation: independent oscillators (IO) and coupled oscillators (CO).

From these data we can conclude that the vacancy formation enthalpy in ferromagnetic fcc Ni is $H_{Ni,V}^{for} = 1.75 \pm 0.10$ eV and the vacancy migration enthalpy is $H_{Ni,V}^{mig} = 1.1 \pm 0.05$ eV. These values are slightly larger than in NM Ni (which must not be confused with PM Ni). They are also close to experimental ones, measured in paramagnetic Ni. This suggests that there are no strong differences between the FM and PM Ni.

For the activation energy, the results vary around $Q = 2.5 - 2.9$ eV, which are slightly smaller than the experimental value of 2.83 eV.

- *Pure Iron*

Similar studies have been carried out in fcc Fe. In 2012, Klaver *et al.* (Klaver, Hepburn, and Ackland 2012) found that the vacancy formation energy is between 1.76 and 1.95 eV with DFT calculations in a supercell of 256 atoms (Table II.9). The calculations have been done for different magnetic states, including single-layer antiferromagnetic (afmI), double-layer antiferromagnetic (afmD) and also some ferromagnetic high-spin magnetic state. Indeed, many of the magnetic states of γ-Fe are mechanically unstable and for the FM state, the most stable is face centered tetragonal high spin. For austenite at 0 K, the fct afmI and afmD states have been proposed to be the most suitable, as they have the lowest energies. The values are given in Table II.8. Other calculations performed in NM Fe are summarized in Table II.9 and Table II.10.

Table II.8. Vacancy formation energy (eV) for different magnetic states in Fe (Klaver, Hepburn, and Ackland 2012)

fcc afmD	fct afmD	fct afmI	fct fm-HS
1.76	1.82	1.95	1.69

Ecut=400 eV; supercell=4×4×4, 256 atoms; k-point=2^3; convergence condition: 0.03 eV.

Table II.9. Vacancy formation/migration enthalpy/entropy in fcc Fe by DFT calculations

$H_{Fe,V}^{for}(eV)$	$H_{Fe,V}^{mig}(eV)$	$S_{Fe,V}^{for}(k_B)$	Method	Reference
1.80-1.95			VASP PAW GGA afm	(Klaver, Hepburn, and Ackland 2012)[1]
2.37	1.42		VASP PAW GGA-PBE NM	(Tsuru and Kaji 2013)[2]
2.32	1.38		VASP PAW GGA-PBE NM	(Angsten et al. 2014)[3]
2.36	1.39	2.47	VASP PAW GGA-PBE NM	(Wang et al. 2018)[4]
2.42			GPAW with PBE NM	(Karimi and Auinger 2020)[5]

1: Ecut=400 eV; supercell=4×4×4, 256 atoms; k-point=2^3; convergence condition: less than 0.03 eV.
2: Ecut=500 eV; supercell=3×3×3, 108 atoms; k-point=5^3; convergence condition: 0.02eV/Å.
3: Ecut: 1.5 times that of the maximum energy cutoff in the PAW potential file; supercell=3×3×3, 108 atoms; k-point=4^3; convergence condition: 1 meV.cell^{-1}.
4: Ecut=350 eV; supercell=3×3×3, 108 atoms; k-point=9^3; residual atomic forces < 0.01 eV/Å.
5: Ecut=900 eV; supercell=3×3×3, 108 atoms; k-point=6^3; convergence condition: < 0.02 eV for each supercell size

Table II.10: Activation energy and pre-exponential factor of the self-diffusion coefficient in fcc Fe

D_0 (m^2s^{-1})	Q (eV)	Method	Reference
9.47×10^{-3}	3.75	VASP PAW GGA-PBE NM	(Wang et al. 2018)

Ecut=350 eV; supercell=3×3×3, 108 atoms; k-point=9^3; residual atomic forces < 0.01 eV/Å.

From these results we can conclude that the vacancy formation enthalpy in fcc Fe is about $H_{Fe,V}^{for} = 2.3 - 2.4$ eV in non magnetic and $H_{Fe,V}^{for} = 1.80 - 1.95$ in anti-ferromagnetic fcc Fe. The vacancy migration enthalpy is about $H_{Fe,V}^{mig} = 1.4$ eV in NM fcc Fe. Therefore, the activation energy Q, is about 3.8 eV in NM Fe, which is much higher than the experimental values of 2.80-2.95 eV (Table II.4): the calculations in the NM state are clearly not representative of the PM fcc Fe.

For later parametrization, we will assume that the vacancy formation enthalpy in fcc Fe is 1.943 eV from the DFT study who considers the magnetic effects for fcc Fe at 0 K (Klaver, Hepburn, and Ackland 2012). We will then consider that the vacancy migration enthalpy is $H_{Fe,V}^{mig} = Q - H_{Fe,V}^{for} =$ 1.0 eV (with $Q = 2.943$ eV, from the experiments of Heumann (Heumann and Imm 1968), which is

representative of the average experimental values for the self-diffusion in fcc Fe). Due to the large differences between the different experimental values and between the different DFT calculations, one must admit that these values are more uncertain than those of pure Ni. For this value of Q, slightly different choices of $H_{Fe,V}^{mig}$ and $H_{Fe,V}^{mig}$ would have been possible. Finally, as in pure nickel, we will assume that $H_{Fe,V}^{mig}$ and $H_{Fe,V}^{mig}$ are the same in FM and PM iron, since no data suggests a strong effect of the magnetic state.

II.2.3.3 Impurity diffusion in fcc Fe and fcc Ni

Tucker *et al.* (Tucker et al. 2010) computed the tracer diffusion coefficients of Ni, Cr and Fe in a Ni host based on *ab initio* calculations and the five frequency model (equations (II-11) and (II-12)). The modeling results were used to determine the matrix of phenomenological coefficients and the tracer diffusion coefficients for both vacancy and interstitial mediated diffusion in Ni based alloys, including Ni-Fe. For diffusion in Ni-Fe alloys, the authors gave the parameters needed to be used in the five-frequency model by Le Claire (Le Claire 1978), including $H_2^{mig} = 0.97$ eV. The vacancy formation entropy is also calculated, which is $S_{Ni,V}^{for} = 1.82\, k_B$. However, with these parameters, they found smaller D_{Ni}^{Ni*} and D_{Ni}^{Fe*} than in the experiments by approximately a factor 10. The difference between their calculation and experiments was explained by the pre-exponential factor since there is a good agreement for the slopes of the Arrhenius laws with experimental data.

Toijer *et al.* also calculated these different migration barriers and the impurity diffusion coefficient of Fe in fcc Ni. For the impurity diffusion coefficient D_{Ni}^{Fe*}, they found a good agreement with the experiment of Bakker (Bakker 1968) at high temperature, which is in the average range of experimental studies (Figure II.4). The values of Tucker are a little higher than that proposed by Toijer (Toijer et al. 2021). A comparison for those values of barriers are given in Table II.11.

Table II.11. The migration barriers of the five frequency model in ferromagnetic Ni, according to DFT calculations (Toijer et al. 2021; Tucker et al. 2010)

Barrier in eV	H_0^{mig}	H_1^{mig}	H_2^{mig}	H_3^{mig}	H_4^{mig}
Tucker[1]	1.09	1.13	0.97	1.07	1.07
Toijer[2]	1.05	1.09	0.93	1.05	1.03

1: Ecut=270 eV; supercell=3×3×3, 108 atoms; k-point=3^3; convergence condition: 35 meV.
2: Ecut=350 eV; supercell=4×4×4, 256 atoms; k-point=3^3; convergence condition: 20 meV/Å in force convergence

Regarding the impurity diffusion of Ni in fcc Fe, only one reference by Tsuru and Kaji (Tsuru and Kaji 2013) is available. They evaluated the binding energy between Ni and the vacancy, $H_{Ni-V}^{bin} = 0.114$ eV.

II.2.3.4 Diffusion in concentrated Fe-Ni alloys

● *Point defect properties:*

There are very few studies relevant to diffusion in concentrated Fe-Ni alloys. Li and coworkers (Li, private communication) have recently estimated the vacancy formation and migration enthalpies in ordered structures of the FeNi system by DFT calculations. The values of the formation enthalpies are given in Table II.12.

Table II.12. Vacancy formation energies in $FeNi_3 - L1_2$ and $FeNi - L1_0$ ordered structures. DFT calculations. (Li et al. Private communication).

$H_{V_{Fe}}^{for}(FeNi_3 - L1_2)$	$H_{V_{Ni}}^{for}(FeNi_3 - L1_2)$	$H_{V_{Fe}}^{for}(FeNi - L1_0)$	$H_{V_{Ni}}^{for}(FeNi - L1_0)$
1.388	1.594	1.897	1.847

Ecut=400 eV; supercell=3×3×3, 108 atoms; k-point=16^3; convergence condition: 0.02eV/Å

where $H_{V_{Fe}}^{for}$ is the formation enthalpy of a vacancy replacing a Fe atom on its sublattice.

Recently Osetsky *et al.* performed a series of atomistic modelling of diffusion in Fe-Ni alloys, using various EAM potentials developed by Bonny *et al.* (Bonny et al. 2011), classical or *ab initio* molecular dynamics and kinetic Monte Carlo simulations (Anento, Serra, and Osetsky 2017; Osetsky et al. 2018; Zhao, Osetsky, and Zhang 2019; Ferasat et al. 2020). The same potentials were used, with the k-ART, off lattice, kinetic Monte Carlo method to study diffusion mechanisms in the $L1_0$-FeNi phase (Mahmoud and Mousseau 2018). These simulations show how the details of migration barriers affect the diffusion properties of vacancies and self-interstitials. The simulations of Zhao *et al*. (Zhao et al. 2019) , for example, show that the vacancy diffuse more slowly in the ordered phase $FeNi_3$ than in a solid solution at the same composition (Figure II.15). However, for a quantitative modelling of the Fe and Ni diffusion coefficients in concentrated alloys, these approaches present two limitations. The first one comes from the EAM potential, which predicts a strong decrease of the average migration barriers for the Fe-V jumps with the iron concentration (Table II.13). As a result, the simulations predict that the Fe diffusion coefficient varies by orders of magnitude between pure Ni and pure Fe (Figure II.14), in contrast to what is experimentally observed.

Table II.13. Average migration energies for vacancy jumps in the simulations of Ferasat et al. (Ferasat et al. 2020)

x_{Fe}	E_{Ni}^{mig} (eV)	E_{Fe}^{mig} (eV)
0	1.182	
0.1	1.224	1.196
0.2	1.261	1.168
0.3	1.290	1.136
0.4	1.303	1.090
0.5	1.305	1.039
0.6	1.301	0.976
0.7	1.298	0.916
0.8	1.278	0.834
0.9	1.251	0.736
1.0		0.622

The other limitation is that these simulations are performed with a single vacancy. In such a case, time rescaling techniques must be used to get the absolute values of the Fe and Ni diffusion coefficients. The atomic diffusion coefficients are indeed proportional to the equilibrium vacancy concentration, which depends on the composition of the solid solutions and, at low temperatures, on possible ordering effects. This is not accounted for in these studies. We will try to deal with this important but non trivial issue with our model, as will be explained below.

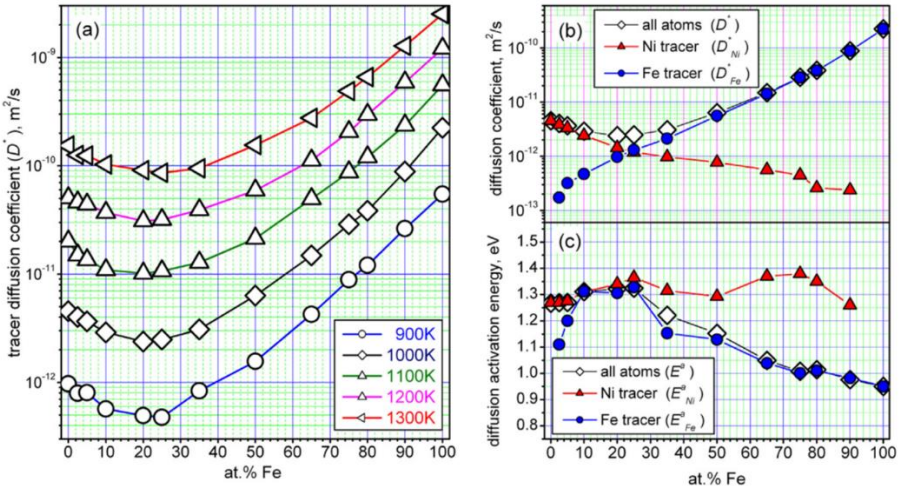

Figure II.14. Variation of the tracer diffusion coefficient with the concentration and temperature by MD: (a) tracer diffusion coefficients of vacancies; (b) tracer diffusion coefficients of Fe, Ni and all atoms; (c) effective activation energy of total (all atoms are tracers) and partial (Ni or Fe atom are tracers) tracer diffusion (Osetsky et al. 2018)

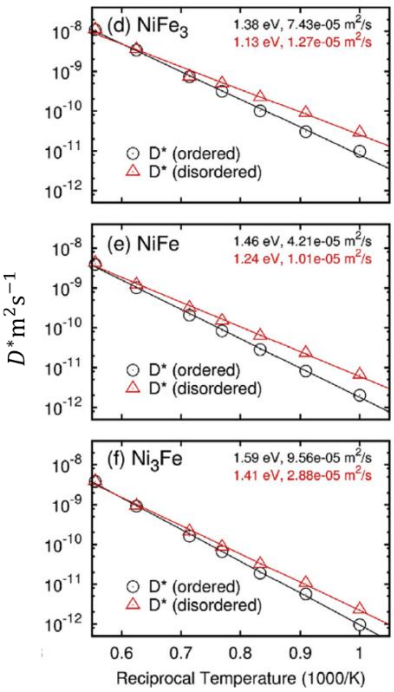

Figure II.15. Tracer diffusion coefficients of a vacancy in different alloys with ordered and disordered structures (Zhao, Osetsky, and Zhang 2019). Classical MD with the EAM potential of Bonny et al. (Bonny et al. 2011)

Regarding the influence of magnetism on diffusion, Schneider and coworkers (Schneider et al. 2020) have studied the temperature evolution of self-diffusion coefficient in bcc Fe using Monte Carlo simulations, with ab initio-based effective interaction models. Li *et al.* (Li, Fu, and Schneider 2021) used the same approach to investigate the influence of magnetism on vacancy formation in fcc Ni, and in bcc and fcc Fe. The vacancy formation energy in AFD fcc Fe and FM fcc Ni was found to be respectively 1.83 eV and 2.20 eV. When the temperature increases, an influence of the magnetic transition can be observed in Figure II.16, however much less pronounced than in bcc Fe. Accounting for this recent result will be a perspective for future work.

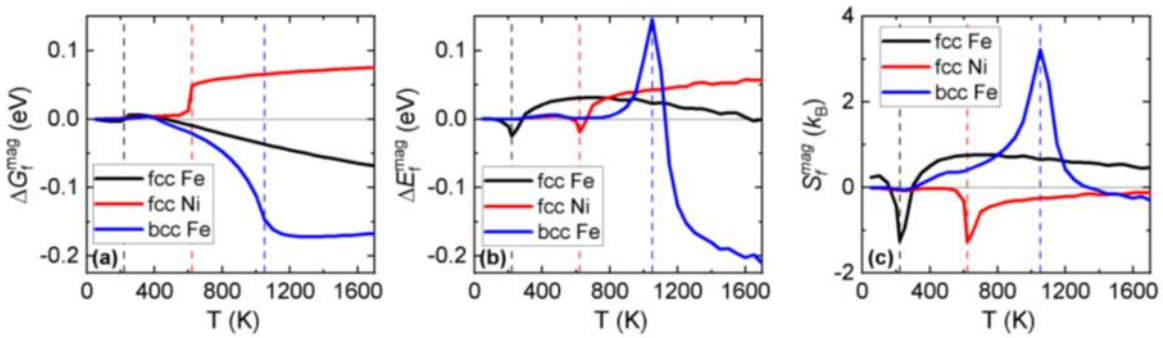

Figure II.16. Magnetic contribution to vacancy formation properties in the three systems (Li, Fu, and Schneider 2021)

II.2.4 Conclusions

The diffusion properties in the Fe-Ni system have been investigated using both experimental and theoretical approaches. Key parameters such as the formation and migration energy of vacancies have been measured, using various experimental methods. Let us summarize the essential results that we will retain for pure metals (Table II.14 and II-15), and that will be used to determine the parameters of our model.

For pure fcc Ni, we have independent recommended values for the formation and migration energy of vacancies at high temperature ($H_{Ni,V}^{for} = 1.79$ eV and $H_{Ni,V}^{mig} = 1.04$ eV), consistent with the value of the diffusion enthalpy ($Q = 2.84$ eV). In the case of pure fcc Fe, fewer experimental data of vacancy formation and migration energy exist and those values are not in good agreement with one another. However, many experiments proposed an activation energy in the range of 2.8-3.0 eV in fcc Fe. Therefore, we use the value of $H_{Fe,V}^{for} = 1.94$ eV which is adjusted to DFT calculation value by assuming that there is not much influence of the magnetic transition on the vacancy formation, and $H_{Fe,V}^{mig} = 1.0$ eV, which is adjusted on experimental value of activation energies.

For the entropies of vacancy migration and formation, theoretical results are used as references because they are not available by experiments. For example, the vacancy migration entropy in Ni of Ortega (Garcia Ortega, Ramos de Debiaggi, and Monti 2002), obtained with an empirical potential, $S_{Ni,V}^{mig} = 1.58\, k_B$, are used since this is the only reference found for this value. Then the vacancy formation entropy is adjusted to experimental results of Ni self-diffusion coefficients via the pre-exponential factor D_0 as shown in equation (II-8). Then the $S_{Ni,2}^{mig}$ is adjusted to the experimental impurity diffusion coefficient of Ni in fcc Fe.

The vacancy migration is supposed to be $H_{Fe,V}^{mig} = 1$, and then the $H_{Fe,V}^{for}$ is deduced from experimental value of activation energy (Heumann and Imm 1968). The vacancy migration entropy $S_{Fe,V}^{for}$ in fcc Fe is the DFT value of Wang *et al*. (Wang et al. 2018). Finally, the vacancy formation entropy is adjusted to experimental results of Ni self-diffusion coefficients via the pre-exponential factor.

Table II.14: parameters concerning the exchange between a vacancy and a Ni atom

a_0^{Ni}(nm)	ϑ_0^{Ni}(Hz)	$H_{Ni,V}^{for}$(eV)	$H_{Ni,V}^{mig}$(eV)	$S_{Ni,V}^{for}(k_B)$	$S_{Ni,V}^{mig}(k_B)$	$H_{Ni,2}^{mig}$(eV)	$S_{Ni,2}^{mig}(k_B)$
0.3524	0.59×10^{13}	1.79	1.04	3.22	1.58	0.96	2.7

Table II.15: parameters concerning the exchange between a vacancy and a Fe atom

a_0^{Fe}(nm)	ϑ_0^{Fe}(Hz)	$H_{Fe,V}^{for}$(eV)	$H_{Fe,V}^{mig}$(eV)	$S_{Fe,V}^{for}(k_B)$	$S_{Fe,V}^{mig}(k_B)$	$H_{Fe,2}^{mig}$(eV)	$S_{Fe,2}^{mig}(k_B)$
0.3571	1.245×10^{13}	1.943	1.0	2.47	1.32	0.97	1.75

Regarding the alloys, other interesting data are the migration barriers computed by Tucker *et al*. in the dilute Ni-Fe system (Table II.11). We will use additional DFT calculations to parametrize the parameters of the dilute Fe-Ni system, as explained later.

In concentrated alloys, several experimental studies clearly show – in spite of minor differences – that the tracer diffusion coefficients of Fe and Ni change little with the alloy composition. The study by Million *et al.* (Million et al. 1981) is especially interesting because it presents a rare case of direct experimental comparison between of tracer and interdiffusion coefficients. Finally, a few experimental and theoretical results suggest that the FM/PM magnetic transition has little effect on the vacancy properties in Fe-Ni fcc alloys, except for the recent results shown in Figure II.16.

II.3 Atomistic modelling of diffusion in Fe-Ni alloys

II.3.1 Introduction

As mentioned in II.2.1.4, there is no reliable analytical models to deal with diffusion properties in concentrated alloys. On the other hand, an atomistic modelling can be a promising approach for diffusion and phase transformation kinetics. Key points of the model are how to describe the vacancy jump frequencies and vacancy concentrations in the system.

Atomistic methods have been previously used in other systems and have improved over time. Pareige *et al*. studied ordering and precipitation in the Ni-Cr-Al system (Pareige et al. 1999). Soisson and Fu investigated the precipitation kinetics of Cu in α-Fe, taking into account the dependence of vacancy concentration and migration barriers on the local atomic environment (Soisson and Fu 2007).

Later Martinez *et al*. studied the decomposition in Fe-Cr system (Martínez et al. 2012). In these alloys the ferro-to-paramagnetic transition affects both the thermodynamic and diffusion properties: the effect on the precipitation kinetics has been simulated by Senninger *et al*., using a model where the effects of the magnetic transitions are taken into account through the concentration and temperature dependence of pair interactions (Senninger et al. 2014). We will use a similar approach, by extending the PIM of Chapter I to deal with vacancy formation and migration properties in Fe-Ni fcc alloys.

In the following, we will first give the general expression of the vacancy migration barriers of the k-PIM (II.3.2). Then, in section II.3.3, we will explain the parametrization of the model and compare its results with the experiments, in the relatively simple situation of self- and impurity-diffusion, where accounting for the equilibrium vacancy concentration is straightforward. In section II.3.4, we will present a new method based on Widom integration, to determine the vacancy equilibrium concentration in concentrated Fe-Ni alloys. Last, in section II.3.5, we will study diffusion properties in concentrated Fe-Ni alloys. Tracer diffusion coefficients and interdiffusion coefficients will be calculated and

compared to experiments; the Darken equation will be discussed, and we will investigate the effect of the chemical order-disorder transition on diffusion.

II.3.2 Kinetic pair interaction model for Fe-Ni alloys: jump frequencies and migration barriers

We propose to reproduce and predict the diffusion properties in fcc FeNi alloys with a concentrated-and temperature-dependent pair interaction model and kinetic Monte Carlo simulations. This model is based on the PIM given in Chapter I and is an extension of it. To distinguish these two conceptions, we will call them PIM and k-PIM respectively for the rest of this thesis. The k-PIM describes the vacancy jump frequencies in the system. A vacancy-atom exchange in the fcc lattice is shown in Figure II.17: the saddle-point position (m) is surrounded by 4 nearest-neighbor atoms (i).

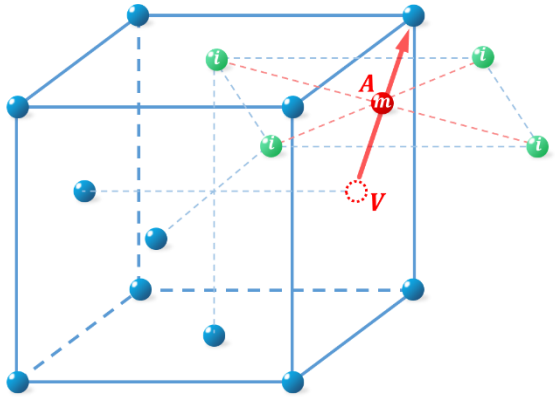

Figure II.17. The vacancy migration in the fcc lattice. The vacancy (dotted circle) exchanges with an A atom. The red sphere shows the saddle point position (m) and the green ones its first nearest neighboring sites (i)

The vacancy migration barrier (i.e. the difference between the Gibbs free energy of the system in the transition state and in the initial state) can be expressed in terms of pair interactions as:

$$\Delta G_{AV}^{mig} = \sum_{i \in n(SP)} g_{Ai}^{SP}(x,T) - \sum_{j \in n(V)} g_{Vj}(x,T) - \sum_{k \in n(A)} g_{Ak}(x,T) \qquad \text{(II-30)}$$

where $g_{Ai}^{SP}(x,T)$ are the interactions between atom A on the saddle point and the atoms on the neighboring fcc sites (i); $g_{Vj}(x,T)$ are the interactions between the vacancy and its neighboring atoms on the fcc lattice and $g_{Ak}(x,T)$ are the interactions between atom A on its initial position and its neighboring atoms on the fcc lattice.

Compared to previous studies (Pareige et al. 1999; Senninger et al. 2014; Soisson and Fu 2007; Martínez et al. 2012), we try to deal with finite temperature effects (the effect of the magnetic transition

but also of the vibrational entropy) in a more systematic ways, as in Chapter I. The interatomic pair interactions, such as $g_{Ak}(x,T)$ in equation (II-30), are those of the PIM (between first and second nearest neighbors, with magnetic and non-magnetic contributions, adjusted on DFT calculations at 0 K and CALPHAD results at high temperatures). Similarly, the saddle-point and vacancy-atom interactions, are written as $g_{ij} = h_{ij} - Ts_{ij}$ (with h_{ij} and s_{ij} the enthalpy and the entropy of the pair, each being the sum of magnetic and non-magnetic terms).

II.3.3 Application to the diffusion in pure and dilute alloys

The self-diffusion coefficients and the impurity diffusion coefficients only depend on a few jump frequencies (see section II.3.3.4 and II.3.3.5), so that it is easy to fit the relevant parameters of the k-PIM on the corresponding migration barriers. The diffusion coefficients can then be directly computed from the jump frequencies, using an exact analytical expression [equation (II-6) for D_{Fe}^{Fe*} and D_{Ni}^{Ni*} or the five frequency or similar models (equation (II-9) for D_{Ni}^{Fe*} and D_{Fe}^{Ni*}]. AKMC simulations are not necessary, but we will use them to provide a simple illustration and to validate our code.

II.3.3.2 Atomistic Kinetic Monte Carlo simulations

The atomistic kinetic Monte Carlo (AKMC) simulations have been carried out using the residence time algorithm (Bortz, Kalos, and Lebowitz 1975) to perform exchanges between atoms and vacancies. With this algorithm, each Monte Carlo step takes place as follows. For a specific configuration of the system, C_i, we identify all available configurations $\{C_k\}_i$ after one possible atom-vacancy exchange. Then for each possible transition state, the probability of change can be calculated using the associated jump frequencies, ω_k, with a migration barrier given by equation (II-30). One of the jumps is chosen using a random number. The higher the jump frequency, the more likely the associated transition to be chosen. After the chosen transition is performed, the system continues as in the first step. For such a Monte Carlo step, the time increment is obtained by the inverse of the sum of the jump frequencies ω_k ($t_{MC} = 1/\sum \omega_k$). The residence time algorithm has the advantage of guaranteeing one exchange atom-vacancy for each Monte Carlo step.

For the Monte Carlo simulations, a simulation box with periodical condition has been used. A typical simulation box contains $N_0 = 4 \times 64^3$ atoms and one vacancy, with periodic boundary conditions. The tracer diffusion coefficient of one species ($i = A, B \text{ or } V$) can be determined by measuring the average square displacement $\langle R_i^2 \rangle$ of i tracers , according to the Einstein relation:

$$D_{i^*} = \frac{\langle R_i^2 \rangle}{6t} \tag{II-31}$$

where t denotes the accumulated physical time.

II.3.3.3 Vacancy concentration and time rescaling

In our simulations, only one vacancy is introduced into the system, leading to a vacancy concentration of $x_V^{MC} = 1/N_0$. Therefore, the accumulated time t must be rescaled as :

$$t = t_{MC} \frac{x_V^{MC}}{x_V^{eq}} \tag{II-32}$$

where x_V^{eq} is the real vacancy concentration (we assume that the vacancy concentration is at equilibrium on the timescale of the diffusion and ordering processes considered in this study). In the dilute limit, $x_V^{eq} = \exp(-G_V^{for}/k_B T)$ where G_V^{for} is the Gibbs free energy of vacancy formation in the pure metal, Fe or Ni.

II.3.3.4 Self-diffusion coefficient

In pure A (Fe or Ni) the migration barrier is unique. The pair interactions $g_{AA}^{(n)}$ have been fitted of the cohesive energy of the pure metals. The atom-vacancy interactions $g_{AV}^{(n)}$ are then fitted on the Gibbs vacancy formation energies using:

$$G_V^{for}(A) = -\frac{1}{2}\sum_n g_{AA}^{(n)} + \sum_n g_{AV}^{(n)} \tag{II-33}$$

We take into account atom-vacancy interactions between first and second nearest neighbors and we assume a constant ratio: $\beta_{AV} = g_{AV}^{(2)}/g_{AV}^{(1)}$. As for the interatomic pair interactions, they are expressed as a sum of magnetic and non-magnetic term: $g_{AV}^{(i)} = g_{AV}^{mag(i)} + g_{AV}^{nm(i)}$. We have seen in section II.2 that existing experimental and theoretical results do not show significant effects of the magnetic transition on vacancy properties. In this study, we will therefore assume that $G_V^{for}(T)$ and $G_V^{mig}(T)$ show no discontinuity at the Curie temperature in pure Fe and Ni, i.e. that there is a perfect Arrhenius behavior of the self-diffusion coefficients. There are some discontinuities of the pair interactions $g_{FeFe}^{(n)}(T)$ and $g_{NiNi}^{(n)}(T)$ at the Curie temperature, but they are compensated by the variation of $g_{FeV}^{(n)}(T)$ and $g_{FeV}^{(n)}(T)$.

The pair interaction g_{AA}^{SP} can be fitted to the vacancy migration barrier in pure A using:

$$G_0^{mig} = 4g_{AA}^{SP} - \sum_{n=1}^{2} Z_n g_{AV}^{(n)} - (Z_1 - 1)g_{AA}^{(1)} + Z_2 g_{AA}^{(2)} \tag{II-34}$$

The values of $G_V^{for} = H_V^{for} - TS_V^{for}$ and $G_V^{mig} = H_V^{mig} - TS_V^{mig}$, used to fit the $g_{AV}^{(n)}$ and g_{AA}^{SP} parameters, can be found in Table II.14 and Table II.15.

Simulations have been carried out for temperatures between 500 K and 5000 K. Comparison with equation (II-6) and with the experimental results are shown in Figure II.18.

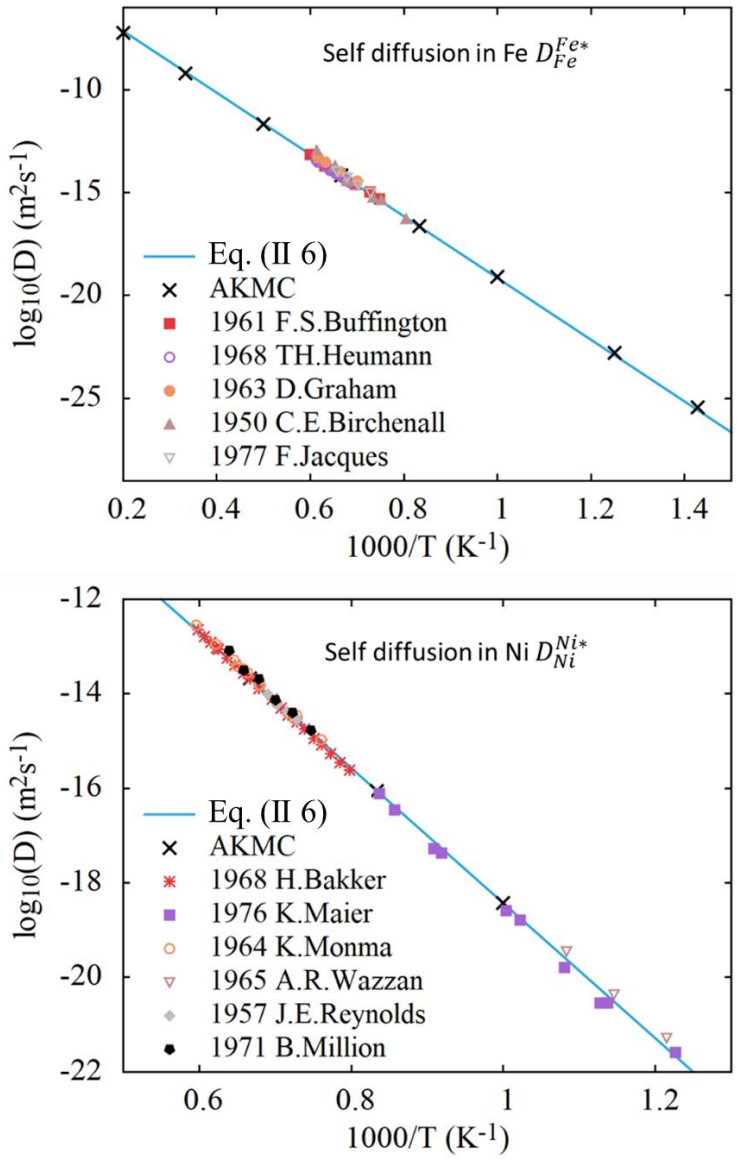

Figure II.18. Self-diffusion coefficients in pure Fe and Ni. Equation (II-6) is represented by the line, the AKMC results by × and experimental results by colored symbols.

These comparisons show a good agreement between the analytical value of equation (II-8), the AKMC simulations, and the experimental values of self-diffusion coefficients of Fe and Ni.

II.3.3.5 Impurity diffusion

With the equation (II-30), one can write the migration barriers of the different frequencies that control the impurity diffusion coefficient $D_{B^*}^{A}$ of B in A. The only parameters that remain to be fitted in

the k-PIM are the saddle-pair interactions $g^{SP}_{FeNi} = h^{SP}_{FeNi} - Ts^{SP}_{FeNi}$ and $g^{SP}_{NiFe} = h^{SP}_{NiFe} - Ts^{SP}_{NiFe}$, which are involved in the H_2^{mig} barriers in Ni and Fe. For example, the g^{SP}_{AB} will be given by

$$G_2^{mig} = 4g^{SP}_{AB} - \sum_{n=1}^{2} Z_n g^{(n)}_{AB} + g^{(1)}_{AB} - \sum_{n=1}^{2} Z_n g^{(n)}_{BV} + g^{(1)}_{BV} - g^{(1)}_{AV} \quad \text{(II-35)}$$

h^{SP}_{FeNi} is fitted to the DFT calculation of H_2^{mig} in FM Ni, by Tucker (Tucker et al. 2010). The values of the other barriers of the five frequency model are then imposed. We find (Table II.17) that the k-PIM model is in good agreement with the calculations of Tucker *et al* for these barriers, and also with the DFT calculations of Toijer *et al*. (Toijer et al. 2021). On another hand, the h^{SP}_{NiFe} parameter is fitted on the value of H_2^{mig} in Fe, given by the DFT calculations of Kangming Li (K. Li, private communication). The entropic contributions are adjusted on the experimental pre-exponential factors of D^{Ni*}_{Fe} and D^{Fe*}_{Ni} (Figure II.19).

To test the model, AKMC simulations have been performed for temperatures between 500 K and 2000 K and 1% of impurities, i.e. 1% Ni in Fe and 1% of Fe in Ni. The comparison between the AKMC, the five frequency model and the experiments is shown in Figure II.19.

Table II.16: Migration barriers of the five frequency model. Comparison between the k-PIM and the DFT calculations of (Tucker et al. 2010) and (Toijer et al. 2021).

Barrier in eV	H_0^{mig}	H_1^{mig}	H_2^{mig}	H_3^{mig}	H_4^{mig}
Tucker	1.09	1.13	0.97	1.07	1.07
Toijer	1.05	1.09	0.93	1.05	1.03
k-PIM	1.04	1.16	0.97	0.99	1.05

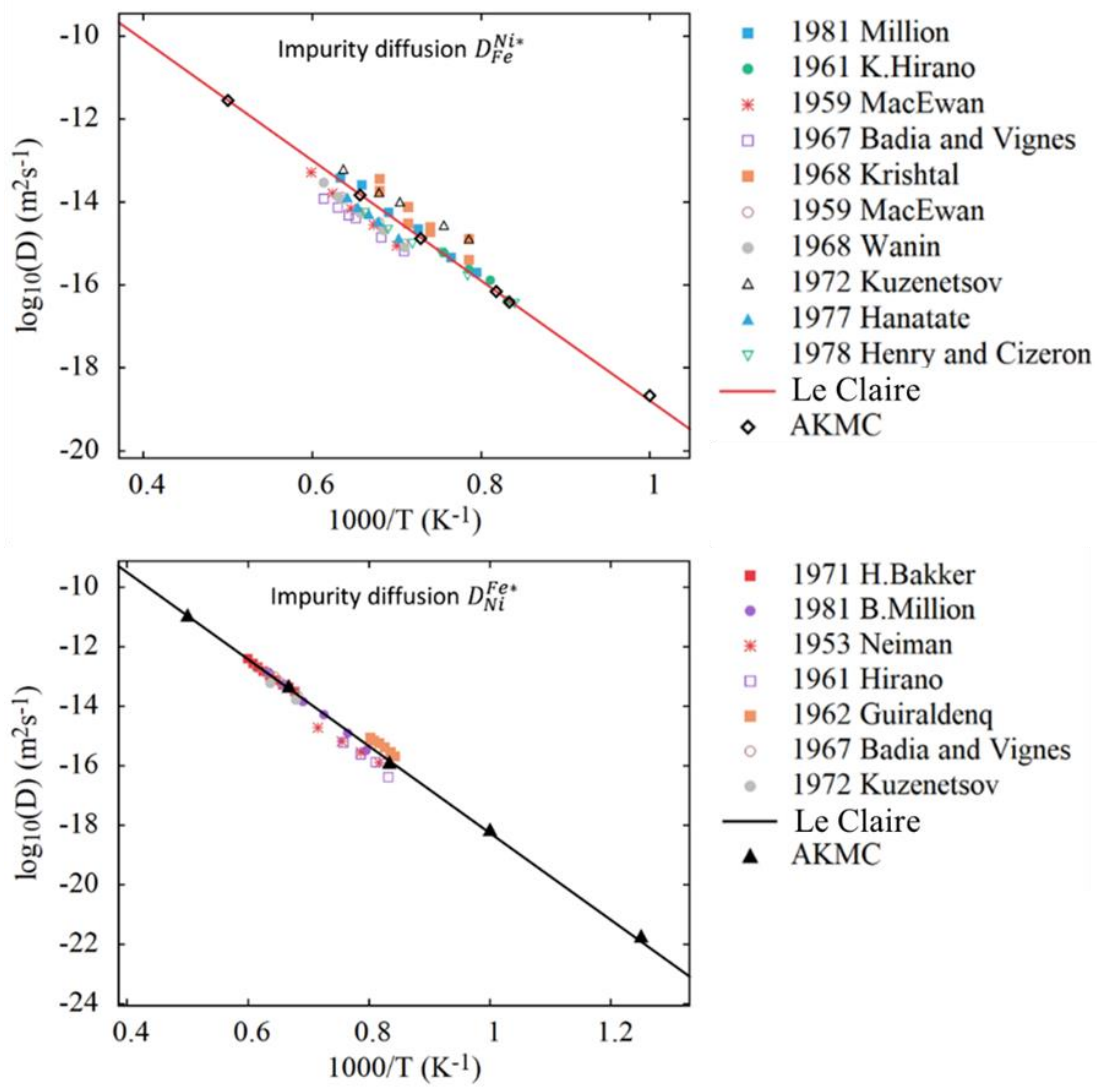

Figure II.19. Impurity diffusion coefficients in pure Fe (top) and Ni (bottom). The symbols in colors correspond to the experimental values, the black triangles to the AKMC simulations and the lines to Le Claire model.

There is a good agreement between the AKMC results and the Le Claire model. As already mentioned above the experimental data are scattered, especially for D_{Fe}^{Ni*} (the values can differ by one order of magnitude). The values of the model fall in the middle of the experimental values, for D_{Fe}^{Ni*} and D_{Ni}^{Fe*}. For the later, they are slightly above the average values of Jönsson (Figure II.5)

In order to estimate the relative diffusivity of each element, we present in Figure II.20 the diffusivity of the different elements in the same matrix.

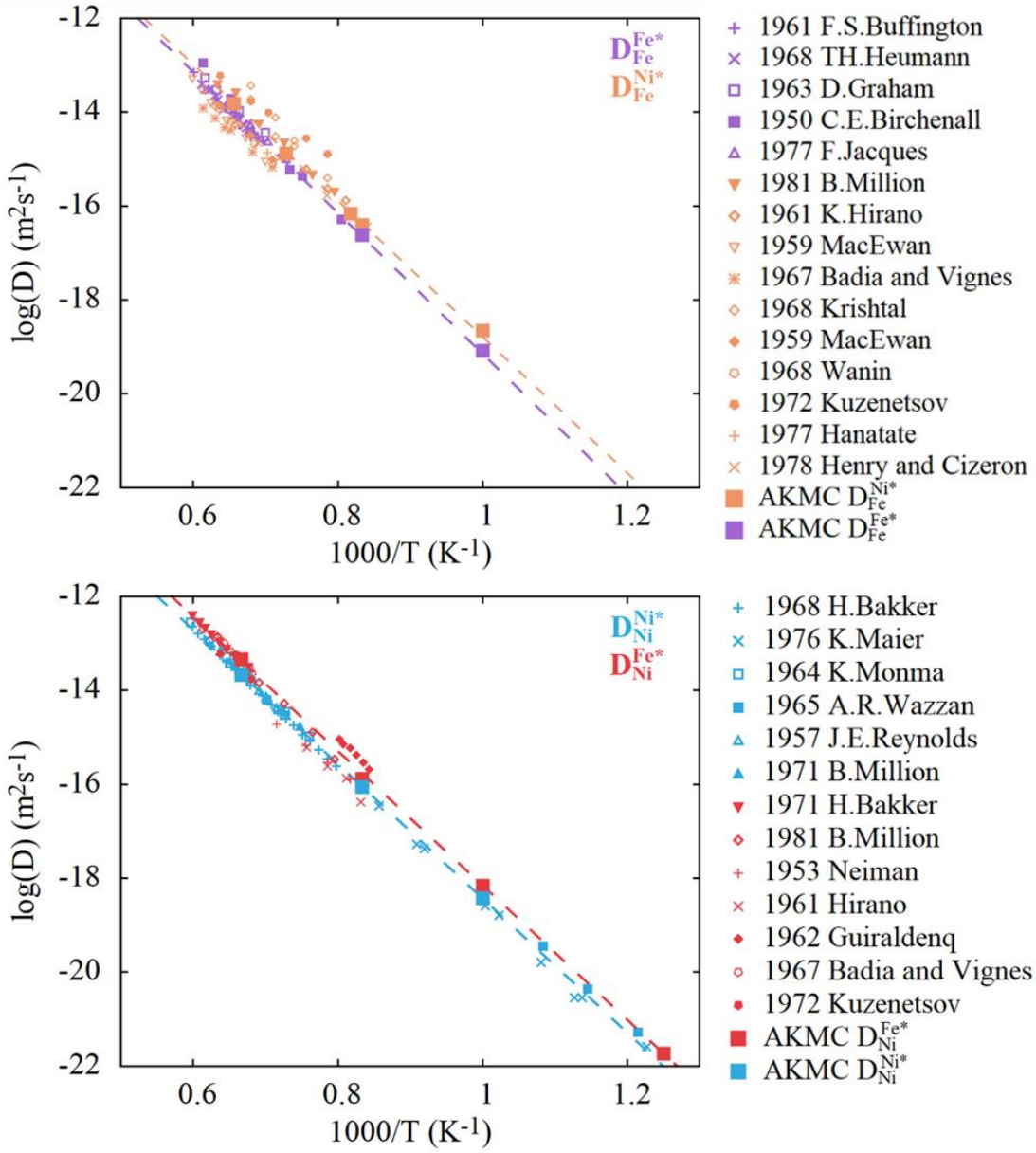

Figure II.20. Comparison of tracer diffusion coefficients in fcc Fe (top) and fcc Ni (bottom): small points are experimental values, large points are AKMC results and the dashed lines are k-PIM values

From Figure II.20, we can see that in fcc Ni, Fe diffuses slightly faster than the Ni; while in fcc Fe, due to the dispersion of experimental data, it is difficult to distinguish the relative diffusivity of Fe and Ni. Our simulations predict a relative faster diffusivity of tracer Ni than tracer Fe in fcc Fe, by a factor 3 approximately.

Finally, let us emphasize that in this section, for the sake of simplicity, we have considered the h^{SP}_{FeNi} and h^{SP}_{NiFe} parameters as constants, independent of the local composition. We will later introduce a dependence of these parameters on the local Ni concentration, in order to better describe the tracer diffusion coefficients in concentrated solid solution. The values given above are thus only the limits in pure Fe and Ni.

II.3.3.6 Conclusions

So far, the k-PIM model has been built and parametrized for pure metals and dilute Fe-Ni alloys. The key parameters have been determined from experimental data and DFT calculations of formation enthalpies and vacancy migration barriers in fcc Fe-Ni systems. Other parameters, controlling the migration and formation entropies, have been fitted on experimental diffusion data. As a result, self and impurity diffusion coefficients are well reproduced in pure fcc Fe and fcc Ni, with uncertainties of the order of a factor of 2 or 3, similar to the differences between various experiments.

II.3.4 Determination of equilibrium vacancy concentration in alloys: Widom integration method

II.3.4.1 Introduction

In the following, we are going to consider diffusion in Fe-Ni concentrated solid solutions (with various degrees of short range order) and in the $L1_2$ phase (partially or perfectly ordered). As explained above, for rescaling the time in Monte Carlo simulations [eq. (II-32)], it is crucial to know the vacancy concentration in the system. This is simple in pure metals but in concentrated A-B alloys there is no general analytical expressions for x_V^{eq} and G_V^{for}, except in limiting cases (such as a fully disordered solid solution, or a perfectly ordered structure). The other problem concerns the alloys undergoing a phase transformation, such as a phase separation or a phase ordering (Chapter III). These systems are not at equilibrium, and one must assume that a vacancy equilibrium concentration can still be defined, which evolves with the system (this assumption, often implicit in the modeling of phase transformation kinetics, is based on the fact that the vacancies diffuse much faster than the atoms). We will see in the next chapter that it poses some problems to estimate x_V^{eq}.

At equilibrium at least, some analytical models exist. In disordered solid solutions, the Bragg-Williams approximation gives the vacancy concentration (Nastar and Soisson 2012):

$$x_V^{eq} = \exp\left[-\frac{x_A G_{A,V}^{for} + x_B G_{B,V}^{for} + Z x_A x_B v/2}{k_B T}\right] \qquad \text{(II-36)}$$

where $G_{A,V}^{for}$ and $G_{B,V}^{for}$ are the Gibbs free energy of vacancy formation in pure A and pure B respectively and v the ordering energy defined in Chapter I. This expression in only valid for pair interactions independent of the composition. In our PIM, they depend on the local concentration, and it can be shown (M. Nastar, private communication) that :

$$x_V^{eq} = \exp\left[-\frac{x_A G_{A,V}^{for} + x_B G_{B,V}^{for} + \frac{Z}{2} x_A x_B \left(v + x_B \frac{dv}{dx_B}\right)}{k_B T}\right] \quad \text{(II-37)}$$

The calculation of vacancy concentrations in perfectly ordered phases is more difficult. The main reason is that generally, at constant numbers of A and B atoms, one cannot create one single vacancy on a sublattice without creating other defects (a vacancy on another sublattice, or an antisite defect). Nevertheless efficient analytical models have been developed, such as the one of Hagen & Finnis, which is described in Appendix (Hagen and Finnis 1998). The method only works for almost perfectly ordered alloys (point defects, vacancies and antisites are assumed to be isolated).

On the other hand, AKMC simulations have been used to determine the equilibrium vacancy concentration, in alloys at equilibrium or during a phase separation (LeBouar and Soisson 2002; Nastar and Soisson 2012). The principle is the same as for the time rescaling of equation (II-32), but using the equilibrium vacancy concentration in a reference phase (for example pure A or pure B). One can rewrite equation (II-32) as, e.g. $x_V^{eq} = x_V^{MC} \times x_V^{eq}(A)/x_V^{MC}(A)$ where x_V^{eq} is the equilibrium vacancy concentration, $x_V^{MC} = 1/N$ the vacancy concentration in the simulation box, and $x_V^{eq}(A) = \exp(-G_{V,A}^{for}/k_B T)$ the equilibrium concentration in pure A. One can therefore get x_V^{eq} by measuring $x_V^{MC}(A)$, the vacancy concentration on the sites of the Monte Carlo simulation that are in a pure A environment. The method works well in systems with an unmixing tendency for example Fe-Cr (Le Bouar and Soisson 2002) and Fe-Cu (Nastar and Soisson 2012). However, we found that it did not work well in systems with an ordering tendency, because fraction of pure A or pure B sites is too small.

Therefore, we propose a new method to calculate the vacancy concentration in concentrated alloys, for general cases. It is based on the Widom integration method, initially developed to estimate the chemical potential of atoms in off-lattice simulations. We will validate our method by comparing the results to Hagen & Finnis method in ordered structures at low temperatures, and to the modified Bragg-Williams approximations of equation (II-37) in random solid solutions, at high temperatures.

II.3.4.2 The Widom method

The Widom method is a statistical thermodynamic approach to the calculation of material and mixture properties. In general, the calculating of quantity Ψ_i for a specie i is of a form of $\Psi_i = \ln\langle\exp(-\Delta\varphi_i/k_B T)\rangle$, where φ_i is the interaction energy of an inserted particle with all other particles in the system. The average is over all possible insertions. This can be understood conceptually as fixing the location of all molecules in the system and then inserting a particle of species i at all locations through the system, averaging over a Boltzmann factor in its interaction energy over all of those

locations. It has been proposed by Widom to give the thermodynamic functions in terms of the potential energy in fluids (Widom 1963).

Applied to our PIM, the Widom integration method calculates the vacancy formation Gibbs free energy as:

$$G_V^{for} = -k_B T ln \langle \exp\left(-\frac{\Delta G_{V_i}}{k_B T}\right)\rangle \quad \text{(II-38)}$$

where ΔG_{V_i} is the Gibbs free energy needed to replace an atom i in the system by a vacancy and the brackets $\langle \quad \rangle$ means the average value, computed on all the atoms of the system. ΔG_{V_i} is defined at constant number of atoms, i.e. :

$$\Delta G_{V_i} = g_i + G_{V_i} - G_0 \quad \text{(II-39)}$$

where G_0 is the Gibbs free energy of the system without vacancy, G_{V_i} the Gibbs free energy of the system with a vacancy on site i, and g_i the Gibbs free energy of atom i (let us recall that all these terms are Gibbs free energies because they include the non-configurational entropic contributions of the system).

In practice, an equilibrium configuration with a certain global concentration x_{Ni} is first created by Monte Carlo simulations (using the semi-grand canonical algorithm described in chapter I). Then G_V^{for} is computed according to equation (II-38). G_{V_i} and G_0 are simply the sums of the pair interactions in system with and without a vacancy. In order to estimate g_i, we propose two different ways:

1. We consider it to be the chemical potential of atom i : $g_i = \mu_i$. This choice will be hereafter referred to as "Widom 1".

2. g_i is computed for each atom i as half the sum of the surrounding pair interactions (considering that a pair interaction g_{ij} belongs one half to i and one half to j). The method will be called "Widom 2".

The first choice may seem more natural, but it has two drawbacks. From a practical point of view, it requires the knowledge of the chemical potentials of A and B. They are indeed provided by semi-grand canonical Monte Carlo simulations (see Chapter I, section III.A), but at low temperatures, in case of strong hysteresis, precise values can be difficult to obtain. In such cases, other models can be used: for example, the model of Hagen and Finnis also provides the values of μ_A and μ_B (see Appendix), but only for a well-ordered stoichiometric phase. The other issue is that the chemical potentials are equilibrium quantities. They can be defined in equilibrium situations, which is the case for the modeling of diffusion coefficients discussed in this chapter. However, it is less clear if they can be used during a phase transformation (as in Chapter III), in a non-equilibrium system, where chemical potentials are not the same everywhere.

The second choice has neither of these two disadvantages, and is very easy to implement in an equilibrium or kinetic Monte Carlo algorithm. It is based on an idea often used to compute vacancy formation energies in simple situations. For example in a pure metal, it is equivalent to the idea that the vacancy formation energy is the energy required to take an atom in the bulk and place it on the surface of the metals where it gets back half of its bonds (Mehrer 2007). However, to our knowledge, the validity of this idea has never been rigorously established in concentrated alloys (Mayer and Fähnle 1997; Cheng, Wynblatt, and Dorn 1967; Hagen and Finnis 1998).

II.3.4.3 Equilibrium vacancy concentrations in Fe-Ni alloys

We are going to apply the above Widom methods to our interaction model for Fe-Ni alloys, first in solid solutions at high temperatures, to get the evolution of $G_V^{for}(x_{Ni})$ in the conditions of the experimental measurements of tracer and interdiffusion coefficients, by Million *et al*. and by other authors, presented in the bibliography part. Then we will model the evolution of $G_V^{for}(x_{Ni})$ at lower temperatures, when the ordered $L1_0$ and $L1_2$ phases appear, as we have seen in Chapter I (section I). We will use the same pair interactions (between atoms and between atoms and vacancies) as in section II.3.3, and we will see in the next section that these parameters allow a good reproduction of all the existing diffusion data.

In the following simulations, a system with $N = 4 \times 16^3$ atoms with periodic boundary conditions has been used. At a given temperature, the semi-grand canonical algorithm described in chapter I gives the isotherm $= f(\mu_{Ni} - \mu_{Fe})$, as shown e.g. in Figure II.21. Then one can choose the value of $\mu_{Ni} - \mu_{Fe}$ to get an equilibrium configuration of the desired composition (once $\mu_{Ni} - \mu_{Fe}$ is known, the values of μ_{Ni} and μ_{Fe} can be deduced from $G = x_{Ni}\mu_{Ni} + x_{Fe}\mu_{Fe}$). Widom 1 and 2 integration methods are used to compute $G_V^{for}(x_{Ni})$.

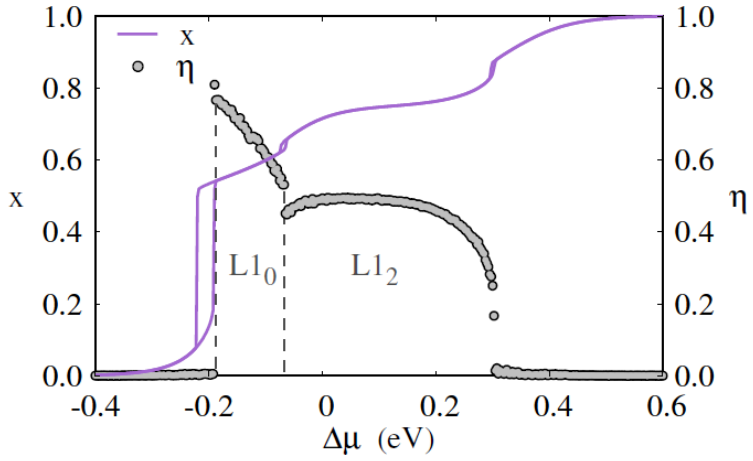

Figure II.21. Evolution of the Ni concentration x and long-range order parameter η of the PIM for Fe-Ni alloys at 600 K, as a function of $\Delta\mu = \mu_{Ni} - \mu_{Fe}$

- *Disordered solid solutions*

Examples of four isotherms $G_V^{for} = f(x_{Ni})$, at $T = 1000$, 1523, 2000 and 3000 K are shown in Figure II.22. The comparison shows some minor differences between the results obtained with Widom 1 and 2. At $T = 1000$ K, the difference reaches a maximum value of about 0.04 eV around the concentration of $x_{Ni} = 0.55$ (it corresponds to a factor 0.63 on the vacancy concentration) and decreases outside this concentration range. The difference reduces to 0 at the two sides of concentrations for about $x_{Ni} < 0.05$ and $x_{Ni} > 0.85$. It decreases with increasing temperature and vanishes at $T = 3000$ K. Both methods agree well with the modified Bragg-Williams approximation, equation (II-36), at sufficient temperatures (approx. $T > 1500$ K). The agreement is slightly better with Widom 1.

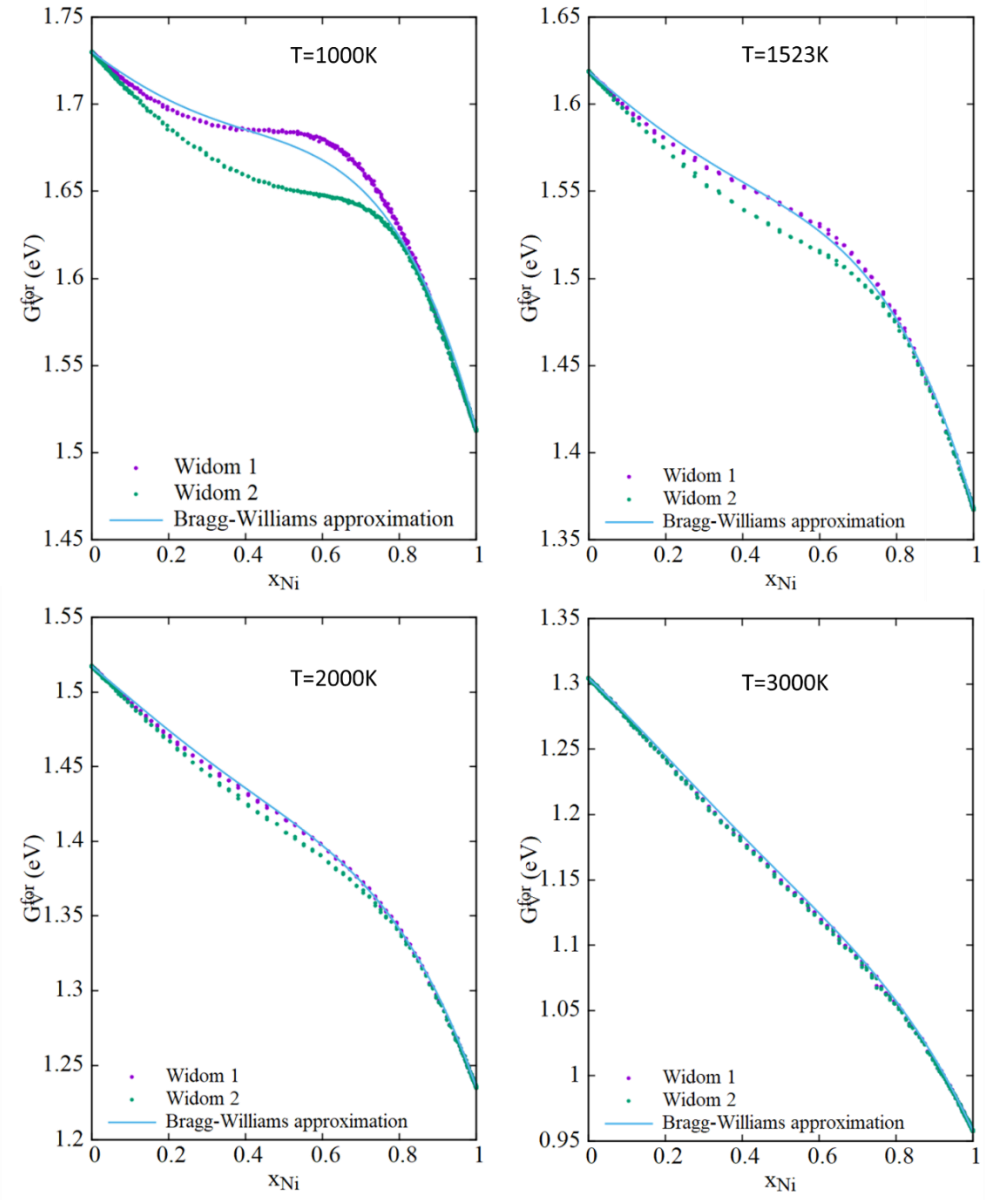

Figure II.22. Gibbs free energy of vacancy formation energy in Fe-Ni solid solutions at different temperatures: comparison between the Bragg-Williams approximation, Widom 1 and Widom 2

- *Ordered phases*

At 700 K (Figure II.23), the γ solid solution is stable in the whole composition range, except between $x_{Ni} = 0.67$ and $x_{Ni} = 0.82$, where the $L1_2$ phase is stable, but not perfectly ordered, with a long range order parameter $\eta = 0.85$ for the stoichiometric composition. Widom 1 and 2 methods give again similar results in the dilute solid solutions, and in the $L1_2$ phase, where G_V^{for} presents a local maximum, with G_V^{for}~1.77 eV. The Hagen and Finnis model gives a slightly larger value G_V^{for}~1.79 eV, because of the partial order (the model is valid for an almost perfect order, with isolated antisites). The difference between Widom 1 and 2 is larger between $x_{Ni} = 0.3$ and 0.6, with a maximum of 0.07 eV, at $x_{Ni} = 0.57$.

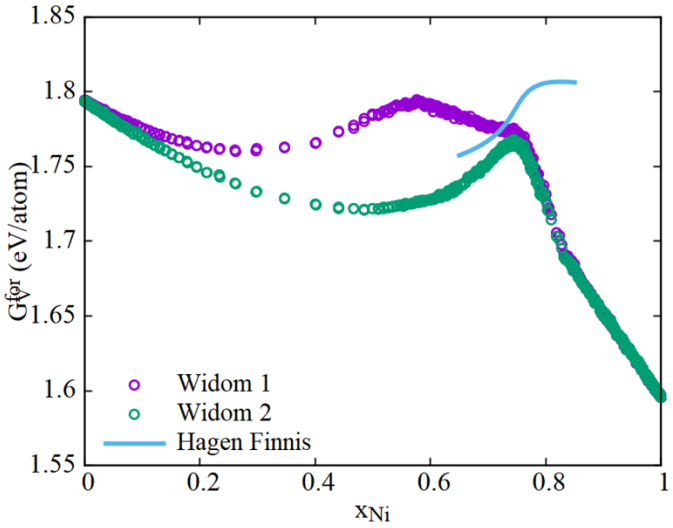

Figure II.23. Gibbs free energies for the vacancy formation in Fe-Ni alloys at 700 K, computed with Widom 1 and Widom 2 methods, and compared with the model of Hagen and Finnis for the $FeNi_3$-$L1_2$ phase

At 500 K (Figure II.24), the $L1_2$ is well ordered (with $\eta = 0.98$), and the two Widom methods are in good agreement with the Hagen and Finnis model for the stoichiometric composition $x_{Ni} = 0.75$, with $G_V^{for} = 1.87$ eV. Widom 1 and Widom 2 methods give also very similar results in the γ solid solution between $x_{Ni} = 0.77$ and $x_{Ni} = 1$. But they significantly differ between $x_{Ni} = 0.20$ and 0.75. For the stoichiometric FeNi-$L1_0$ phase, at $x_{Ni} = 0.5$, the difference is approximately 0.15 eV, Widom 1 method being in better agreement than Widom 2 with the Hagen and Finnis model.

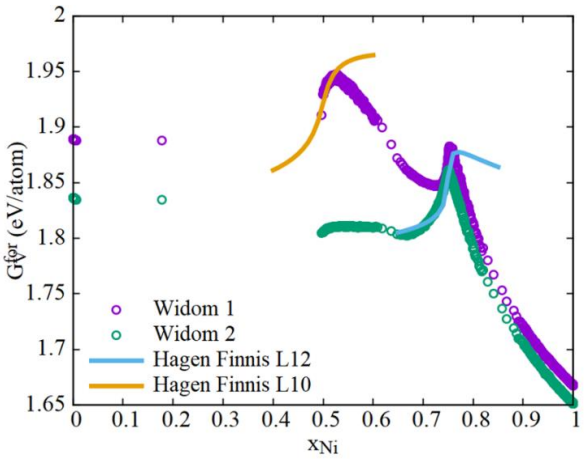

Figure II.24. Gibbs free energies for the vacancy formation in Fe-Ni alloys at 500 K, computed with Widom 1 and Widom 2 methods and compared with the model of Hagen and Finnis for the $L1_0$ and $L1_2$ structure.

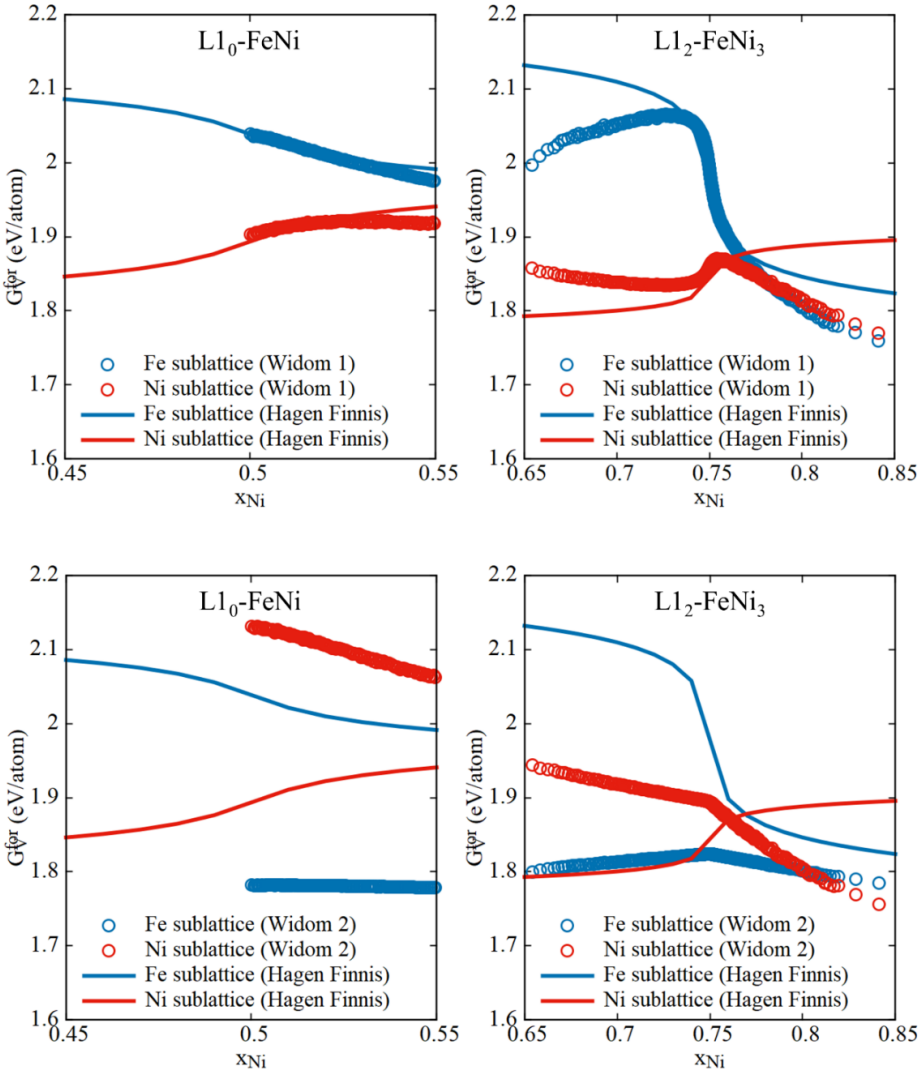

Figure II.25. Gibbs free energies for vacancy formation on the Fe and Ni sublattices of the $L1_0$-FeNi and $L1_2$-FeNi$_3$ phase, at 500 K. Top: Widom 1 method vs Hagen & Finnis, Bottom: Widom 2 method vs Hagen & Finnis model.

In Figure II.25, we distinguish the Gibbs free energy of vacancy formation on the Fe and Ni sublattices, at the same temperature. There is a good agreement between Widom 1 and the model of Hagen and Finnis, in the two ordered structures $L1_0$-FeNi and $L1_2$-$FeNi_3$, in a narrow concentration range around the stoichiometry. The results of Widom 2 are significanctly different from the model of Hagen and Finnis, sometimes by more than 0.2 eV.

As a conclusion, both methods give similar results in solid solutions at high temperatures, in the range of the diffusion experiments. At lower temperatures, in the ordered phases they give also similar Gibbs free energies G_V^{for} in the $L1_2$ phase, near $x_{Ni} = 0.75$. Both agree well with the Hagen and Finnis model, when the phase is perfectly ordered. The Widom 1 method is also in good agreement with the Hagen and Finnis model, for the G_V^{for} on the Fe and Ni sublattices, while Widom 2 is significantly different. For the well-ordered $L1_0$ phase at $x_{Ni} = 0.5$, Widom 1 is also in good agreement with Hagen and Finnis, contrary to Widom 2.

On the whole, the Widom 1 method seems more reliable than Widom 2, especially in the ordered phase, where the Hagen and Finnis model provides a safe reference. We will therefore use it in the following simulations of diffusion in concentrated alloys, and also for ordering kinetics of $FeNi_3$ in the next chapter (even if it uses the equilibrium chemical potentials, we will come back to this point later). It turns out that in these cases – the only ones for which we have some experimental observations – the choice is not a critical one indeed, because Widom 1 and 2 happen to give almost the same results. It would be interesting to test the same methods in other systems, to see if the same conclusions apply.

II.3.5 Diffusion coefficients in concentrated alloys

II.3.5.1 Tracer diffusion coefficients in concentrated alloys

As discussed above, G_V^{for} and the equilibrium vacancy concentration $x_V^{eq} = \exp(-G_V^{for}/k_BT)$ can be calculated by Widom 1 method in a concentrated alloy. The tracer diffusion coefficients of Fe and Ni can then be obtained with AKMC simulations performed with one vacancy and the appropriate time rescaling (eq. II-32).

We will use the same k-PIM parameters as in the dilute alloys, with an additional optimization of the saddle-points interactions, already mentioned in section II.3.3.5: we introduce here a dependence of g_{NiFe}^{SP} and g_{Fe}^{SP} on the local concentration around the saddle-point position, x_{Ni}^{SP}, adjusted to the experiments to improve the results of the AKMC simulations. This concentration is defined by the number of Ni atoms among the four first-nearest neighbors –sites (i) in Figure II.17. The concentration dependence is given by:

$$g_{NiFe}^{SP}(x_{Ni}^{SP}) = (x_{Ni}^{SP})^2[g_{NiNi}^{SP} - g_{NiFe}^{SP}(x_{Ni}^{SP} = 0)] + g_{NiNi}^{SP}$$
$$g_{FeNi}^{SP}(x_{Ni}^{SP}) = (x_{Ni}^{SP})^2[g_{FeNi}^{SP}(x_{Ni}^{SP} = 1) - g_{FeFe}^{SP}] + g_{FeFe}^{SP} \quad \text{(II-40)}$$

The resulting values of g_{NiFe}^{SP} and g_{FeNi}^{SP} are given in Table II.19, and shown in Figure II.29. The comparison between the experiments and the AKMC simulations, before and after optimization, is given in Figure II-28.

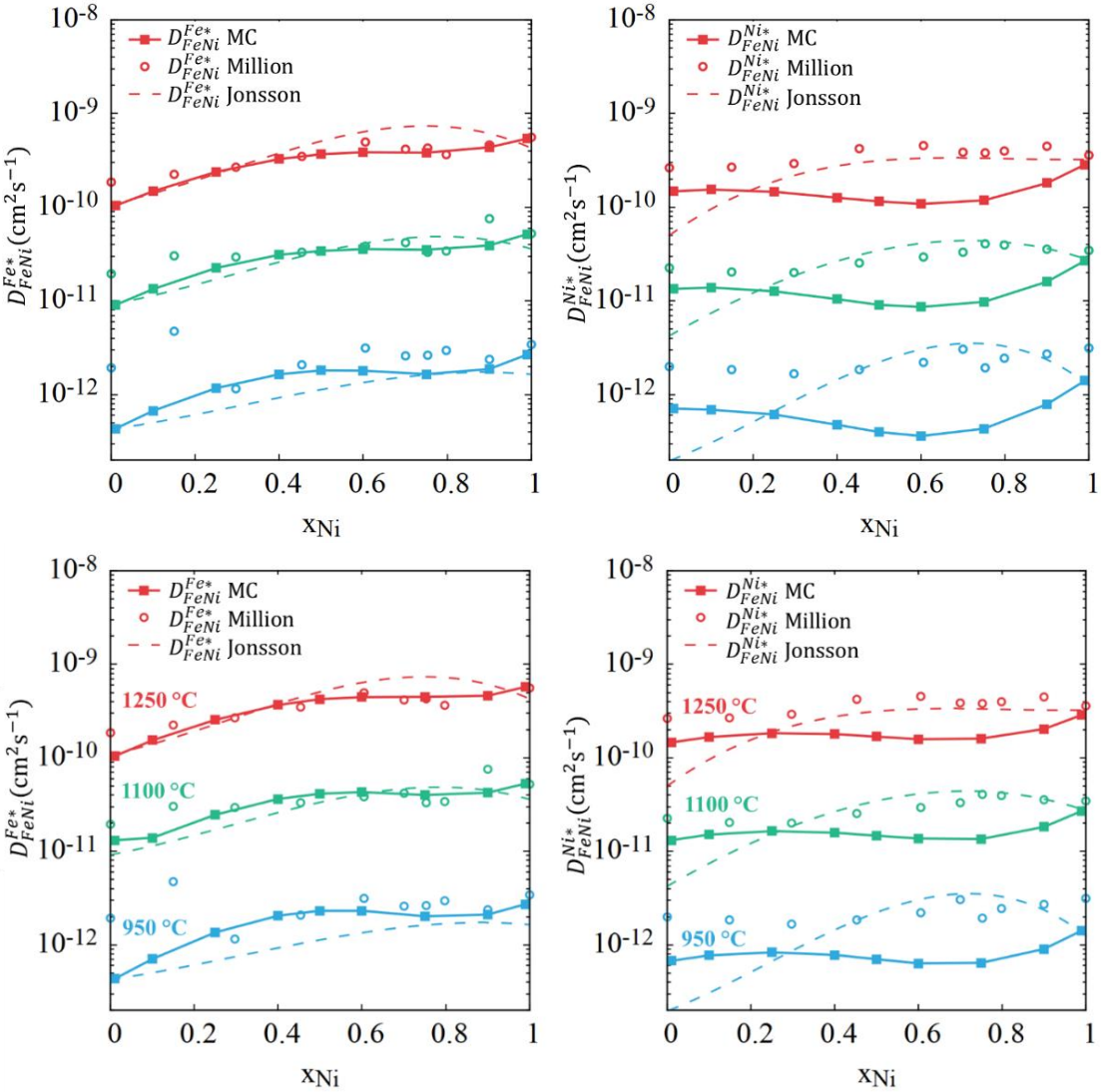

Figure II.26. Tracer diffusion coefficients of Fe and Ni in fcc Fe-Ni alloys at different temperatures and concentrations: comparison between the AKMC simulations (full squares), the experiments of Million (open circles), and the estimation of Jönsson (dotted line). Top figures: before optimization (g_{NiFe}^{SP} and g_{FeNi}^{SP} constant); bottom figures: after optimization (g_{NiFe}^{SP} and g_{FeNi}^{SP} depend on x_{Ni}^{SP})

Table II.17. The local concentration dependence of $g^{SP}_{NiFe}(x^{SP}_{Ni})$ and $g^{SP}_{FeNi}(x^{SP}_{Ni})$ in eV [see eq. (II-40)]

x^{SP}_{Ni}	0	0.25	0.5	0.75	1
g^{SP}_{FeNi}	-2.66934	-2.68207	-2.72025	-2.78389	-2.87298
g^{SP}_{NiFe}	-2.76156	-2.76689	-2.78287	-2.80951	-2.8468

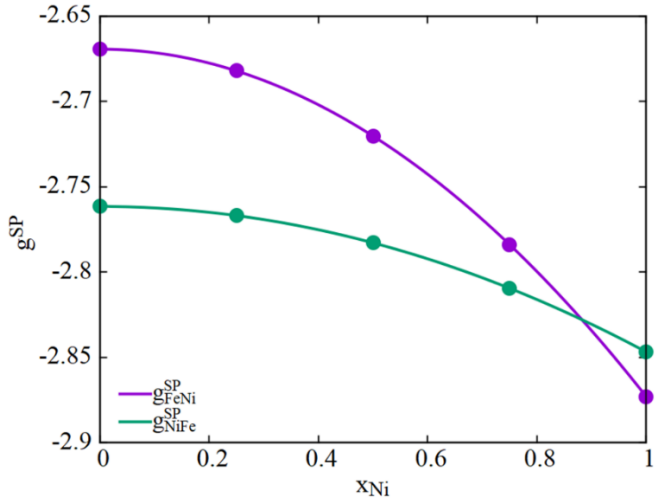

Figure II.27: function showing the concentration dependence for $g^{SP}_{NiFe}(x^{SP}_{Ni})$

There is a good general agreement between the results of the Fe tracer diffusion coefficients between the AKMC simulations and the experiments. The optimization slightly improves the agreement with the experiments of Million *et al.* at 950°C and for $x_{Ni} > 0.5$. The main discrepancy is between the value of Million *et al.* at $x_{Ni} = 0$, and both our results and the estimation of Jönsson. The reason is that the values of the self-diffusion coefficients $D^{Fe^*}_{Fe}$ of Million *et al*. are above those of most other studies. The discrepancy is limited, except at 950°C, but here one must mention a very practical problem. There is an ambiguity for this temperature in the paper of Million *et al*.: the same data is given with a different temperature in the figure (950°C) and in the table (985°C). We have retained the value 950°C (this value is also retained, without any comment, in the Landolt-Bornstein database. Therefore, for the comparison with these experiments, we will rely more on the two other temperatures (1100 and 1250°C).

For the tracer diffusion coefficients of Ni, there are more differences between the AKMC simulations, Jönsson and Million *et al*., especially on the Fe rich side. At $x_{Ni} = 0$, this is again because the values of Million *et al.* for $D^{Ni^*}_{Fe}$ are above those selected by Jönsson (as discussed in section II.3.3.5, see Figure II.5). The results of our simulations are between the two. At $x_{Ni} = 1$, the three sets of data agree for $D^{Ni^*}_{Ni}$, except Million *et al* at 950°C (with the problem mentioned above for this particular temperature). After optimization, our simulations give an evolution of $D^{Ni^*}_{FeNi}$ with x_{Ni} similar to that of Million *et al*, but shifted downwards by a factor of 2 or 3.

II.3.5.2 Interdiffusion coefficients. Test of the Darken equation.

We will now use the k-PIM to model the interdiffusion coefficients in Fe-Ni solid solutions, compare them with the tracer diffusion coefficients, and test the Darken equations, as in the experiments of Million *et al.* discussed in section II.2.3.4.

It is difficult to model in the simulations the conditions of a typical interdiffusion experiment, i.e. start from a pure Fe/pure Ni couple, simulate the interdiffusion of Fe and Ni, and deduce $\widetilde{D}(x_{Ni})$ from the concentration profile with the Matano method. One of the difficulties is that at the atomic scale, it is difficult to keep a well-defined interface. It quickly becomes rough, with oscillations perpendicular to the interdiffusion direction.

For this reason, we will use the sinusoid method, which can also be used in real experiments. This method consists in measuring the attenuation rate of a sinusoidal concentration wave of small amplitude (Chang and Giessen 1985). The initial configuration in the x direction is shown schematically in Figure II.28, with a concentration profile $x_{Ni}(x, t = 0) = x_{Ni} + A_0 \sin(2\pi x/\lambda)$, an initial amplitude A_0 of a few percent and a wavelength λ.

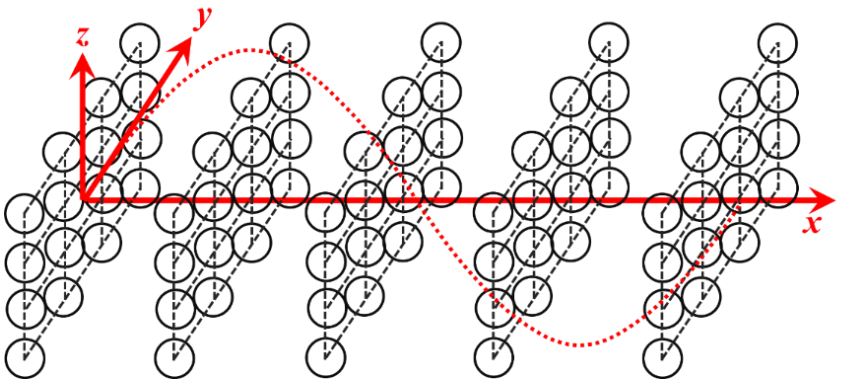

Figure II.28. Sinusoidal profile of Ni concentration on different planes in a lattice.

When the solid solution is stable, the concentration wave vanishes. It can be shown that if λ is large enough, the amplitude decreases exponentially with time (Figure II.29), according to:

$$\frac{d\ln(A - A_0)}{dt} = -\widetilde{D}\left(\frac{2\pi}{\lambda}\right)^2 \qquad \text{(II-41)}$$

$\widetilde{D}$ can be directly estimated by measuring the evolution of the amplitude A.

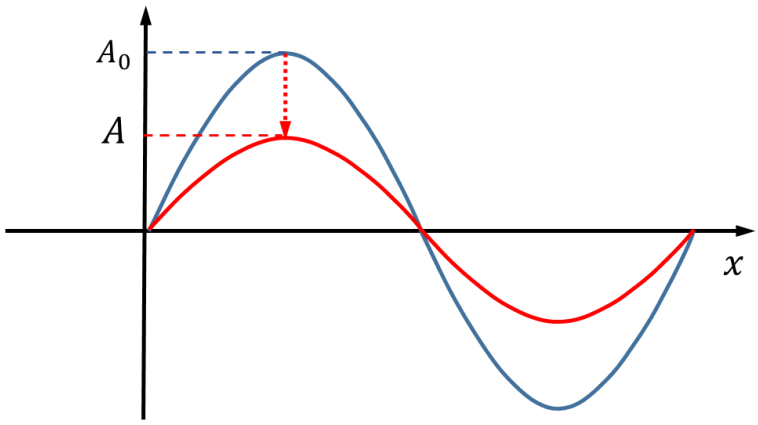

Figure II.29: Attenuation of the concentration wave

The advantage is that the concentration profile remains well defined in the x direction, the main drawback is that one simulation must be performed for each composition x_{Ni} (with the standard method, one gets the whole $\widetilde{D}(x_{Ni})$ curve with one concentration profile).

The kinetic Monte Carlo simulations have been performed with an initial amplitude $A = 0.02$, $N = 64 \times 1024 \times 1024/2$ atoms (64 atomic planes in the *x* directions, and 1024×1024 fcc sites in the perpendicular planes: due to the small amplitude, a large number of atoms per plane is required to get a sufficient precision on the concentration profile). Figure II.30 gives an example of attenuation of the sinusoidal concentration profile at $T = 1523$ K. The exponential attenuation predicted by eq. (1) is clearly verified (Figure II.31).

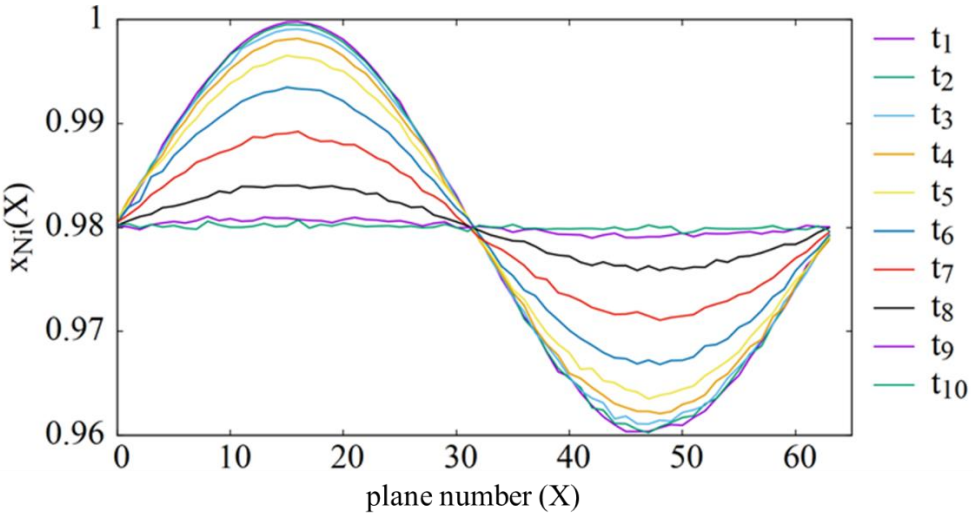

Figure II.30. AKMC simulation: evolution of a sinusoidal concentration profile in a Fe-98%Ni solid solution at 1523 K.

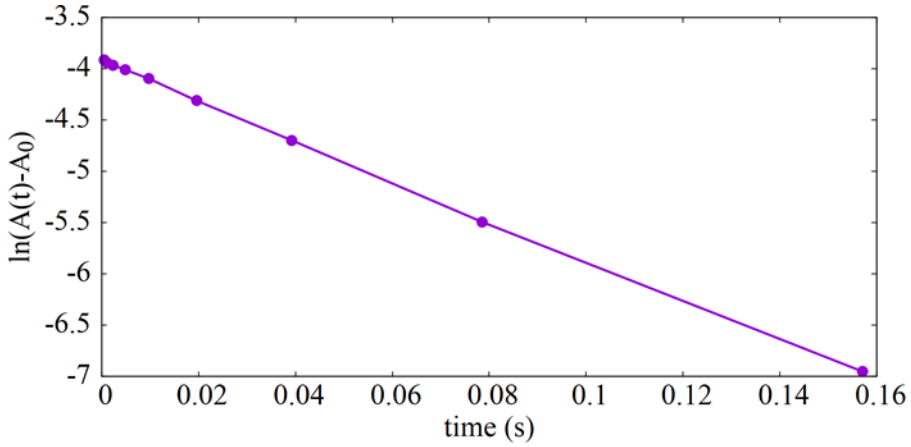

Figure II.31. AKMC simulation: evolution of the amplitude A with time.

The simulations have been performed with the same k-PIM parameters and with the same time rescaling method as for the tracer diffusion coefficients, with the averaged concentrations $x_{Ni} = 0.02, 0.1, 0.25, 0.4, 0.5, 0.6, 0.75, 0.9, 0.98$ at $T = 1223$, 1373 and 1523 K (as in the experiments of Million *et al.* (Million et al. 1981)). The results are shown in Figure II.32.

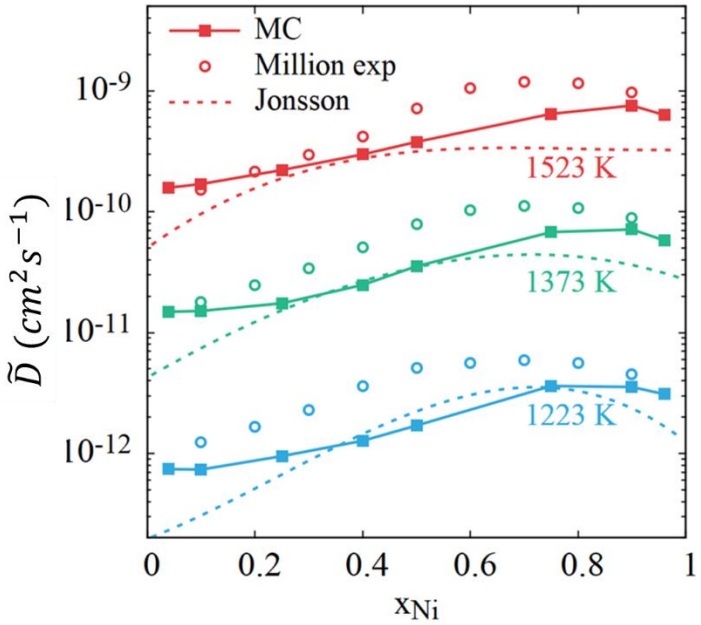

Figure II.32. Interdiffusion coefficients measured by AKMC simulations (solid lines with full squares), by Million's experiments (open circles) and by Jönsson's fitting functions (dashed lines)

The AKMC measurements are between the results of Million *et al.* and Jönsson fitting functions. In the dilute alloys, $x_{Ni} \to 0$ and $x_{Ni} \to 1$, the Monte Carlo simulations predict values higher than Jönsson, by a factor 3 approximately, and are closer to those of Million *et al*. The $\widetilde{D}(x_{Ni})$ relationship is less curved than in the experiments.

One can then test Darken equation:

$$\widetilde{D} = \left(x_A D_{AB}^{B^*} + x_B D_{AB}^{A^*}\right)\Phi \qquad \text{(II-42)}$$

using the thermodynamic factor Φ of our PIM and the tracer diffusion coefficients obtained in our previous simulations (Figure II.26).

Let us first recall that in the experiments of Million *et al.*, some differences were observed between the measured interdiffusion coefficient $\widetilde{D}$ and those predicted from the Darken equation. Million *et al*. did not conclude that the Darken equation was invalid in Fe-Ni alloys, due to the experimental uncertainties (coming e.g. from diffusion at grain boundaries). Another possible origin of the discrepancy could be the thermodynamic factor they used, which is slightly different from recent evaluations. Figure II.33 compares the thermodynamic factor of Million *et al*. to the one of Cacciamani *et al* (Cacciamani et al. 2010), used in our PIM (see Chapter I, section III.A).

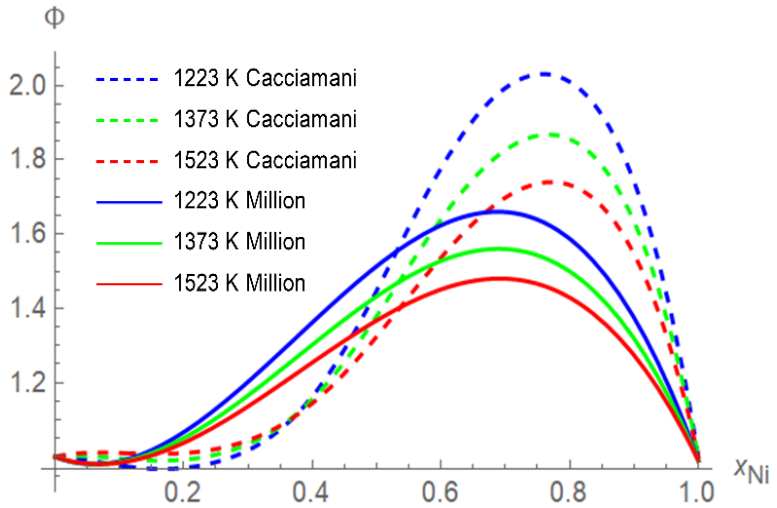

Figure II.33. Evolution of the thermodynamic factor versus Ni content in Fe-Ni, according to Million et al (Million et al. 1981) and to Cacciamani et al. (Cacciamani et al. 2010)

Figure II.34 shows a comparison between the interdiffusion coefficients measured by Million *et al*, to those calculated from their tracer diffusion coefficients and the Darken equation, with the two thermodynamic factors. The differences are slightly reduced when using Cacciamani's thermodynamic factor.

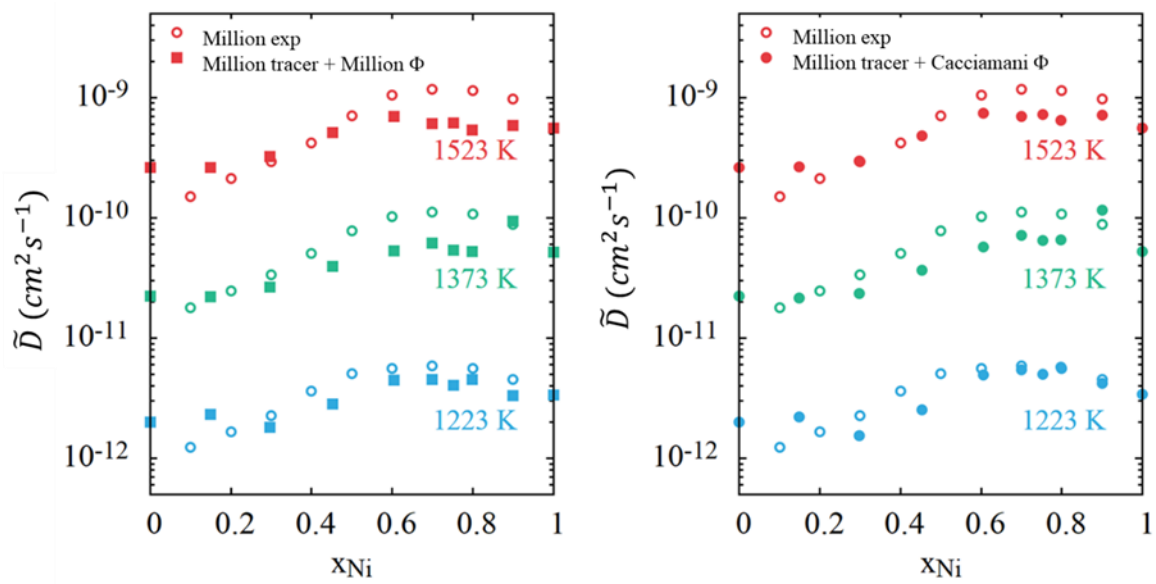

Figure II.34. Interdiffusion coefficients directly measured (open symbols) compared to those obtained using Darken equation (full symbols) and two different thermodynamic factors: left Φ of Million; right: Φ of Cacciamani

The same comparison can be done with the AKMC simulations: the results are shown in Figure II.35. The interdiffusion coefficients calculated from the simulated tracer diffusion coefficient and the Darken equation are very close to those directly simulated (they are slightly lower, contrary to what was obtained by Million *et al*). One can conclude that in our model, the Darken equation is almost valid. This does not mean that this equation is exactly true in Fe-Ni alloys: there is no reason to believe that the non-diagonal terms of the Onsager matrix, such as L_{NiV} and L_{FeV} are completely negligible. However, they cannot be derived safely from the deviation from the Darken equation, observed in the existing experimental studies by Million *et al*., because of uncertainties in the experiments.

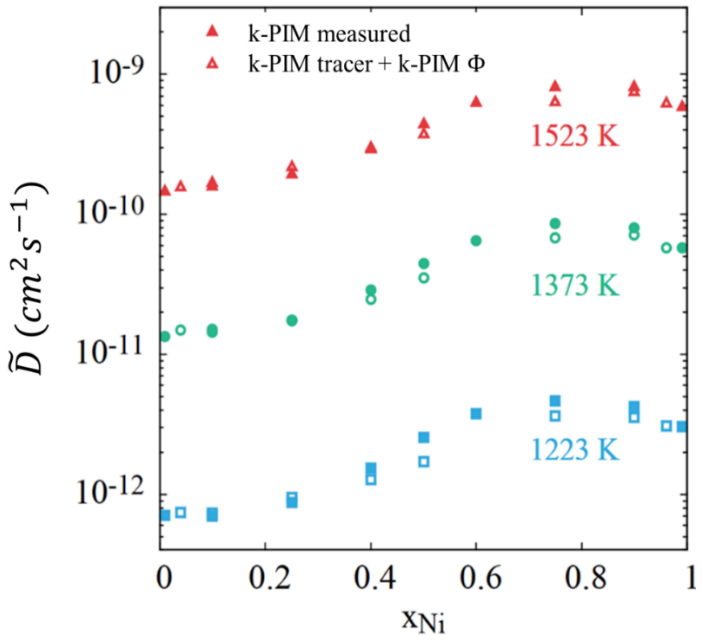

Figure II.35. Interdiffusion coefficients by direct measurement (empty symbols) and using Darken equation (full symbols) obtained by kinetic Monte Carlo simulations

II.3.5.3 Diffusion coefficients in ordered structure and at the transition of order-disorder

In this section, we are going to predict the effect of the $L1_2$ order-disorder transition on the diffusion of Fe in Ni in a Fe-75%Ni alloy, using the k-PIM and same AKMC method as in section II.3.5.1. Unfortunately, no experimental data are available in that case, probably because diffusion is slow below the transition temperature $T_c^{L1_2}$ (slow but not null: the growth of ordered domains is observed over times of the order of 100-1000 h, down to 60°C below the transition temperature, as we will see in Chapter III. Experimental measurements of diffusion may not be impossible).

AKMC simulations of Fe and Ni tracer diffusion coefficients in Fe-75%Ni, for temperatures from T = 500 K to T = 1500 K, are shown in Figure II.36. At high temperature, in the solid solution, Fe atoms diffuse slightly faster than the Ni atoms (as in pure Ni). Below $T_c^{L1_2}$, one observes a curvature of the Arrhenius plot, similar to what was observed in other systems (section II.2.2.4). The curvature is more pronounced for Fe than for Ni and in the ordered $L1_2$ phase, Ni diffuses faster than Fe.

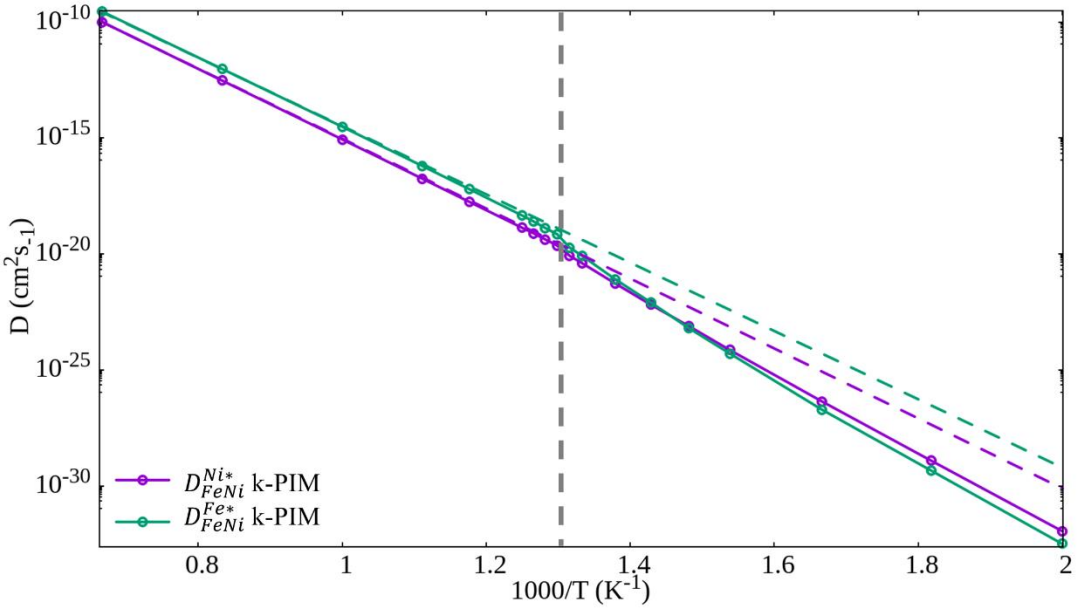

Figure II.36: AKMC simulations of the tracer diffusion coefficients of Fe and Ni in Fe-75%Ni. The dashed lines represent the extrapolation of the Arrhenius law of the disordered alloy below $T_c^{L1_2}$ (vertical dashed line)

The tracer diffusion coefficients in the disordered solid solutions can be fitted by $D_{FeNi_3}^{Fe^*} = 1.8\exp(-2.93\ [\text{eV}]/k_BT)\ [\text{cm}^2.\text{s}^{-1}]$ and $D_{FeNi_3}^{Ni^*} = 1.2\exp(-3.0\ [\text{eV}]/k_BT)\ [\text{cm}^2.\text{s}^{-1}]$. In the ordered $L1_2$-$FeNi_3$ phase, they can be fitted to Girifalco's model: $D = D_0\exp[-\Delta H_{dis}(1+\alpha S^2)/k_BT]$ (equation (II-29)), with $\alpha \approx 0.11$ for Fe^* and $\alpha \approx 0.06$ for Ni^* (Figure II.36).

Let us emphasize that these results have been obtained with the k-PIM parameters used to model diffusion at high temperatures, in the solid solutions. We have seen that these parameters give vacancy formation enthalpies in the $L1_2$-$FeNi_3$ phase which are significantly larger than those calculated from first principles methods by Li (Table II.18). (Note that the DFT calculations have been performed at 0 K, whereas the values of the k-PIM model are given at T = 50 K, to avoid divergences coming from the magnetic contributions, see Chapter I, section II.C.2). Contrary to the k-PIM, the DFT calculations predict that the vacancy formation enthalpies in the $L1_2$-$FeNi_3$ ordered phase are lower than in the solid solution.

Table II.18. Vacancy formation energies on the Fe and Ni sublattices of the $L1_2$ and $L1_0$ ordered structures. Comparison between the DFT calculation and the k-PIM (unit: eV)

	$G_{V_{Fe}}^{for}(FeNi_3 - L1_2)$	$G_{V_{Ni}}^{for}(FeNi_3 - L1_2)$	$G_{V_{Fe}}^{for}(FeNi - L1_0)$	$G_{V_{Ni}}^{for}(FeNi - L1_0)$
Li	1.388	1.594	1.897	1.847
This work	2.115	1.956	2.140	1.996

- *Modified k-PIM*

For the diffusion in the ordered phase, we therefore propose a modified k-PIM, hereafter referred as k-PIM2, which includes a transition between high-temperature parameters, derived from experiments, and low temperatures parameters, derived from DFT calculations (as has been done for the thermodynamic properties and phase diagram, see Chapter I, section II.C.3).

This adjustment is introduced through the change of the vacancy formation energy in Fe and Ni, while the vacancy migration barriers will be kept the same. At low temperatures, k-PIM2 is adjusted on the vacancy formation energies in the ordered structure $L1_2$ $FeNi_3$ of DFT calculations. At temperatures higher than the order-disorder transition temperature, the k-PIM2 parameters remain the same as in k-PIM, so that the diffusion properties in solid solutions do not change. The resulting evolution of the Gibbs free energies for vacancy formation with the temperature, on the two sublattices of the ordered $L1_2$ $FeNi_3$ phase, is shown in Figure II.37.

The new tracer diffusion coefficients are shown in Figure II.38, and compared with those obtained with the original k-PIM: one observes that the curvature is strongly reduced with k-PIM2. This is due to the change in the vacancy formation energy. For example, at T = 600K, the k-PIM gives $G_V^{for}(FeNi_3 - L1_2) = 1.95$ eV while the k-PIM 2 gives $G_V^{for}(FeNi_3 - L1_2) = 2.20$ eV. The difference of 0.25 eV gives a factor of $\exp(0.25/(k_B T) \approx 125$, which corresponds to the difference on the tracer diffusion coefficients in Figure II.38.

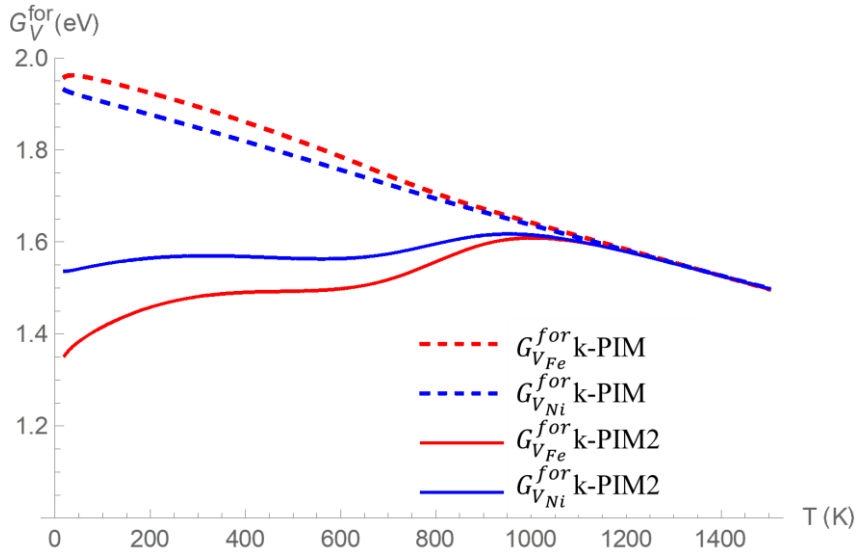

Figure II.37. Gibbs free energies for vacancy formation on the Fe and Ni sublattices of the ordered $L1_2$ $FeNi_3$ phase, in k-PIM and k-PIM2

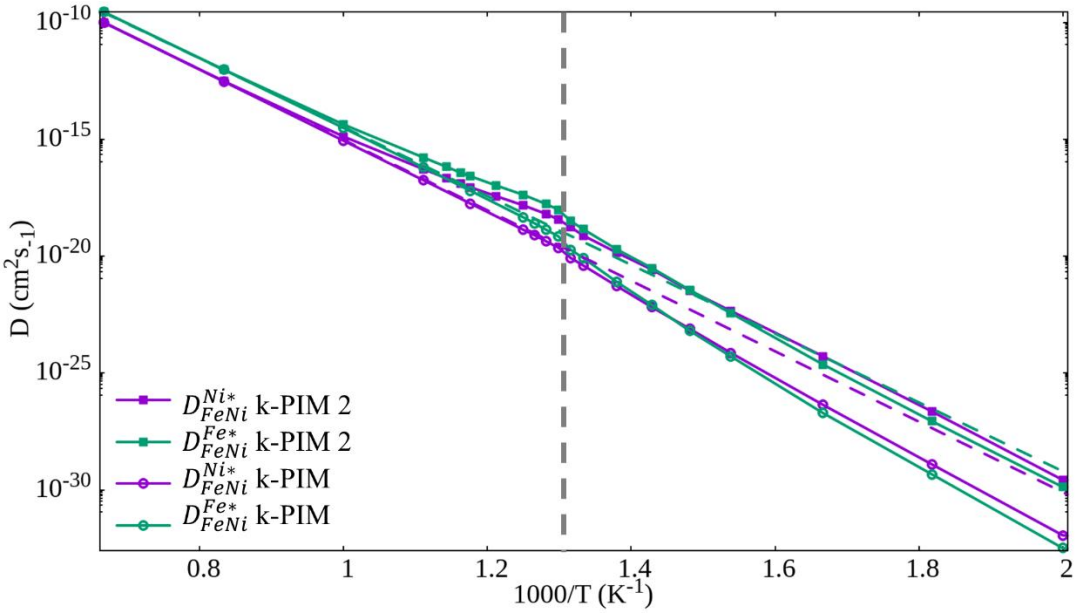

Figure II.38. AKMC simulations of tracer diffusion coefficients of Fe and Ni in Fe-75%Ni: comparison between k-PIM and k-PIM 2.

II.4 Conclusions

In this chapter, the pair interaction model (PIM) developed in Chapter I, to model the thermodynamic properties of Fe-Ni alloys, has been extended to a kinetic model (k-PIM) to model vacancy and atomic diffusion properties. As in Chapter I, our strategy has been to fit the k-PIM parameters on existing DFT calculations (usually at 0 K) and experimental data (usually at high temperatures). The additional k-PIM parameters (atom-vacancy and saddle-point pair interactions) are temperature and concentration-dependent pair interactions, divided in enthalpic and (non-configurational) entropic terms, and in magnetic and non-magnetic terms.

The tracer and interdiffusion coefficients of the k-PIM are measured by AKMC simulations, using a time rescaling to take into account the evolution of the vacancy concentration with the alloy composition. For this purpose, we have used a new method, based on the Widom insertion technique. This new method is in good agreement with the Bragg-Williams approximation at high temperatures, in fully disordered solid solutions, and with the model of Hagen & Finnis at low temperatures, in perfectly ordered structures.

One limitation of the approach is that existing DFT and experimental data are scarcer for point defects and diffusion than for thermodynamic properties, especially in concentrated alloys. Important assumptions have therefore been made to “fill the gaps”: for example, based on partial experimental and theoretical evidences, we have assumed that the magnetic transition does not affect the point defect properties and the diffusion coefficients.

In spite of these limitations, we were able to reproduce with one set of parameters all existing experimental diffusion data: tracer and interdiffusion coefficients, in a large range of temperatures and compositions. The difference between the model and the experiments (typically a factor 2 or 3) are of the same order as the differences between the experiments. If new experimental or theoretical results were to lead us change some of our assumptions, it should be easy to modify the relevant parameters within the same formalism. To give an example, the very recent results of Li *et al*. (Li, Fu, and Schneider 2021), based on Monte Carlo simulations DFT based effective interaction models, suggest that there is a small discontinuity of G_V^{for} at the Curie point in pure fcc Fe and Ni, less important that in bcc Fe but not zero.

The approach is applied to a system that has actually a simple behavior: in Fe-Ni solid solutions, the evolution of the tracer diffusion with the composition is limited and almost linear. We think however that the same methods could be useful to model other systems, with more complex behaviours. We have found that the difference between the tracer and interdiffusion coefficients can be reasonably well predicted by the Darken equation. Finally, our first AKMC simulations predict a strong effect of the A1/$L1_2$ ordering transition in the $FeNi_3$ alloy on the tracer diffusion coefficients, when using the k-PIM (i.e. an increase of the diffusion enthalpy in the $L1_2$ phase). The effect is significantly reduced however, when the k-PIM is modified to give at low temperatures the vacancy formation enthalpies calculated from first principles.

Chapter III Kinetics of ordering in fcc Fe-Ni alloys

III.1 Introduction

We are now going to study the kinetics of ordering in Fe-Ni alloys, using the k-PIM and AKMC tools developed in the two previous chapters. We will limit ourselves to the ordering of the $FeNi_3$-$L1_2$ phase, for which three experimental studies are available, dating back to the 1970s (Calvayrac and Fayard 1973; Morris et al. 1976; Ferjani, Bley, and Calvayrac 1977). These studies provide detailed information on the evolution of the long range parameter, $\eta(t)$, and of the size of ordered domains, $L(t)$, during isothermal annealings at temperatures slightly below the critical ordering temperature, $T_c^{L1_2}$. The ordering of the FeNi-$L1_0$ phase occurs at lower temperatures, on (literally) astronomic times: is has been only observed in meteorites (Scorzelli 1997), or under irradiation where it can be accelerated by the increase of point defects concentrations (Reuter, Williams, and Goldstein 1989). It is thus beyond the scope of our study.

After a brief review of the experimental results (section III.2), we will give some details on the AKMC simulations (section III.3). The simulations will use the two sets of parameters developed in the previous chapter: k-PIM, derived from the modelling of diffusion coefficients in the paramagnetic solid solutions and k-PIM2, fitted on the enthalpies of vacancy formation in the $L1_2$ phase computed by DFT calculations. We will present the methods used in the simulations to measure the evolution of the long range order parameter $\eta(t)$ and the domain size $L(t)$, and discuss the use of the Widom method to take into account the evolution of the vacancy concentration during the ordering process (i.e. in a non-equilibrium situation). The comparison between the simulations and the experiments will be presented in section III.4.

III.2 Experimental observations of ordering process in $L1_2$-$FeNi_3$

Calvayrac and Fayard studied the evolution of the long-range order parameter and average domain size during the ordering process of $L1_2$-$FeNi_3$ by X-ray diffraction (Calvayrac and Fayard 1973). The evolution of the long-range order parameter at $T = 480$°C (753 K) and $T = 497$°C (770 K) in the stoichiometric Fe-75%at.Ni alloy is shown in Figure III.1, together with the one of the Fe-73%at.Ni

alloy at $T = 480$°C (753 K). According to the authors, the absolute values of the long-range order parameter (LRO) are difficult to determine in their experiments: they therefore only provide a "relative" LRO parameter, $\eta(t)/\eta_\infty$, where η_∞ is the value of $\eta(t)$ after a long time, sufficient for the alloy to reach equilibrium (500 h in that case). In these conditions, the LRO parameter has almost reached its equilibrium value after approximately 100 h.

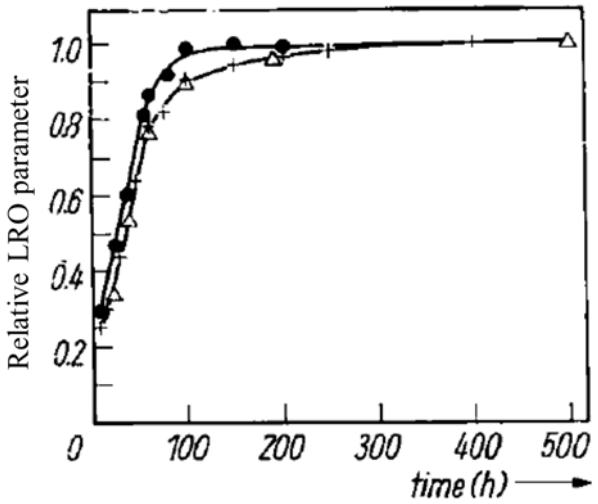

Figure III.1. Evolution of the relative long-range order parameter with time: ● Fe-73%Ni at T = 480°C (753 K); Δ Fe-75%Ni at T = 480°C (753 K); + Fe-75%Ni at T = 497°C (770 K) (Calvayrac and Fayard 1973)

The evolution of the average domain size is shown in Figure III.2. According to Calvayrac and Fayard, two stages can be distinguished: a rapid one at the beginning of the ordering, then a slower one with a growth exponent close to 1/2 (i.e. $L^2 - L_0^2 \cong kt$).

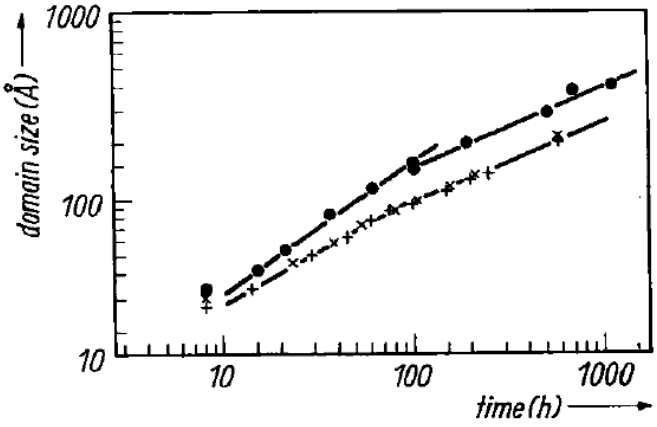

Figure III.2. Kinetics of the growth of ordered domains during isothermal annealing: ● Fe-75%Ni at T = 497°C (770 K); + Fe-75%Ni at T = 480°C (753 K); × Fe-73%Ni at T=480 °C (753 K)(Calvayrac and Fayard 1973)

Morris *et al.* did a somewhat more systematic study of the ordering process and domain growth in $L1_2$-$FeNi_3$ over the temperature range from 434°C (707 K) to 497°C (770 K) using transmission electron microscopy (TEM) and X-ray diffraction (Morris et al. 1976). The evolution of the long-range order parameter η obtained at different temperatures is shown in Figure III.3. Note that these authors give the absolute values of the LRO parameter: at 497°C (770 K) for example, just below the order-disorder transition temperature of $L1_2$-$FeNi_3$ ($T_C^{L1_2}$), the alloy is only partially ordered at equilibrium, with $\eta \sim 0.8$.

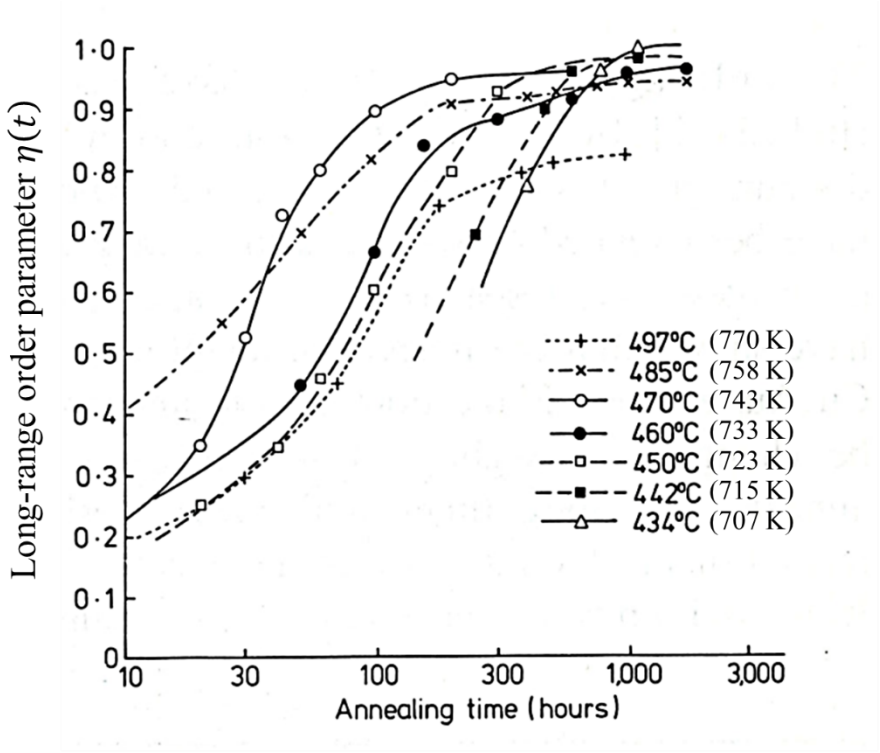

Figure III.3. Evolution of the long-range order parameter as a function of annealing time at different temperatures in Fe-75%Ni (Morris et al. 1976)

The effect of the temperature on the ordering kinetics is summarized on the Time-Temperature-Transformation (TTT) diagram of Figure III.4, which gives the time required to get a value of the LRO parameter at different temperatures. One observes a standard behavior: the ordering rate is maximum at

approximately 480°C (753 K) and decreases at lower temperature (due to a slower diffusion) and at higher temperature (due to the decrease of the ordering driving force).

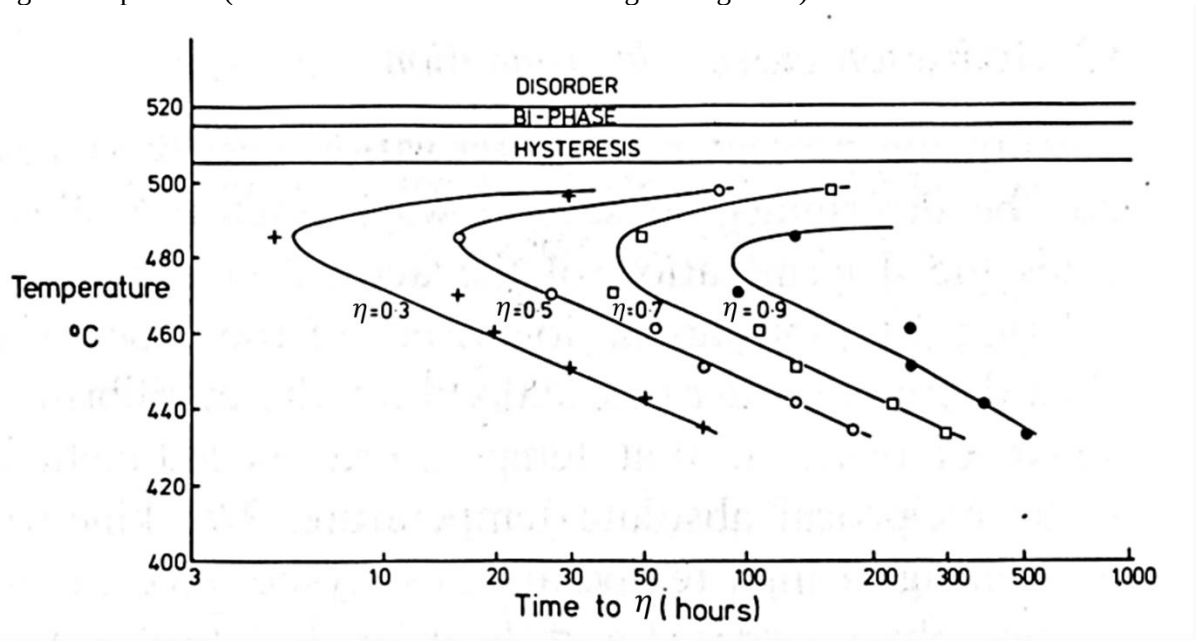

Figure III.4. Time-Temperature-Transformation diagram of ordering kinetics in Fe-75%Ni during isothermal annealing (Morris et al. 1976)

The evolution of the average domain size, measured by TEM, is given in Figure III.5. As Calvayrac and Fayard, Morris found that at high temperature [470°C (743 K) – 497°C (770 K)], two successive stages for the domain growth can be distinguished. At lower temperature, only one stage was observed. The evolution of the domain size L can be fitted by a power law: $L \sim t^n$, the constant n varing from 0.21 to 0.49 depending on the annealing temperature.

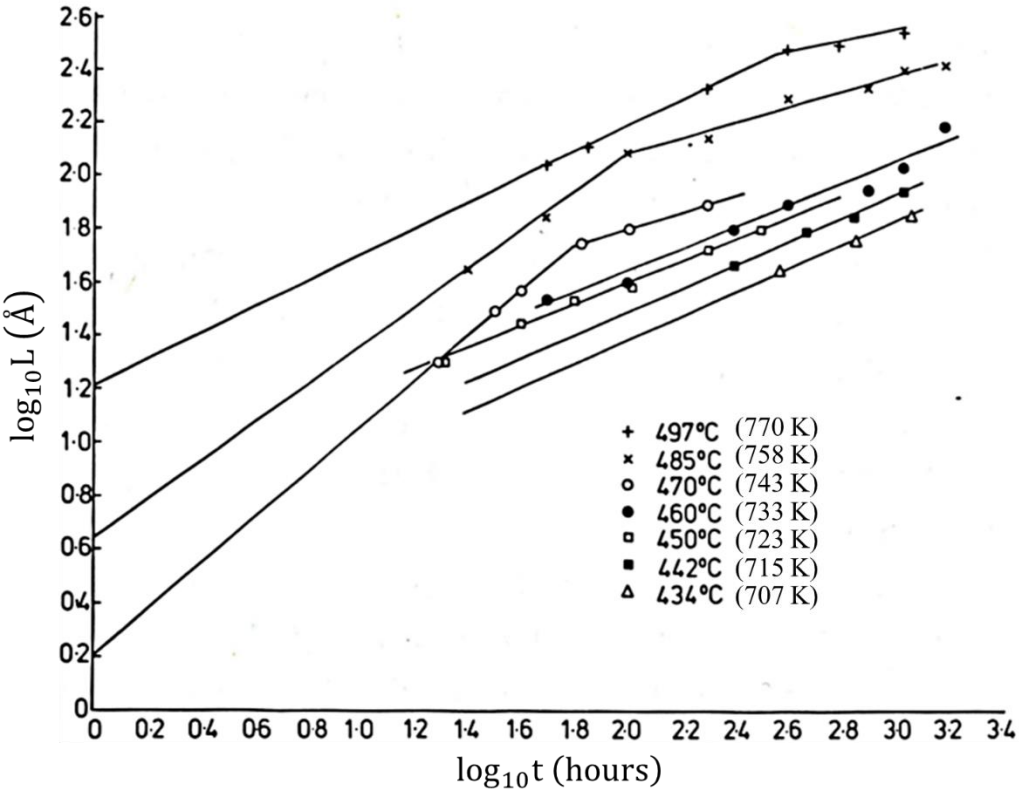

Figure III.5. Domain growth as a function of time and temperature in Fe-75%Ni (Morris et al. 1976)

Ferjani *et al.* did similar measurements in Fe-75%Ni at $T = 470$°C (743 K) and $T = 478$°C (751 K) (Ferjani, Bley, and Calvayrac 1977). Their results are shown in Figure III.6 and Figure III.7. As Calvayrac and Fayard, they only considered the relative LRO parameters, which reach unity at the final annealing time.

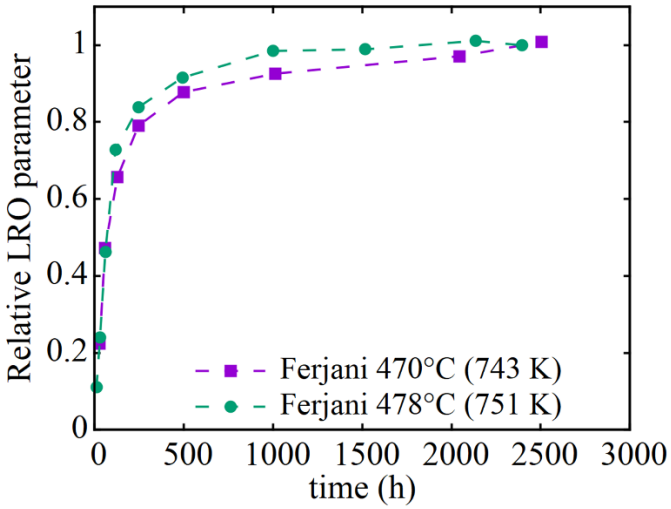

Figure III.6. Evolution of the relative long-range order in Fe-75%Ni at 470°C (743 K) and 480°C (753 K) (Ferjani, Bley, and Calvayrac 1977)

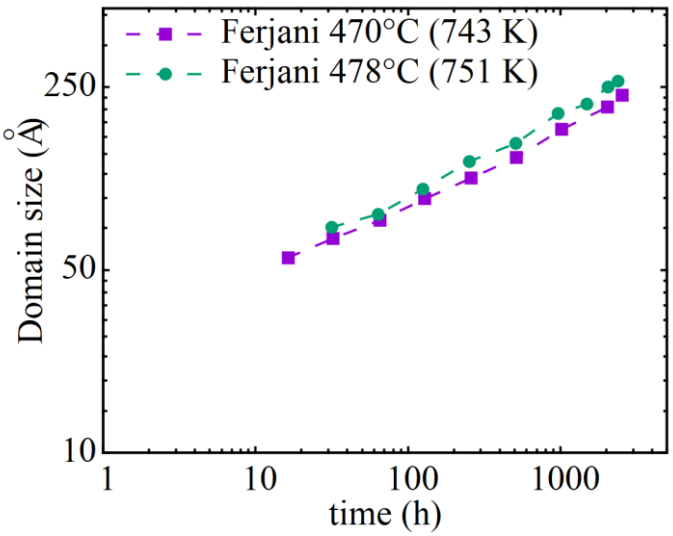

Figure III.7. Evolution of the average domain size versus annealing time in Fe-75%Ni at 470°C (743 K) and 480°C (753 K) (Ferjani, Bley, and Calvayrac 1977)

As discussed above, these studies were carried out at different temperatures (Table III.1). Fortunately, one is common to Calvaray and Fayart and to Morris *et al.* [470°C (743 K)] and one to Ferjani *et al.* and to Morris *et al.* [497°C (770 K)], which allows a direct comparison.

Table III.1. Temperature condition of different experiments (°C)

Calvayrac							480		497
Morris	434	442	450	460	470			485	497
Ferjani					470	478			
T in K	(707)	(715)	(723)	(733)	(743)	(751)	(753)	(758)	(770)

The comparison between the results of Morris *et al.* and those of Ferjani *et al.* at $T = 470$°C (743 K) is shown in Figure III.8. We show the LRO parameters of Morris *et al.* in relative value (divided by the value at the maximum annealing time), so that they can be directly compared to those of Ferjani *et al.*

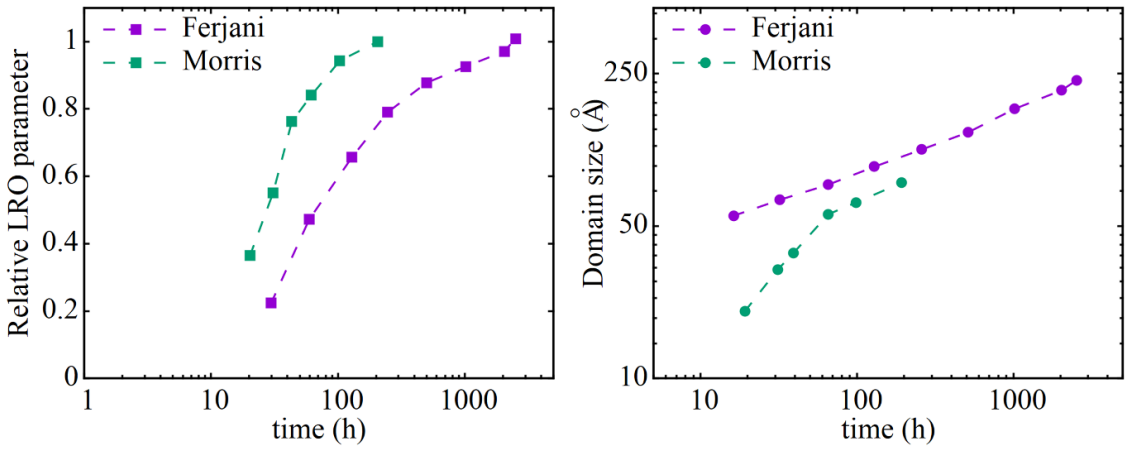

Figure III.8. Evolution of relative long-range order (left) parameter and the domain size (right) in Fe-75%Ni: comparison between Ferjani (Ferjani, Bley, and Calvayrac 1977) and Morris (Morris et al. 1976) at T=470 °C (743 K).

One observes some significant differences between the two studies. Morris *et al.* observed a faster evolution of the LRO parameter than Ferjani *et al.*, by approximately a factor 2 at the beginning and 10 at the end of the annealing. By contrast, the domain size evolution is about 3 times slower in Morris *et al.* than in Ferjani *et al.* Morris *et al.* observed two stages on the growth of domain, with a change in the growth rate at $t \sim 65$ h, while Ferjani *et al.* reported only one stage at this temperature.

By eliminating the time, one can show the evolution of the domain size as a function of the relative long-range order parameter, $L(\eta/\eta_\infty)$. In this way, the results of Morris and Ferjani are compared in Figure III.9. The two experiments shown two different kinetic paths, Morris *et al.* predicting a slower growth of more ordered domains than Ferjani *et al.*

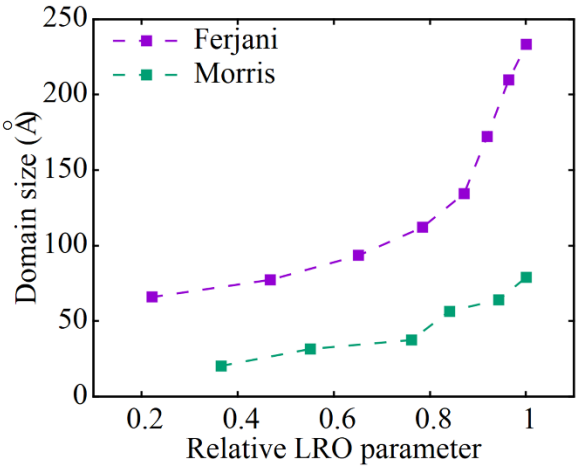

Figure III.9. Evolution of the ordered domain size as a function of relative long-rang order parameter in Fe-75%Ni at T=470 °C (743 K): comparison between the observations of Ferjani et al. (Ferjani, Bley, and Calvayrac 1977) and Morris et al. (Morris et al. 1976).

The same comparison can be done between the results of Morris *et al.* and Ferjani *et al.* at $T =$ 497°C (770 K), as shown in Figure III.10 and Figure III.11.

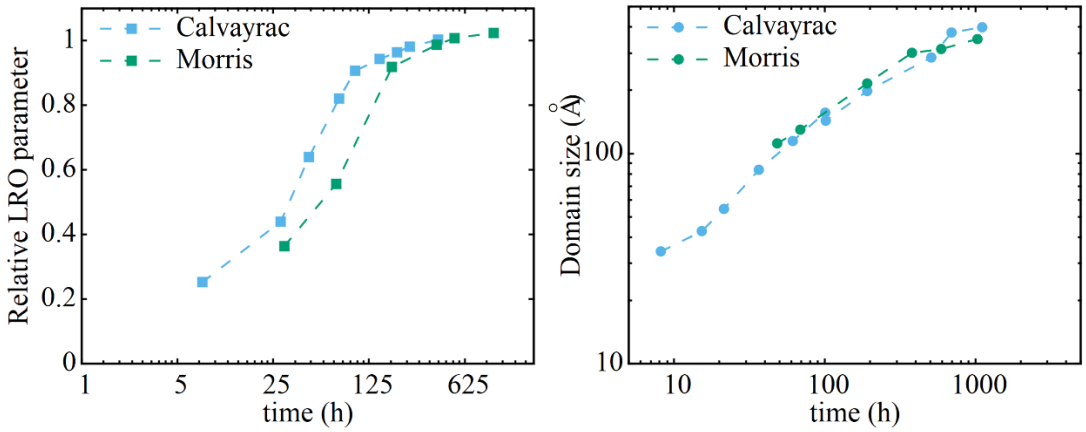

Figure III.10. Evolution of the relative long-range order parameter (left) and the domain size (right) in Fe-75%Ni at T=497°C. Comparison between the observations of Calvayrac and Fayard (Calvayrac and Fayard 1973) and Morris et al. (Morris et al. 1976).

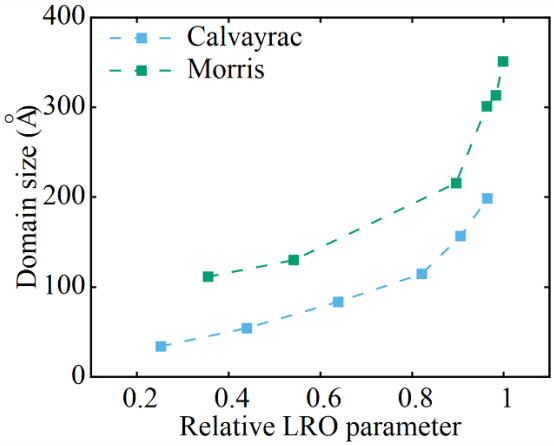

Figure III.11. Evolution of the domain size as a function of relative long-rang order parameter in Fe-75%Ni at T=497°C (770 K): comparison between the observations of Calvayrac and Fayard (Calvayrac and Fayard 1973) and Morris et al. (Morris et al. 1976).

The two studies are in good agreement for the evolution of the domain size, while Morris *et al.* observed an evolution of long-rang order parameter slightly slower than that of Calvayrac and Fayard. The shapes of the $\eta(t)$ curves are nevertheless similar.

III.3 AKMC simulations: methods

III.3.1 Vacancy concentrations and the Widom method

The k-PIM and k-PIM2 parameters are used in the following AKMC simulations, performed with one vacancy and the time rescaling method as described in Chapter II. However, unlike the previous chapter we now consider an alloy that is not at equilibrium, and where the vacancy concentration changes with time. We use a standard adiabatic approximation, by considering that for each transient state of the alloy, the vacancy concentration immediately adjusts to its equilibrium value, because vacancies diffuse much more rapidly than atoms.

To estimate the equilibrium value at each time, $x_v^{eq}(t)$, we use the Widom 1 method as presented in section II.3.4.2 (Chapter II). In practice, we start from a random solid solution and performed vacancy jumps using the residence time algorithm. From time to time, $G_V^{for}(t)$ and $x_v^{eq}(t)$ are evaluated with the Widom 1 method. The time between two evaluations must be short enough, so that the system has changed very little in between, but not too short, to save some computation time (in practice, 1000 measurements are typically done during an AKMC simulations of 6×10^9 MCS). We have chosen to use the Widom 1 method because we have seen that, in some cases (for example in the Fe-50%Ni alloy), it gives better estimations of x_v^{eq}. As already mentioned, this method uses the equilibrium potentials of Fe and Ni atoms, μ_{Fe} and μ_{Ni}, for the composition and temperature of interest. During the ordering process, the alloy is not at equilibrium and therefore μ_{Fe} and μ_{Ni} are not the same on the different sublattices, as long as they have not reached their equilibrium concentration (similarly, in a case of precipitation, they would not be the same in the precipitate and the matrix). The use of the equilibrium potentials can nevertheless be justified if we assume that a local equilibrium is very rapidly reached around the vacancy – because diffusion occurs rapidly in its vicinity. Note that in this specific case (the Fe-75%Ni alloy), we found that the Widom 2 method gave very close vacancy concentration and ordering kinetics. For example at T=434 °C (707 K), in the Fe-75%Ni alloy, the Gibbs free energies of vacancy formation given by Widom 1 and 2 only differ by 0.003 eV, which corresponds to a factor 1.05 on the timescale. But as indicated in section II.3.4.3 (Chapter II), Widom 1 gives a better estimation of the equilibrium vacancy concentrations on the Fe and Ni sublattices. In the Fe-50%Ni alloy, the difference between Widom 1 and 2 would also be more important (0.15 eV at 500 K). Therefore we will consider that in general, Widom 1 is a safer choice.

III.3.2 Measurement of long-range order parameter and domain size

As discussed in III.2, in the experiments the ordering process of a system is characterized by the evolution of the long-range order parameter, η, and the size of the ordered domains, L. These domains

belong to one of the 4 variants of the $L1_2$ phase, which corresponds to the four sublattices defined in Chapter I (III.A), and are separated by antiphase boundaries (APB). The LRO parameter of a given domain, η can be measured from the concentration of Ni atoms upon the four different sublattices of the fcc structure. However, the method cannot be used to measure the averaged value of η when several domains of different variants coexist. In such a case, it is better to measure the LRO parameter from the structure factor $S(\boldsymbol{k}, t)$, of the system (Domb, Green, and Lebowitz 1976):

$$S(\boldsymbol{k}, t) = \frac{1}{N} \langle \left| \sum_{\boldsymbol{r}} e^{i\boldsymbol{k}\cdot\boldsymbol{r}} (x(\boldsymbol{r}, t) - \bar{x}) \right|^2 \rangle \tag{III-1}$$

where $x(\boldsymbol{r}, t) = 0$ or 1 is the Ni atomic fraction on each site $\boldsymbol{r}$ and $\bar{x}$ the average Ni atomic fraction. $S(\boldsymbol{k}, t)$ is computed using a fast Fourier transform algorithm. In an ordered $L1_2$ structure, some superstructure peaks appear for specific vectors $\boldsymbol{k_S}$ in the reciprocal space – in addition to those of the fcc lattice. The intensity of one peak, I_s, is obtained by integrating the structure factor in a volume centered around $\boldsymbol{k_s}$. Then the long-range order η can be calculated as:

$$\eta = \sqrt{\frac{I_s}{I_s^0}} \tag{III-2}$$

where I_s^0 is the peak intensity in a perfect $L1_2$ structure. In our simulations, we compute the intensity of around the $\boldsymbol{k_s} = (1,1,0)$ peak, over all the vectors with $|\boldsymbol{k} - \boldsymbol{k_s}| < 0.1\boldsymbol{k_s}$ (Le Floc'h, Bellon, and Athènes 2000). The average size of domains (L) is calculated with the second moment of the structure factor, k_2 :

$$L \propto \sqrt{\frac{1}{k_2}} \tag{III-3}$$

where

$$k_2 = \frac{\sum_{\boldsymbol{k}}^{\boldsymbol{k}_{max}} |\boldsymbol{k}|^2 S(\boldsymbol{k}, t)}{\sum_{\boldsymbol{k}}^{\boldsymbol{k}_{max}} S(\boldsymbol{k}, t)} \tag{III-4}$$

The summations in equation (III-4) must be done will all the values of $\boldsymbol{k}$ in the reciprocal space where the structure factor $S(\boldsymbol{k}, t)$ is less than the background values obtained for a completely disordered configuration. For the calibration of the relation given by equation (III-3), several test simulations were carried out in systems of specific domain size. We found that equation (III-3) gives the correct values of the domain size.

On the other hand, in a homogeneous system the measurement of the LRO parameter by equation (III-2) gives the same value as that measured from the concentrations on the four sublattices, used in Chapter I. There is little size effect of the size of system on the evolution of the LRO parameter: we have compared the simulation results in systems of $N_0 = 4 \times 32^3$ and $N_0 = 4 \times 64^3$ and found practically no difference, except that in a larger system, there are less fluctuations.

III.4 Results and discussions

III.4.2 Long-range order parameter: comparisons between MC and experiments

Atomistic Kinetic Monte Carlo simulations of ordering kinetics have been carried out at different temperatures. All simulations were done in a system containing $N = 4 \times 64^3$ fcc sites (except specifically mentioned), with periodic boundary conditions. Therefore, the length of the system is about 225 Å. An example of microstructure evolution (using k-PIM2 parameters), in Fe-75%Ni, is shown in Figure III.12. To visualize the ordered domains, we use a different color for the Fe atoms located on the 4 sublattices, as in (Pareige et al. 1999). Starting from a random solution, one rapidly observes the formation of a high density of small ordered domains, equally distributed among the four variants. The evolution of LRO parameter, the domain size and the vacancy concentration are shown in Figure III.13.

The system starts to be partially ordered very shortly after the simulation begins (about several hours), and becomes completely ordered ($\eta \sim 0.8$, or $\eta/\eta_\infty \sim 1$) after approximately 10^3 hours. We can see that the measurement of the domain size by equation (III-3) (Figure III.13) actually matches the one observed on the microstructure, in direct space (Figure III.12.). During the ordering transformation, one observes a decrease of the vacancy concentration, from $x_v^{eq} \sim 1.6 \times 10^{-11}$ in the initial random solid solution, to $x_v^{eq} \sim 4.5 \times 10^{-12}$ in the final ordered state.

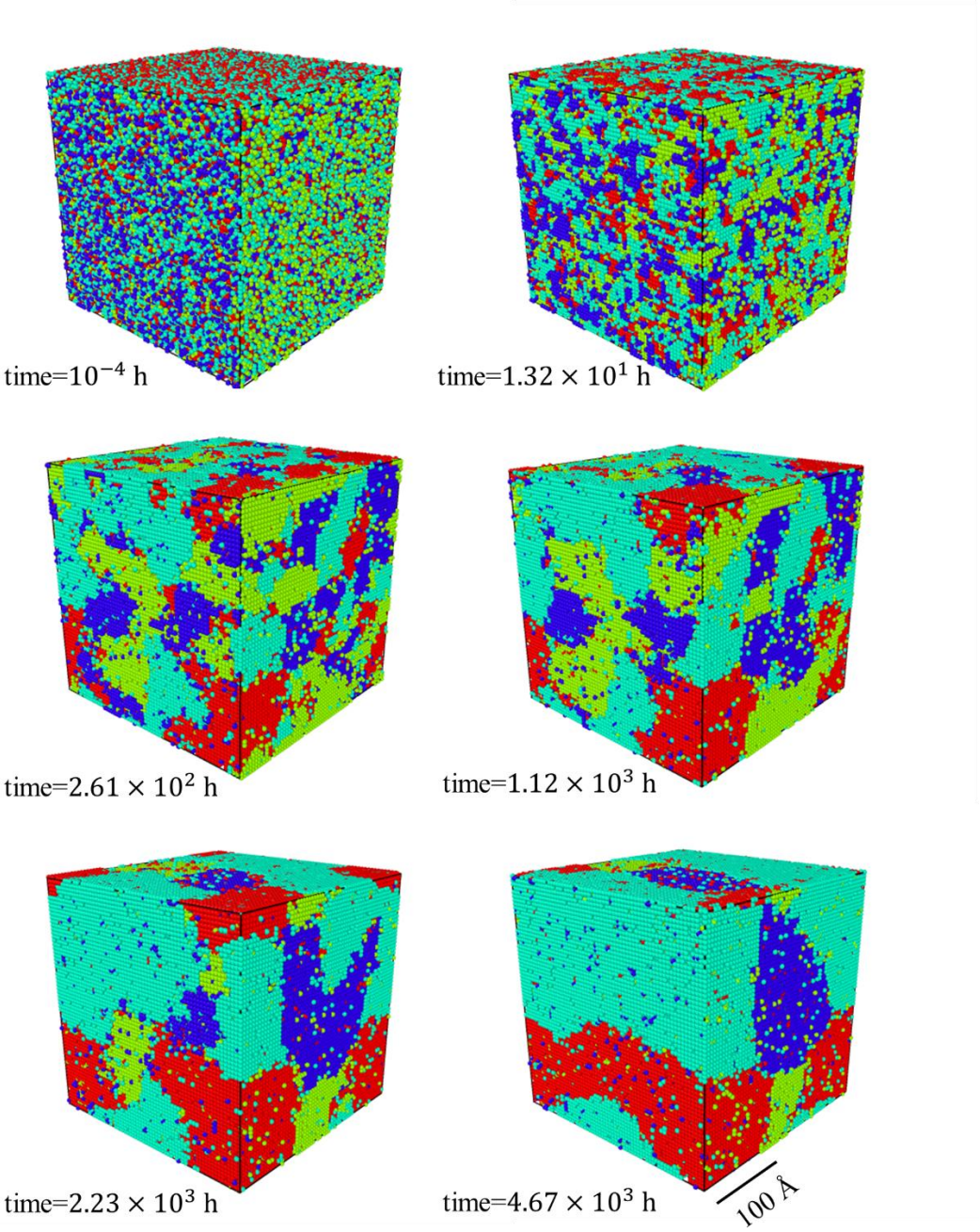

Figure III.12. AKMC simulation of ordering in Fe-75%Ni at 434°C (707 K), with the k-PIM2 parameters: evolution of the microstructure (with time in hours, only the Fe atoms are shown, with a different color for each variant).

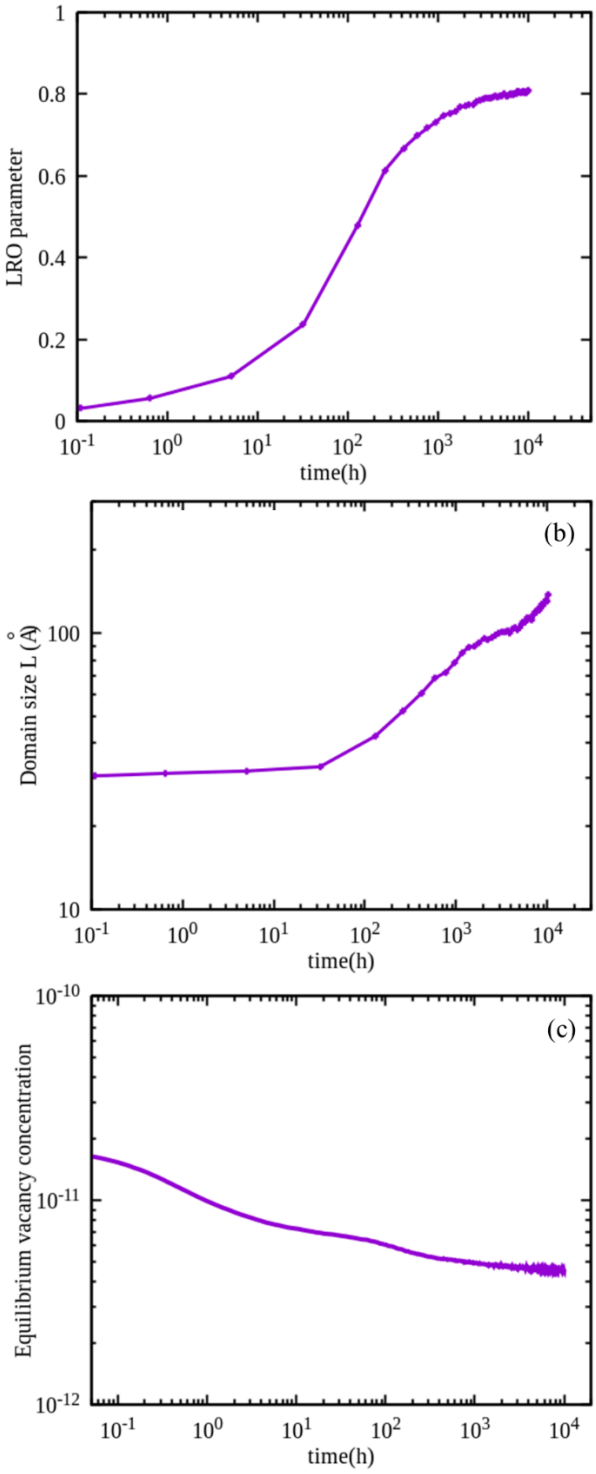

Figure III.13. AKMC simulation of ordering in Fe-75%Ni at T=434°C (707 K), with the k-PIM2 parameters. (a) evolution of the LRO parameter, (b) evolution of the domain size, (c) evolution of the equilibrium vacancy concentration.

In Figure III.14, the evolutions of the LRO parameter are compared with the experiments presented in section III.2. For the sake of the comparison we show the evolution of the relative LRO parameters η/η_∞, the only one given in the studies of Calvayrac and Fayard, and of Ferjani *et al.*

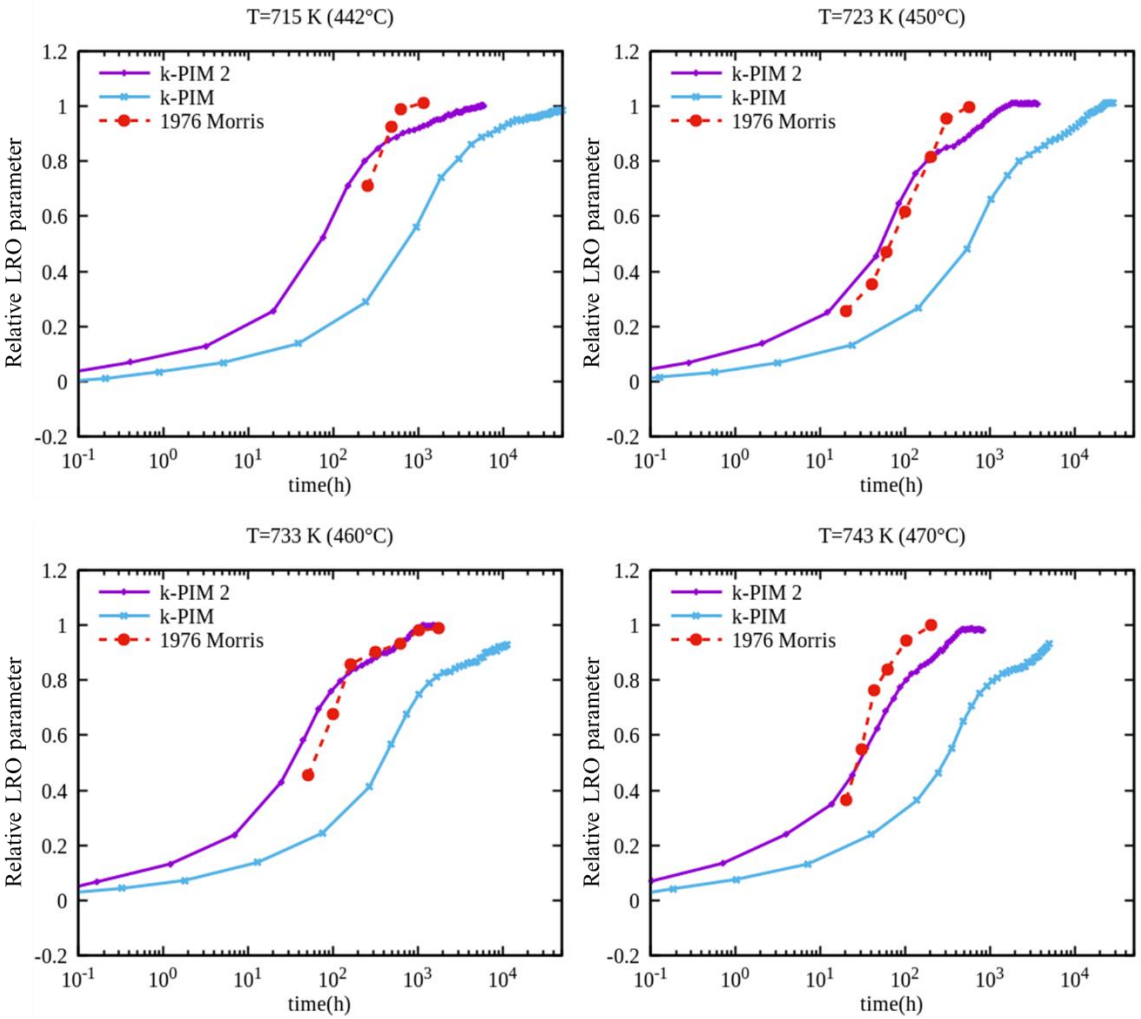

Figure III.14. Evolution of the relative long-range order parameter at T=442 °C (715 K), T=450 °C (723 K) ,T=460 °C (733 K) and T=470 °C (743 K) in Fe-75%Ni: comparisons between the experiments of Morris et al.(Morris et al. 1976) and the AKMC simulations.

The AKMC simulations performed with the k-PIM2 parameters are in good agreement with the experiments of Morris et al. (Morris et al. 1976). The simulations performed with the k-PIM parameters are approximately 10 times slower in this range of temperatures. This is due to the smaller Gibbs free energies of vacancy formation in the $L1_2$-$FeNi_3$ phase i.e. to the larger $x_v^{eq}(t)$, obtained by the k-PIM2 parameters, as shown in Figure III.15.

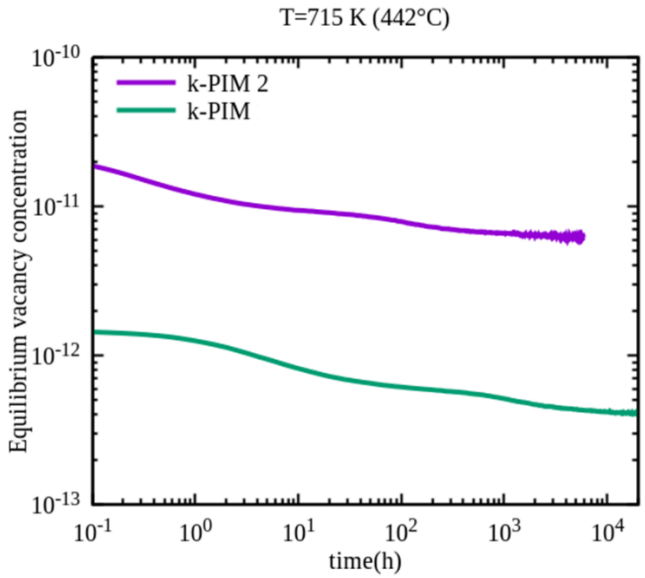

Figure III.15. Evolution of the equilibrium vacancy concentration during the ordering of a Fe-Ni75% alloy at T=442°C (715 K). AKMC simulations with k-PIM and k-PIM 2 parameters.

The comparison with the experiments of Ferjani *et al.* is shown in Figure III.16. As mentioned above, the kinetics of ordering is slower than the one observed by Morris *et al*. It falls between the kinetics predicted with the two sets of AKMC parameters.

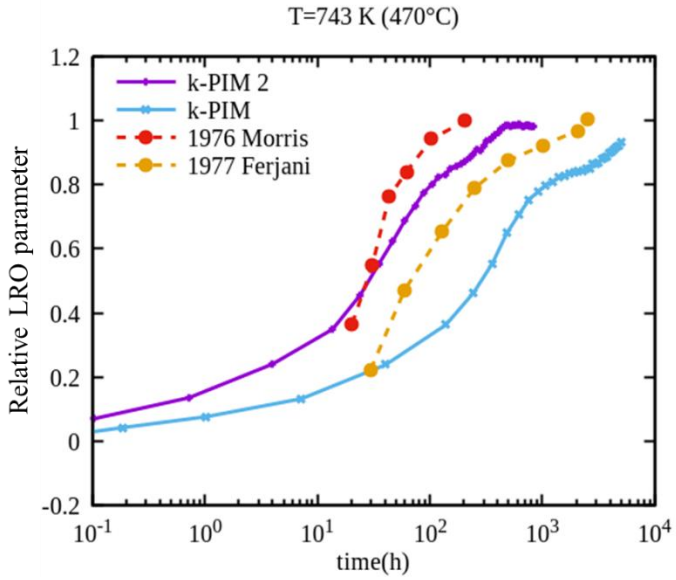

Figure III.16. Evolution of the long-range order parameter at T=470 °C (743 K) in Fe-75%Ni: comparison between the experiments of Ferjani et al (Ferjani, Bley, and Calvayrac 1977), Morris et al(Morris et al. 1976) and the AKMC simulations with k-PIM and k-PIM 2 parameters

Figure III.17 shows the TTT diagram obtained with the AKMC simulations (with the k-PIM and k-PIM 2 parameters), compared with the one of Morris *et al*. When plotting the absolute values of η, for the k-PIM 2, we observe that the simulations are in good agreement with the experiments at low

temperatures, but become slower above 730 K : this is due to the fact that our model gives a critical ordering temperature $T_c^{L1_2} = 765$ K, below the one estimated by Morris *et al.* (by approximately 25 K). The ordering driving force therefore decreases more rapidly in our model than in the experiments, when T increases. With the k-PIM parameters, the evolution of the LRO parameter is slower than in the experiments of Morris *et al.* by approximately a factor 10.

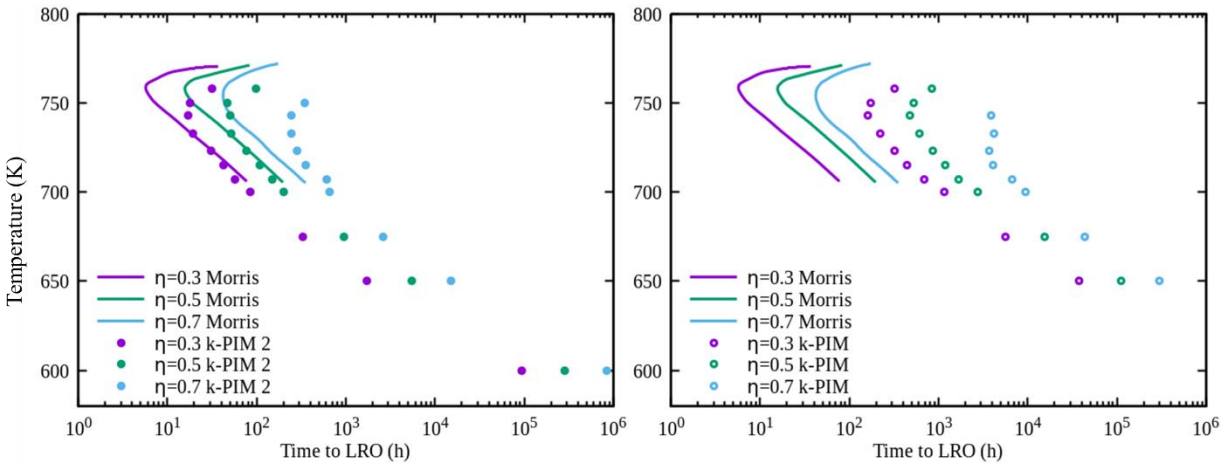

Figure III.18. Time-Temperature-Transformation diagram of LRO evolution in Fe-75%Ni comparison between the AKMC simulations and experiments of Morris et al.

III.4.3 Domain growth: comparisons between MC and experiments

The evolutions of the domain size, measured in the AKMC simulations are compared with the observations of Morris *et al*. in Figure III.19. With the k-PIM 2 parameters, there is a good overall agreement [slightly worse than for the LRO parameters: the simulations are 2 times faster than the experiments at 450°C (723 K), up to three times faster at 460°C (733 K)]. As for the LRO parameter, the simulations performed with the k-PIM parameters are too slow, by approximately one order of magnitude.

According to Morris et al., their results follow a power law $L - L_0 \sim t^n$, with various exponents (Morris et al. 1976). For the highest temperatures (e.g. at 743 K on Figure III.19), two successive regimes are observed (one faster, then one slower, with different exponents). For most temperatures, one may consider that the growth exponent is not far from 1/2 (the yellow dotted line in Figure III.19). Note that these conclusions are based on a small number of experimental points, and on times that vary by only one or two orders of magnitude. It is also difficult to draw definite conclusions from the AKMC simulations. The results, with k-PIM and k-PIM2 parameters, are often compatible with a growth exponent close to 1/2 between $t = 10^2$ and $t = 10^3$ hours. The fast regime observed by Morris *et al.* for short times at 743 K is not seen in the simulations. The simulations display a faster evolution at long times, when the domain are larger than approximately 100 Å, with an exponent $n > 1/3$, but this is a

well-known artefact due to the finite size of the simulation box (see e.g. Le Floc'h, Bellon, and Athènes 2000). It is due to the fact that at the end of the simulation, only one large domain remains and rapidly invades the small ones – with no other large domain to compete with it.

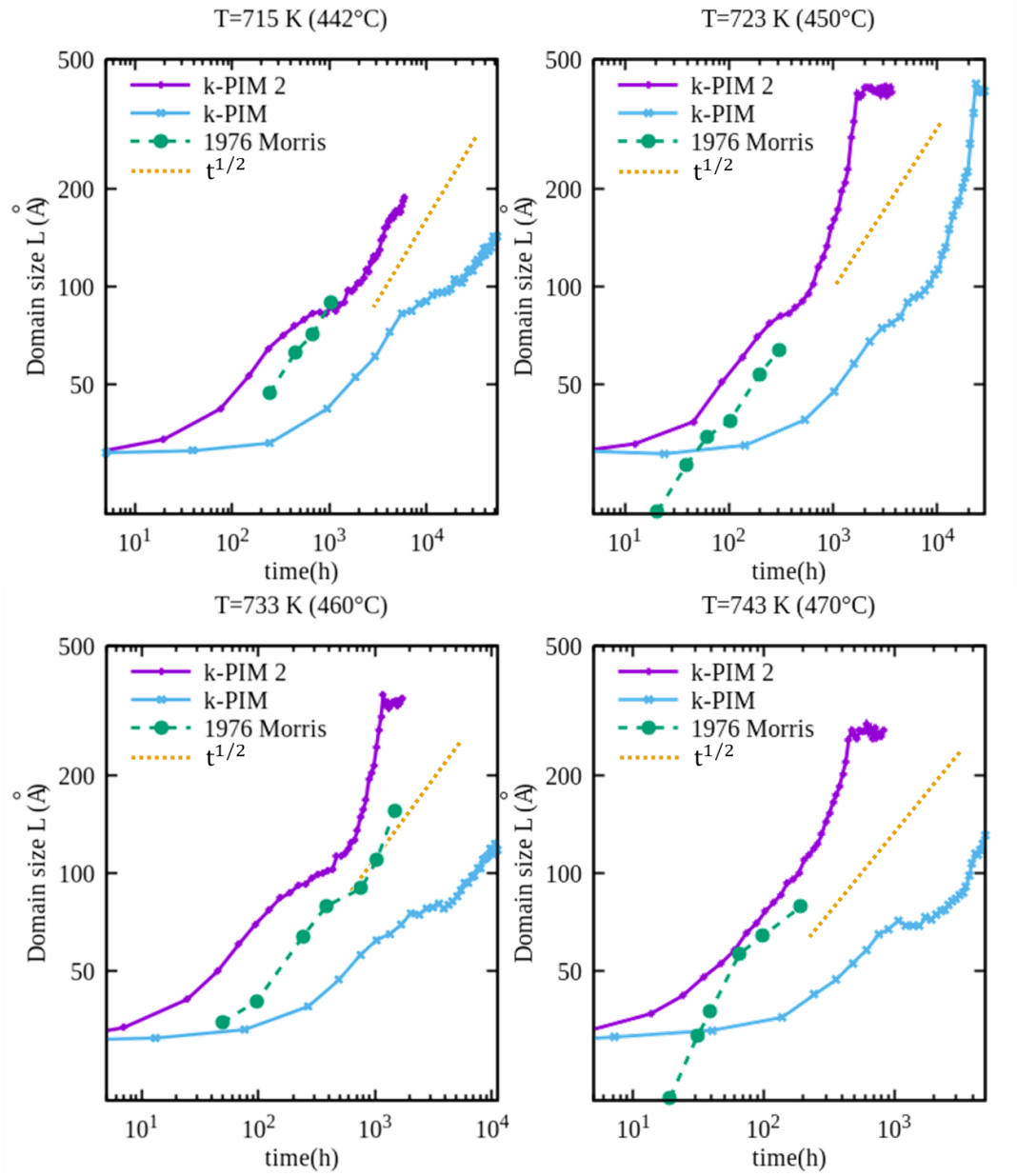

Figure III.19. Evolution of domain size with time at different temperatures (715 K, 723 K,733 K and 743K): comparison between experiments (points) and MC results (lines)

The comparison with Ferjani et al. and Morris et al. is shown in Figure III.20. Compared to Ferjani, the AKMC simulation using k-PIM is slower but has approximately the same slope for the curve $L(t)$, while the AKMC simulations using k-PIM2 predicts a growth rate larger than Ferjani *et al*. and a slope closer to experiments of Morris *et al*.

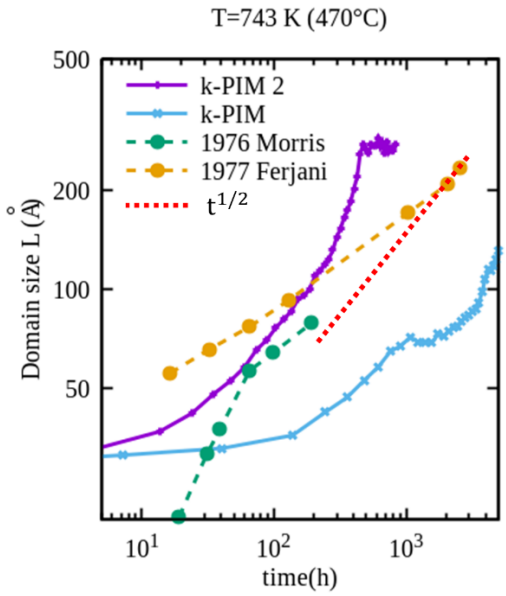

Figure III.20. Evolution of domain size with time at T=743 K: comparison between experiments (points) and MC results (lines)

As in III.3.2, the evolution of the domain size L as a function of the relative LRO parameter η/η_∞, in the AKMC simulations, has been obtained by elimination of the time. The results at $T = 743$ K are shown in Figure III.21 and compared with the experiments. The simulations using k-PIM and k-PIM2 parameters follow a similar kinetic path (except at the larger times), which is between those of the experiments of Ferjani *et al.* and those of Morris *et al.*, but closer to the second one.

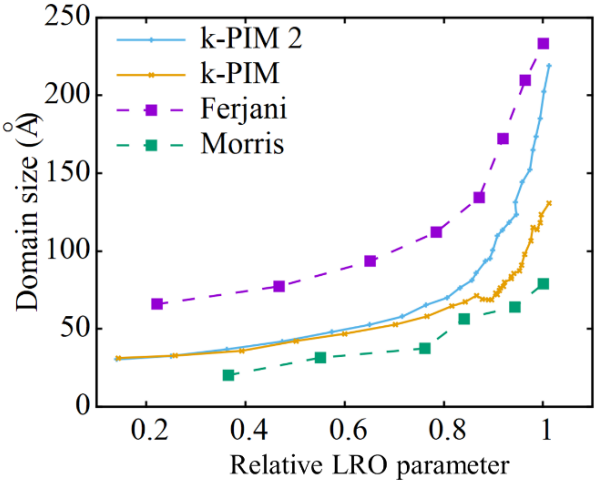

Figure III.21. Evolution of the ordered domain size as function of relative long-rang order parameter in Fe-75%Ni at T=743 K (470 °C): comparison between the AKMC results and experiments of Ferjani et al. (Ferjani, Bley, and Calvayrac 1977) and Morris et al. (Morris et al. 1976).

III.5 Conclusions

In this chapter, we have investigated the ordering process in the $L1_2$ $FeNi_3$ alloy with AKMC simulations. Two different sets of pair interaction model, k-PIM and k-PIM2, have been used. Using a fast Fourier transformation, the LRO parameter and the domain size have been computed from the structure factor of the system.

In general, the simulations performed with the k-PIM2 parameters are in agreement with the experiments -- with an uncertainty that is in the order of differences between experimental studies. The simulations performed with the k-PIM parameters are significantly slower, because they lead to an overestimation of the Gibbs free energies of the vacancy formation in the $L1_2$ phase, therefore to an underestimation of the vacancy concentrations and to a too slow diffusion.

This work needs to be completed: for example, we have not attempted a detailed analysis of the growth exponents of the domain size, partly because the experimental observations are not fully conclusive and partly for lack of time. The analysis would require costly simulations on large simulation boxes, and the determination of growth exponents can be tricky (on a log-log diagram, it is often easy to fit a power law of the type $L - L_0 = kt^{\alpha}$ with several values of α, especially for transient kinetic regimes if they do not extend over several decades of the time scale). Moreover, it would be useful in connection with a detailed study of the diffusion processes in the $L1_2$ phase (diffusion in ordered phases usually occurs by vacancy jumps cycles that can affect the kinetic laws). This is left for future work.

The k-PIM could also be improved. For example, the present models overestimates the critical ordering temperature by approximately 25 K: this could be easily corrected by an optimization of the pair interactions, and we hope it would improve the agreement between the simulations of the experiments and Morris *et al.* with regard to the absolute value of the LRO parameters. The use of the present transition between the parameters based on DFT and those derived from high temperature measurements (Figure II.37) is probably a more important issue. Magnetic interactions models may provide a more physical input for these kinds of simulations in the future.

General conclusions and perspectives

We have developed in this work a pair interaction model, within the rigid lattice approximation. It is used in atomistic equilibrium and kinetic Monte Carlo simulations, to describe the thermodynamic properties, diffusion coefficients and ordering kinetics in Fe-Ni alloys with face-centered cubic structures.

The parameters of the model have been fitted both on ab initio calculations and on experimental data. For the thermodynamic part, we tried to establish a direct link between the interatomic pair interactions of the model and the data of a CALPHAD study, by distinguishing in these pair interactions an enthalpic and an entropic (non-configurational) contribution on the one hand, and a magnetic and non-magnetic contribution on the other hand. We have thus been able to construct a phase diagram that is in good agreement with experiments, when available, i.e. at temperatures above about 400°C. We have also been able to predict the stability domain of the FeNi-$L1_0$ phase, at temperatures too low to reach thermodynamic equilibrium under ordinary conditions. This method has some advantages: distinguishing the magnetic energy contributions, for example, makes it possible to reproduce a phase separation between two solid solutions, one paramagnetic and one ferromagnetic, which had already been predicted by some theoretical studies. We also believe that it could be applied to other alloys and contribute to a more methodical approach to the parameterisation of this type of atomic model.

The kinetic version of the interaction model and simulations, which so far only describes the vacancy diffusion mechanism, allowed us to reproduce all the experimentally known diffusion coefficients with good accuracy, taking into account the scattering between experimental results. For this purpose, we had to introduce a new method to describe the evolution of the equilibrium vacancy concentration, based on the Widom insertion technique. This method, unlike others previously developed for alloys with a tendency to phase separation, works well in alloys with an ordering tendency. It allows the rescaling of the time in Monte Carlo simulations and to obtain a physical time scale, which is obviously essential to simulate diffusion properties. Here again, we believe that this method can be profitably used in other ordering alloys, including systems where the vacancy formation enthalpies and diffusion coefficients evolve much more with the composition than in Fe-Ni alloys. To give an example, one can think of fcc Ni-Al alloys, where the difference in vacancy formation enthalpy is approximately 1 eV and the difference in the self-diffusion coefficients is more than 6 orders of magnitude at 1000 K. Finally, we were able to model the ordering kinetics of the $FeNi_3$ phase, again in good agreement with the available experiments.

A direct perspective of this work is to extend the model to ternary Fe-Ni-Cr alloys, for the modelling of austenitic steels and to the self-interstitial diffusion mechanism, to simulate irradiation effects (in particular radiation induced segregation (RIS), as it has already been done in ferric Fe-Cr alloys). It is also possible to improve our approach in many ways. Some minor changes of the pair interactions should remove the small discrepancy with the experimental value of the critical temperature for the $L1_2$-FeN_3 ordering, thus improving the ordering driving force and the simulation of ordering kinetics just below this temperature. We could also improve the description of the migration barriers in the $L1_0$ and $L1_2$ phases, by further comparison and adjustment on *ab initio* calculations. More fundamentally, one of the difficulties encountered in this study was the lack of data, either experimental or derived from first-principles calculations, to adjust some of the model parameters. There are little data on the entropies of formation and migration of vacancies in concentrated alloys; or on the effect of the ferro-paramagnetic transition on the same properties. This led us to make some fairly strong assumptions, in particular that the magnetic transition does not modify the enthalpies of formation and migration of vacancies at the Curie point. We also had to introduce, in the thermodynamic part of the model as well as in the kinetic part, an empirical rule for the transition between the properties at 0 K (calculated *ab initio*) and the properties at high temperature (experimentally measured). The transition between these two regimes directly affects the diffusion coefficients in the $FeNi_3$ phase and the ordering kinetics. On this last point, we believe that the model of composition- and temperature-dependent pair interactions is sufficiently adaptable to integrate any new data that could be obtained on these properties, while remaining sufficiently numerically cost-effective, which is essential for simulating phase transformation kinetics. From this point of view, we can think that magnetic interaction models will provide very valuable information in the near future. We can mention for example the results of Kangming Li and Chu-Chun Fu (Li, Fu, and Schneider 2021) on the effect of the magnetic transition on the enthalpy of formation of vacancies in iron and nickel. It will be easy to modify our model slightly to take this variation into account, and see its impact on the migration of vacancies and more generally diffusion properties as well as phase transition kinetics.

Appendix

The Hagen & Finnis Model: calculation of vacancy formation energy for ordered structures at their stoichiometry

At high temperatures, it is relatively easy to obtain the equilibrium vacancy concentration by experiments. However, manipulation difficulties arise due to the slow rate of diffusion at low temperature, and consequently long time to reach equilibrium. Furthermore, the order-disordering process makes it even more complicated for experiments. Therefore, it is of great interest to obtain these values by means of theoretical analysis and calculations. Hagen and Finnis (Hagen and Finnis 1998) have proposed analytical expressions for the vacancy and antisite concentration in ordered systems at their stoichiometry. Both may be present to an extent which depends on the alloy and its stoichiometry as well as the temperature. The formulas are constructed based on the assumptions that several key energies can be calculated.

To clarify this theory, we consider an ordered system A_mB_n. We suppose that in a perfect ordered state, all atoms A locate in the sub-lattices α and all atoms B locate on the sub-lattices β. For a real system, we denote that the global concentration of atom A of the system is x and thus the system can be expressed as A_xB_{1-x}. It should be noticed that the Hagen and Finnis formula is only valid within a very narrow change of concentration x around the stoichiometry *m/(m+n)*. With the evolution of the system, we assume that the sites can be occupied by its own atom, an atom of the other kind or a vacancy. In this way, in total six different concentration are defined:

$c_{A\alpha}$: concentration of atoms A on the α site
$c_{A\beta}$: concentration of atoms A on the β site
$c_{B\alpha}$: concentration of atoms B on the α site
$c_{B\beta}$: concentration of atoms B on the β site
$c_{V\alpha}$: concentration of vacancies on the α site
$c_{V\beta}$: concentration of vacancies on the β site

Correspondingly, the key energies $e_{A\alpha}$, $e_{A\beta}$, $e_{B\alpha}$, $e_{B\beta}$, $e_{V\alpha}$, $e_{V\beta}$ are defined as well. For instance, $e_{A\alpha}$ and $e_{B\beta}$ are defined in a perfect ordered system and denoted the energy of atom A on the sub-lattice α and the energy of atom B on the sub-lattices β. As a result, the cohesive energy of the system can be expressed by the sum: $e_{mol} = me_{A\alpha} + ne_{B\beta}$. However, Hagen pointed out that this is just a conventional allocation in for these two variables. As long as the sum e_{mol} remains the same, the calculated concentration of defects will not affect any measurable properties. Then $e_{B\alpha}$ is defined as the

energy of the system where we replace one A atom on the α sub-lattice in the perfect ordered system by a B atom. $e_{V\alpha}$ is defined as the energy of the system where we replace one atom A on the sub-lattices α in the perfect ordered system by a vacancy. Similar definition applies for $e_{A\beta}$ and $e_{V\beta}$.

With the definition of these variables, we have:

$$\begin{aligned} mk_3 c_{V\alpha}^{2(m+n)/n} &+ k_1(m - mx + mk_2k_3x)c_{V\alpha}^{2+m/n} \\ &- k_1(m - mx + mk_2k_3x - nx - nk_2k_3 + nk_2k_3x)c_{V\alpha}^{1+m/n} \\ &+ nk_1^2(1-x)(1-k_2k_3)c_{V\alpha} - k_1^2k_2 = 0 \end{aligned} \tag{1}$$

Where k_1, k_2 and k_3 denote respectively:

$$\begin{aligned} k_1 &= \exp\left(-\frac{me_{V\alpha} + ne_{V\beta}}{nk_BT}\right) \\ k_2 &= \exp(-\frac{e_{V\alpha} - e_{V\beta} + e_{A\beta} - e_{A\alpha}}{k_BT}) \\ k_3 &= \exp(-\frac{e_{V\beta} - e_{V\alpha} + e_{B\alpha} - e_{B\beta}}{k_BT}) \end{aligned} \tag{2}$$

By resolving equation (1), the concentration of vacancy on the α sub-lattice is obtained. Then we can further calculate the concentration of point defects on all sites by:

$$\begin{aligned} c_{V\alpha}^m c_{V\beta}^n &= \exp\left(-\frac{me_{V\alpha} + ne_{V\beta}}{k_BT}\right) \\ \frac{c_{V\alpha}c_{A\beta}}{c_{V\beta}c_{A\alpha}} &= \exp\left(-\frac{e_{V\alpha} - e_{V\beta} + e_{A\beta} - e_{A\alpha}}{k_BT}\right) \\ \frac{c_{V\beta}c_{B\alpha}}{c_{V\alpha}c_{B\beta}} &= \exp\left(-\frac{e_{V\beta} - e_{V\alpha} + e_{B\alpha} - e_{B\beta}}{k_BT}\right) \\ c_{A\alpha} + c_{B\alpha} + c_{V\alpha} &= 1 \\ c_{A\beta} + c_{B\beta} + c_{V\beta} &= 1 \end{aligned} \tag{3}$$

In addition, with Hagen & Finnis method, one is able to calculate the chemical potential as well by the following expressions:

$$\begin{aligned} \mu_A &= \frac{m}{m+n}e_{A\alpha} + \frac{n}{m+n}e_{A\beta} + \frac{m}{m+n}k_BTlnc_{A\alpha} + \frac{n}{m+n}k_BTlnc_{A\beta} \\ \mu_B &= \frac{n}{m+n}e_{B\beta} + \frac{m}{m+n}e_{B\alpha} + \frac{n}{m+n}k_BTlnc_{B\beta} + \frac{m}{m+n}k_BTlnc_{B\alpha} \end{aligned} \tag{4}$$

References

Allnatt, A.R., Lidiard, A.B., 1993. Atomic Transport in Solids, 1st ed. Cambridge University Press. https://doi.org/10.1017/CBO9780511563904

Anento, N., Serra, A., Osetsky, Y., 2017. Effect of nickel on point defects diffusion in Fe – Ni alloys. Acta Materialia 132, 367–373. https://doi.org/10.1016/j.actamat.2017.05.010

Angsten, T., Mayeshiba, T., Wu, H., Morgan, D., 2014. Elemental vacancy diffusion database from high-throughput first-principles calculations for fcc and hcp structures. New J. Phys. 16, 015018. https://doi.org/10.1088/1367-2630/16/1/015018

Badia, M., Vignes, A., 1969. Diffusion du fer, du nickel et du cobalt dans les metaux de transition du groupe du fer. Acta Metallurgica 17, 177–187. https://doi.org/10.1016/0001-6160(69)90138-2

Badia, M., Vignes, A., 1967. Diffusion dans le Systeme Fe-Ni. C. R. Acad. Sci. Paris 264, 1528–1531.

Bakker, H., 1968. A Curvature in the InD versus 1/T Plot for Self-Diffusion in Nickel at Temperatures from 980 to 1400°C. Phys. Stat. Sol. (b) 28, 569–576. https://doi.org/10.1002/pssb.19680280214

Birchenall, C.E., Mehl, R.F., 1950. Self-diffusion in alpha and gamma iron. JOM 2, 144–149. https://doi.org/10.1007/BF03398989

Bonny, G., Terentyev, D., Pasianot, R.C., Poncé, S., Bakaev, A., 2011. Interatomic potential to study plasticity in stainless steels: the FeNiCr model alloy. Modelling Simul. Mater. Sci. Eng. 19, 085008. https://doi.org/10.1088/0965-0393/19/8/085008

Bortz, A.B., Kalos, M.H., Lebowitz, J.L., 1975. A new algorithm for Monte Carlo simulation of Ising spin systems. Journal of Computational Physics 17, 10–18. https://doi.org/10.1016/0021-9991(75)90060-1

Buffington, F.S., Hirano, K., Cohen, M., 1961. Self diffusion in iron. Acta Metallurgica 9, 434–439. https://doi.org/10.1016/0001-6160(61)90137-7

Cacciamani, G., Dinsdale, A., Palumbo, M., Pasturel, A., 2010. The Fe–Ni system: Thermodynamic modelling assisted by atomistic calculations. Intermetallics 18, 1148–1162. https://doi.org/10.1016/j.intermet.2010.02.026

Calvayrac, Y., Fayard, M., 1973. Structural state and mechanical properties of polycrystalline Ni3Fe Alloys. Phys. Stat. Sol. (a) 17, 407–421. https://doi.org/10.1002/pssa.2210170204

Caplain, A., Chambron, W., 1977. Energies de formation et de migration des lacunes dans les alliages fer-nickel de structure C.F.C. par la methode de l'anisotropie magnetique induite. Acta Metallurgica 25, 1001–1011. https://doi.org/10.1016/0001-6160(77)90128-6

Chambron, W., Caplain, A., 1974. Etude des lacunes en très faible concentration dans l'alliage fer-nickel à 70% de nickel par la methode de l'anisotropie magnetique. Acta Metallurgica 22, 357–366. https://doi.org/10.1016/0001-6160(74)90175-8

Cheng, G.Y., Wynblatt, P.P., Dorn, J.E., 1967. Vacancy models for concentrated binary alloys - II long-range ordered alloys. Acta Metallurgica 15, 1045–1056. https://doi.org/10.1016/0001-6160(67)90268-4

Ding, H., Huang, S., Ghosh, G., Liaw, P.K., Asta, M., 2012. A computational study of impurity diffusivities for 5d transition metal solutes in α-Fe. Scripta Materialia 67, 732–735. https://doi.org/10.1016/j.scriptamat.2012.06.010

Dinsdale, A.T., 1991. SGTE data for pure elements. Calphad 15, 317–425. https://doi.org/10.1016/0364-5916(91)90030-N

Domb, C., Green, M.S., Lebowitz, J.L. (Eds.), 1976. Phase transitions and critical phenomena. Vol. 1: Exact results. Acad. Press, London.

Ehrhart, P., 1991. Ni, in: Ullmaier, H. (Ed.), Atomic Defects in Metals, Landolt-Börnstein - Group III Condensed Matter. Springer-Verlag, Berlin/Heidelberg, pp. 242–250. https://doi.org/10.1007/10011948_63

Ferasat, K., Osetsky, Y.N., Barashev, A.V., Zhang, Y., Yao, Z., Béland, L.K., 2020. Accelerated kinetic Monte Carlo: A case study; vacancy and dumbbell interstitial diffusion traps in concentrated solid solution alloys. J. Chem. Phys. 153, 074109. https://doi.org/10.1063/5.0015039

Ferjani, H., Bley, F., Calvayrac, Y., 1977. Ordering and domain coarsening kinetics in substiteted premalloys. J. Phys. Colloques 38, C7-55-C7-56. https://doi.org/10.1051/jphyscol:1977710

Fillion, J., Calais, D., 1977. Autodiffusion dans les alliages concentres fer-palladium. Journal of Physics and Chemistry of Solids 38, 81–89. https://doi.org/10.1016/0022-3697(77)90150-0

Ganesan, V., Seetharaman, V., Raghunathan, V.S., 1984. Interdiffusion in the nickel-iron system. Materials Letters 2, 257–262. https://doi.org/10.1016/0167-577X(84)90125-3

Garcia Ortega, M., Ramos de Debiaggi, S.B., Monti, A.M., 2002. Self-Diffusion in FCC Metals: Static and Dynamic Simulations in Aluminium and Nickel. phys. stat. sol. (b) 234, 506–521. https://doi.org/doi.org/10.1002/1521-3951(200211)234:2<506::AID-PSSB506>3.0.CO;2-Q

Girifalco, L.A., 1964. Vacancy concentration and diffusion in order-disorder alloys. Journal of Physics and Chemistry of Solids 25, 323–333. https://doi.org/10.1016/0022-3697(64)90111-8

Graham, D., Tomlin, D.H., 1963. Self-diffusion in iron. Philosophical Magazine 8, 1581–1585. https://doi.org/10.1080/14786436308207320

Greer, A.L., Spaepen, F., 1985. Diffusion, in: Synthetic Modulated Structures. Elsevier, pp. 419–486. https://doi.org/10.1016/B978-0-12-170470-4.50015-4

Guiraldenq, P., 1962. Metallographie-Influence des Impuretés et de la Structure Fritée sur les Coefficients de Diffusion en Volume et aux Joints des Grains du Fer dans le Nickel. C. R. Acad. Sci 254, 1994–1996.

Hagen, M., Finnis, M.W., 1998. Point defects and chemical potentials in ordered alloys. Philosophical Magazine A 77, 447–464. https://doi.org/10.1080/01418619808223764

Hanatate, Y., Yamamoto, M., Mitani, H., 1977. On the Grain Boundary Diffusion of Ni into gamma-Fe. J.Japan Inst.Metals 41, 1211–1216. https://doi.org/10.2320/jinstmet1952.41.12_1211

Hancock, G.F., Leak, G.M., 1967. Diffusion of Nickel in Binary Alloys of Iron with Nickel, Manganese, and Chromium. Metal Science Journal 1, 33–36. https://doi.org/10.1179/msc.1967.1.1.33

Hargather, C.Z., Shang, S.-L., Liu, Z.-K., 2018. A comprehensive first-principles study of solute elements in dilute Ni alloys: Diffusion coefficients and their implications to tailor creep rate. Acta Materialia 157, 126–141. https://doi.org/10.1016/j.actamat.2018.07.020

Henry, G., Cizeron, G., 1978. Diffusion of nickel into FCC iron nickel alloys-comparison with other results related to diffusion into FCC solid. Annales de chimie et de physique 3, 167–176.

Heumann, Th., Imm, R., 1968. Self-diffusion and isotope effect in γ-iron. Journal of Physics and Chemistry of Solids 29, 1613–1621. https://doi.org/10.1016/0022-3697(68)90103-0

Hirano, K., Cohen, M., Averbach, B.L., 1961. Diffusion of nickel into iron. Acta Metallurgica 9, 440–445. https://doi.org/10.1016/0001-6160(61)90138-9

Howard, R.E., Manning, J.R., 1967. Kinetics of Solute-Enhanced Diffusion in Dilute Face-Centered-Cubic Alloys. Phys. Rev. 154, 561–568. https://doi.org/10.1103/PhysRev.154.561

Iijima, Y., Kimura, K., Hirano, K., 1988. Self-diffusion and isotope effect in α-iron. Acta Metallurgica 36, 2811–2820. https://doi.org/10.1016/0001-6160(88)90127-7

Jönsson, B., 1995. Assessment of the Mobilities of Cr, Fe and Ni in bcc Cr-Fe-Ni Alloys. ISIJ International 35, 1415–1421. https://doi.org/10.2355/isijinternational.35.1415

Jönsson, B., 1994. Mobilities in Fe-Ni alloys : assessment of the mobilities of Fe and Ni in fcc Fe-Ni alloys. Scandinavian Journal of Metallurgy 23, 201–208.

Karimi, A., Auinger, M., 2020. Thermodynamics of the iron-nitrogen system with vacancies. From first principles to applications. Journal of Alloys and Compounds 821, 153343. https://doi.org/10.1016/j.jallcom.2019.153343

Kim, S.M., Buyers, W.J.L., 1978. Vacancy formation energy in iron by positron annihilation. J. Phys. F: Met. Phys. 8, L103–L108. https://doi.org/10.1088/0305-4608/8/5/001

Klaver, T.P.C., Hepburn, D.J., Ackland, G.J., 2012. Defect and solute properties in dilute Fe-Cr-Ni austenitic alloys from first principles. Physical Review B 85. https://doi.org/10.1103/PhysRevB.85.174111

Körmann, F., Dick, A., Grabowski, B., Hallstedt, B., Hickel, T., Neugebauer, J., 2008. Free energy of bcc iron: Integrated ab initio derivation of vibrational, electronic, and magnetic contributions. Phys. Rev. B 78, 033102. https://doi.org/10.1103/PhysRevB.78.033102

Krishtal, MA., Mokrov, AP., Stepanova, UV., Goncharenko, IA., 1968. Zashchitnye Pokrytija Na Metallakh 2, 209–216.

Kuznetsov, E.V., 1972. Uchenye Zapiski Kazanskogo Universiteta. 148, 38–48.

Lavrentiev, M.Yu., Dudarev, S.L., Nguyen-Manh, D., 2009. Magnetic cluster expansion simulations of FeCr alloys. Journal of Nuclear Materials 386–388, 22–25. https://doi.org/10.1016/j.jnucmat.2008.12.052

Le Bouar, Y., Soisson, F., 2002. Kinetic pathways from embedded-atom-method potentials: Influence of the activation barriers. Phys. Rev. B 65, 094103. https://doi.org/10.1103/PhysRevB.65.094103

Le Floc'h, D., Bellon, P., Athènes, M., 2000. Slow coarsening of *B* 2-ordered domains at low temperatures: A kinetic Monte Carlo study. Phys. Rev. B 62, 3142–3152. https://doi.org/10.1103/PhysRevB.62.3142

Li, K., Ph.D. Thesis 2021. Magnetochemical coupling effects on thermodynamics, point deffect formation and diffusion in Fe-Ni alloys: a theoretical study. Paris-Saclay University.

Li, K., Fu, C.-C., Schneider, A., 2021. Effects of magnetic excitations and transitions on vacancy formation: Cases of fcc Fe and Ni compared to bcc Fe. Phys. Rev. B 104, 104406. https://doi.org/10.1103/PhysRevB.104.104406

Liu, J., Barmak, K., 2015. Interdiffusion in nanometric Fe/Ni multilayer films. Journal of Vacuum Science & Technology A: Vacuum, Surfaces, and Films 33, 021510. https://doi.org/10.1116/1.4905465

MacEwan, J.R., MacEwan, J.U., Yaffe, L., 1959. Diffusion of Ni63 in Iron, Cobalt, Nickel and two Iron-Nickel alloys. Can. J. Chem. 37, 1629–1636. https://doi.org/10.1139/v59-237

Mahmoud, S., Mousseau, N., 2018. Long-time point defect diffusion in ordered nickel-based binary alloys: How small kinetic differences can lead to completely long-time structural evolution. Materialia 4, 575–584. https://doi.org/10.1016/j.mtla.2018.11.013

Maier, K., Mehrer, H., Lessmann, E., Schüle, W., 1976. Self-diffusion in nickel at low temperatures. phys. stat. sol. (b) 78, 689–698. https://doi.org/10.1002/pssb.2220780230

Manning, J.R., 1964. Correlation Factors for Impurity Diffusion. bcc, Diamond, and fcc Structures. Phys. Rev. 136, A1758–A1766. https://doi.org/10.1103/PhysRev.136.A1758

Manning, J.R., Bruner, L.J., 1968. Diffusion Kinetics for Atoms in Crystals. American Journal of Physics 36, 922–923. https://doi.org/10.1119/1.1974325

Mantina, M., Wang, Y., Arroyave, R., Chen, L.Q., Liu, Z.K., Wolverton, C., 2008. First-Principles Calculation of Self-Diffusion Coefficients. Phys. Rev. Lett. 100, 215901. https://doi.org/10.1103/PhysRevLett.100.215901

Martínez, E., Senninger, O., Fu, C.-C., Soisson, F., 2012. Decomposition kinetics of Fe-Cr solid solutions during thermal aging. Phys. Rev. B 86, 224109. https://doi.org/10.1103/PhysRevB.86.224109

Matano, C., 1933. On the Relation between Diffusion-Coefficients and Concentrations of Solid Metals. Japanese Journal of Physics 8, 109–113.

Matter, H., Winter, J., Triftshäuser, W., 1979. Phase transformations and vacancy formation energies of transition metals by positron annihilation. Appl. Phys. 20, 135–140. https://doi.org/10.1007/BF00885934

Mayer, J., Fähnle, M., 1997. On the meaning of effective formation energies, entropies and volumes for atomic defects in ordered compounds. Acta Materialia 45, 2207–2211. https://doi.org/10.1016/S1359-6454(96)00334-5

Mehrer, H., 2007. Diffusion in solids: fundamentals, methods, materials, diffusion-controlled processes, Springer series in solid state science. Springer, Berlin ; New York.

Messina, L., Nastar, M., Garnier, T., Domain, C., Olsson, P., 2014. Exact *ab initio* transport coefficients in bcc Fe − X (X = Cr , Cu , Mn , Ni , P , Si) dilute alloys. Phys. Rev. B 90, 104203. https://doi.org/10.1103/PhysRevB.90.104203

Million, B., Kučera, J., 1971. Concentration dependence of nickel diffusion in nickel-cobalt alloys. Czech J Phys 21, 161–171. https://doi.org/10.1007/BF01702804

Monma, K., 1964. Diffusion of Ni63 and Cr51 in nickel-chromium alloys. Journal of the Japan Institute of Metals 28, 188–192.

Morris, D.G., Broln, G.T., Piller, R.C., Smallman, R.E., 1976. Ordering and domain growth in Ni3Fe. Acta Metallurgica 24, 21–28. https://doi.org/10.1016/0001-6160(76)90142-5

Nastar, M., Soisson, F., 2012. Atomistic modeling of phase transformations: Point-defect concentrations and the time-scale problem. Phys. Rev. B 86, 220102. https://doi.org/10.1103/PhysRevB.86.220102

Neiman, M., Shinyaev, Ay., Dzantiew, B., 1953. Akad Nauk SSSR 91, 265–267.

Okada, T., 1966. Determination of self-diffusion constants and observation of autoradiograph in iron–nickel and iron–cobalt alloys by radioactive iron. Radioisotopes.

Osetsky, Y.N., Béland, L.K., Barashev, A.V., Zhang, Y., 2018. On the existence and origin of sluggish diffusion in chemically disordered concentrated alloys. Current Opinion in Solid State and Materials Science 22, 65–74. https://doi.org/10.1016/j.cossms.2018.05.003

Pareige, C., Soisson, F., Martin, G., Blavette, D., 1999. Ordering and phase separation in Ni–Cr–Al: Monte Carlo simulations vs three-dimensional atom probe. Acta Materialia 47, 1889–1899. https://doi.org/10.1016/S1359-6454(99)00054-3

Reuter, K.B., Williams, D.B., Goldstein, J.I., 1989. Ordering in the Fe−Ni system under electron irradiation. MTA 20, 711–718. https://doi.org/10.1007/BF02667588

Reynolds, J.E., Averbach, B.L., Cohen, M., 1957. Self-diffusion and interdiffusion in gold-nickel alloys. Acta Metallurgica 5, 29–40. https://doi.org/10.1016/0001-6160(57)90152-9

Ruch, L., Sain, D.R., Yeh, H.L., Girifalco, L.A., 1976. Analysis of diffusion in ferromagnets. Journal of Physics and Chemistry of Solids 37, 649–653. https://doi.org/10.1016/0022-3697(76)90001-9

Růžičková, J., Million, B., 1981. Self-diffusion of the components in the F.C.C. phase of binary solid solutions of the Fe-Ni-Cr system. Materials Science and Engineering 50, 59–64. https://doi.org/10.1016/0025-5416(81)90086-0

Schneider, A., Fu, C.-C., Soisson, F., Barreteau, C., 2020. Atomic Diffusion in α -iron across the Curie Point: An Efficient and Transferable *Ab Initio* –Based Modeling Approach. Phys. Rev. Lett. 124, 215901. https://doi.org/10.1103/PhysRevLett.124.215901

Schuler, T., Messina, L., Nastar, M., 2020. KineCluE: A kinetic cluster expansion code to compute transport coefficients beyond the dilute limit. Computational Materials Science 172, 109191. https://doi.org/10.1016/j.commatsci.2019.109191

Scorzelli, R.B., 1997. A study of phase stability in invar Fe--Ni alloys obtained by non-conventional methods. Hyperfine Interactions 110, 143–150. https://doi.org/10.1023/A:1012679517295

Senninger, O., Martínez, E., Soisson, F., Nastar, M., Bréchet, Y., 2014. Atomistic simulations of the decomposition kinetics in Fe–Cr alloys: Influence of magnetism. Acta Materialia 73, 97–106. https://doi.org/10.1016/j.actamat.2014.03.019

Soisson, F., Fu, C.-C., 2007. Cu-precipitation kinetics in α − Fe from atomistic simulations: Vacancy-trapping effects and Cu-cluster mobility. Phys. Rev. B 76, 214102. https://doi.org/10.1103/PhysRevB.76.214102

Toijer, E., Messina, L., Domain, C., Vidal, J., Becquart, C.S., Olsson, P., 2021. Solute-point defect interactions, coupled diffusion, and radiation-induced segregation in fcc nickel. Phys. Rev. Materials 5, 013602. https://doi.org/10.1103/PhysRevMaterials.5.013602

Tran, V.-T., Fu, C.-C., Schneider, A., 2020. Effective interaction model for coupled magnetism and phase stability in bcc Fe-Co systems. Computational Materials Science 183, 109906. https://doi.org/10.1016/j.commatsci.2020.109906

Tsuru, T., Kaji, Y., 2013. First-principles thermodynamic calculations of diffusion characteristics of impurities in γ-iron. Journal of Nuclear Materials 442, S684–S687. https://doi.org/10.1016/j.jnucmat.2013.03.051

Tucker, J.D., Najafabadi, R., Allen, T.R., Morgan, D., 2010. Ab initio-based diffusion theory and tracer diffusion in Ni–Cr and Ni–Fe alloys. Journal of Nuclear Materials 405, 216–234. https://doi.org/10.1016/j.jnucmat.2010.08.003

Vernyhora, I.V., Tatarenko, V.A., Bokoch, S.M., 2012. Thermodynamics of f.c.c. Ni–Fe Alloys in a Static Applied Magnetic Field. ISRN Thermodynamics 2012, 1–11. https://doi.org/10.5402/2012/917836

Voter, A.F., Chen, S.P., 1986. Accurate Interatomic Potentials for Ni, Al and Ni3Al. MRS Proc. 82, 175. https://doi.org/10.1557/PROC-82-175

Walsöe De Reca, E., Pampillo, C., 1967. Self-diffusion of Ni in Ni-Fe alloys. Acta Metallurgica 15, 1263–1268. https://doi.org/10.1016/0001-6160(67)90001-6

Wang, H., Gao, X., Ren, H., Chen, S., Yao, Z., 2018. Diffusion coefficients of rare earth elements in fcc Fe: A first-principles study. Journal of Physics and Chemistry of Solids 112, 153–157. https://doi.org/10.1016/j.jpcs.2017.09.025

Wang, Y., Li, K., Soisson, F., Becquart, C.S., 2020. Combining DFT and CALPHAD for the development of on-lattice interaction models: The case of Fe-Ni system. Phys. Rev. Materials 4, 113801. https://doi.org/10.1103/PhysRevMaterials.4.113801

Wanin, M., Khon, A., 1968. Determination by tracer technics of iron and nickel diffusioncoefficients in iron-nickel alloys and of iron and cobalt in iron-cobalt alloys. C.R.Acad. Sci C, 1558–1561.

Wazzan, A.R., 1965. Lattice and Grain Boundary Self-Diffusion in Nickel. Journal of Applied Physics 36, 3596–3599. https://doi.org/10.1063/1.1703047

Widom, B., 1963. Some Topics in the Theory of Fluids. The Journal of Chemical Physics 39, 2808–2812. https://doi.org/10.1063/1.1734110

Zemskii, S.V., L'vov, V.S., Makashova, L.S., 1976. Nickel self-diffusion in nickel-iron alloys. Fiz. Met. Metalloved 41:4, 775–781.

Zhao, S., Osetsky, Y., Zhang, Y., 2019. Diffusion of point defects in ordered and disordered Ni–Fe alloys. Journal of Alloys and Compounds 805, 1175–1183. https://doi.org/10.1016/j.jallcom.2019.07.142

Modélisation atomique des propriétés thermodynamiques, de la diffusion et de la mise en ordre dans les alliages Fe-Ni

Résumé

Nous présentons un modèle d'interactions de paire sur réseau rigide pour étudier les propriétés thermodynamiques, les propriétés de diffusion et la cinétique de mise en ordre dans les alliages Fe-Ni avec une structure cubique à faces centrées (fcc). La raison pour laquelle nous avons choisi ce système binaire à étudier est que d'une part le système Fe-Ni est la base des aciers austénitiques qui ont été largement utilisés dans de nombreux composants de réacteurs nucléaires de génération actuelle et potentiellement future. De plus, il présente aussi lui-même un grand intérêt industriel et a été très étudié au cours des dernières décennies. Cependant, des questions non résolues continuent de se poser concernant ce système car bien que simplement binaire, il reste complexe puisqu'il implique à la fois des transitions magnétiques, chimiques et ordre-désordre. Par conséquent, dans cette thèse, notre objectif est de comprendre et de prédire ces propriétés dans le système Fe-Ni dans le cadre d'un modèle d'interaction de paire simple (PIM). Le modèle développé dans ce travail peut ensuite être étendu à des systèmes ternaires tels que le système Fe-Ni-Cr ou à la modélisation de l'irradiation dans ces alliages. La thèse est constituée de trois chapitres. Le chapitre I présente la partie thermodynamique du modèle. Le chapitre II présente la partie cinétique du modèle. Puis dans le chapitre III, les résultats de mise en ordre dans le système Fe-Ni avec une concentration de 75% Ni sont présentés.

Le chapitre I présente un modèle de paramétrisation systématique des interactions de paire sure réseaux rigides basé sur des données ab-initio et CALPHAD pour le système Fe-Ni. Pour mieux décrire les propriétés thermodynamiques du système Fe-Ni, à 0 K, le modèle d'interaction de paire est ajusté sur des calculs ab initio d'enthalpies de formation de structures ordonnées et désordonnées (spécial quasi-aléatoire) ; à des températures plus élevées, le modèle est systématiquement ajusté sur l'énergie libre de Gibbs des solutions solides gamma Fe-Ni donnée par la méthode CALPHAD. Différentes contributions dans les interactions de paire sont distinguées et comparées séparément. Les interactions comprennent une partie magnétique et une partie non magnétique et dépendent de la température et de la composition locale. Ainsi, le changement magnétique n'est pas traité

explicitement dans les simulations de Monte Carlo mais permet tout de même au modèle de décrire l'influence des transitions magnétiques sur les propriétés thermodynamiques. Nous montrons que les données ab initio et CALPHAD pour la solution solide et pour la phase ordonnée $FeNi_3$-$L1_2$ peuvent être bien reproduites, dans un large domaine de composition et de température, en utilisant des interactions de paire entre les premières et deuxièmes voisins qui dépendent de la température et de la composition locale de l'alliage. Le diagramme de phase du système fcc Fe-Ni est déterminé par des simulations Monte Carlo dans l'ensemble semi-grand canonique et est comparé à des études expérimentales et à d'autres modèles. Nous discutons également en particulier de la stabilité de la phase ordonnée FeNi-$L1_0$ à basse température. L'existence de cette phase est difficile à observer dans les conditions habituelles, du fait d'une diffusion lente, mais elle avait été précédemment suggérée par des observations dans des météorites et par des expériences d'irradiation et notre modèle prédit la stabilité d'une phase FeNi-$L1_0$ à basse température.

Le chapitre II présente des discussions sur les propriétés de diffusion dans le système Fe-Ni. L'objectif est d'étudier les propriétés de diffusion dans le système Fe-Ni par des simulations Monte Carlo cinétiques avec le modèle d'interaction de paire. Par conséquent, le modèle d'interaction de paire du chapitre I est ensuite étendu en tant que modèle d'interaction de paire cinétique (k-PIM) pour prendre en compte la diffusion par les lacunes. En plus des interactions de paire de la partie thermodynamique, nous introduisons des interactions atome-lacune, qui contrôlent les énergies de formation des lacunes et les concentrations à l'équilibre, et des interactions aux positions des cols, qui contrôlent les barrières de migration des lacunes. Comme dans le chapitre I, les interactions magnétiques et non magnétiques sont distinguées. Les paramètres correspondants sont ajustés sur des calculs ab initio des barrières de migration à 0 K, et sur des données expérimentales de diffusion à hautes températures. Nous discutons également en particulier des concentrations de lacunes dans les alliages Fe-Ni concentrés, où aucune expression analytique générale n'existe sauf dans certains cas limites tels qu'une solution solide complètement désordonnée ou une structure parfaitement ordonnée. Par conséquent, une nouvelle méthode basée sur l'intégration de Widom est proposée. Puis avec des simulations Monte Carlo cinétiques, nous montrons qu'il est possible de bien reproduire tous les coefficients de diffusion expérimentaux connus : l'autodiffusion et la diffusion des impuretés dans les alliages dilués, les coefficients de traceur et d'interdiffusion dans les alliages concentrés. L'effet de la transition ordre-désordre sur les coefficients de diffusion du traceur dans l'alliage $FeNi_3$-$L1_2$, qui n'a

pas encore été mesuré expérimentalement, est étudié. Pour simuler la diffusion dans les phases ordonnées, un ajustement supplémentaire du modèle d'interaction de paire cinétiques est effectué basé sure des énergies de formation de lacunes dans la phase ordonnée $FeNi_3$-$L1_2$ données par des calculs DFT à 0 K. L'objectif est d'obtenir un nouveau modèle qui est nommé k-PIM2 dans le travail, pour améliorer les résultats à des températures inférieures à la température de transition ordre-désordre en maintenant les mêmes propriétés de diffusion données par k-PIM à des températures plus élevées.

Enfin le chapitre III présente les discussions sur la cinétique de mise en ordre dans la phase ordonnée $FeNi_3$-$L1_2$. Des simulations Monte Carlo cinétiques avec le k-PIM et le k-PIM2 sont réalisées, avec le calcul de la concentration de lacunes dans le système par la méthode de Widom proposée au Chapitre II. Les évolutions de la taille des domaines et du degré d'ordre à longue distance obtenues avec des simulations Monte Carlo sont mesurées par des transformations de Fourier rapides. Les simulations sont comparées à différentes cinétiques expérimentales à différentes températures. En général, les simulations réalisées avec les paramètres k-PIM2 sont en accord avec les expériences avec une incertitude qui est de l'ordre des différences entre les études expérimentales. Les simulations réalisées avec les paramètres k-PIM sont significativement plus lentes, car elles conduisent à une surestimation des énergies libres de Gibbs de la formation des lacunes dans la phase $L1_2$, donc à une sous-estimation des concentrations de lacunes et à une diffusion trop lente.

Notre travail donne des descriptions globalement satisfaisantes de la thermodynamique, de la diffusion et de la cinétique d'ordre dans le système fcc Fe-Ni avec des simulations Monte Carlo en utilisant un modèle relativement simple d'interaction de paire dépendant à la fois de la composition et de la température. Ce travail peut être potentiellement étendu pour être utilisé dans d'autres systèmes binaires ou les alliages ternaires Fe-Ni-Cr, pour la modélisation des aciers austénitiques. En outre, il peut également être utilisé pour simuler l'effet de l'irradiation, en particulier la ségrégation induite par le rayonnement, comme cela a déjà été fait dans les alliages ferriques Fe-Cr.

disorder transformation

Modélisation atomique des propriétés thermodynamiques, de la diffusion et de la mise en ordre dans les alliages Fe-Ni

Résumé

Nous présentons une modélisation à l'échelle atomique des propriétés thermodynamiques, de la diffusion et des cinétiques de mise en ordre dans les alliages fer-nickel de structure cubique à faces centrées. Le model utilise des interactions de paires qui dépendent de la température et de la composition locale. Ces interactions de paires sont ajustées sur des calculs ab initio à 0 K, et sur des données expérimentales aux températures non nulles. Le diagramme de phases du système est construit et comparé au diagramme de phases expérimental. L'ensemble des coefficients diffusion expérimentaux connus est bien reproduit : les coefficients d'autodiffusion et de diffusion d'impureté dans les alliages dilués, les coefficients de traceur et d'interdiffusion dans les alliages concentrés. Les cinétiques de mise ordre dans l'alliage $FeNi_3$ sont étudies et comparés aux expériences disponibles. Un bon accord est obtenu pour l'évolution du paramètre d'ordre à longue distance et pour l'évolution de la taille des domaines ordonnés.

Mots-Clefs :

alliage Fe-Ni, défauts ponctuels, simulations Monte Carlo, diffusion, transformations ordre-désordre

Atomistic modeling of thermodynamic properties, diffusion and ordering in Fe-Ni alloys

Abstract

We present an atomic-scale modeling of thermodynamic properties, diffusion and ordering kinetics in iron-nickel alloys of face-centered cubic structure. The model uses pair interactions that depend on temperature and local composition. These pair interactions are fitted to ab initio calculations at 0 K, and to experimental data at non-zero temperatures. The phase diagram of the system is constructed and compared to the experimental phase diagram. All known experimental diffusion coefficients are well reproduced: self-diffusion, impurity diffusion coefficients in dilute alloys, tracer and interdiffusion coefficients in concentrated alloys. The ordering kinetics in the $FeNi_3$ alloy are studied and compared to available experiments. A good agreement is obtained for the evolution of the long-range order parameter and for the evolution of the size of the ordered domains.

Key words:

Fe-Ni alloy, point defects, Monte Carlo simulations, diffusion, order-disorder transformation